THESIS

VERTICAL AND HORIZONTAL MIXING IN THE TROPICAL TROPOPAUSE LAYER

Submitted by

Anne Alexandra Glanville

Department of Atmospheric Science

In partial fulfillment of the requirements

For the Degree of Master of Science

Colorado State University

Fort Collins, Colorado

Summer 2015

Master's Committee:

Advisor: Thomas Birner

David A. Randall
Iuliana Oprea

Copyright by Anne Alexandra Glanville 2015

All Rights Reserved

ABSTRACT

VERTICAL AND HORIZONTAL MIXING IN THE TROPICAL TROPOPAUSE LAYER

Nearly all air enters the stratosphere through a single layer in the tropics. The tropical tropopause layer (TTL) is a transition region between the troposphere and stratosphere and its roles include regulating stratospheric chemistry and surface climate. Multiscale dynamics existing in the TTL range from transient convection to the hemispheric wave-driven circulation and the relative influences of these processes still remain unclear. This study pays special attention to vertical and horizontal mixing which are associated with breaking gravity waves and Rossby waves, respectively. Our study quantifies the roles of these dynamics by taking advantage of the conservative nature of water vapor in the lower stratosphere. Unable to change concentration in the lowermost stratosphere after passing through the cold point, water vapor becomes a tracer for total transport and its signal is known as the tape recorder. This tape recorder is studied using observations, reanalysis data, a chemistry-climate model (CCM), and simple idealized modeling. Modifying past methods, we are able to capture the seasonal cycle of effective transport in the TTL and we introduce seasonally-dependent dynamics to a one-dimensional model and perform a parameter-sweep to test all possible dynamical combinations. Simulating with unrealistic annual mean transports results in bimodality where either vertical advection or vertical mixing dominate. The solutions that depend on amplified vertical advection disappear when seasonally-dependent transports are used. Overall, all datasets show that vertical mixing is as important to TTL transport as vertical advection itself even during

boreal winter when advection peaks. The reanalysis and CCM have increased effective transport compared to observations, however, they rely on different dynamics. The reanalysis has amplified vertical mixing while the CCM has amplified vertical advection. This hints at the possible influence of spurious diffusion from data assimilation and its role in amplifying TTL transport.

ACKNOWLEDGEMENTS

Thomas Birner, thank you for working hard to understand my ideas and for giving me time to figure things out on my own. David Randall and Iuliana Oprea, thank you for supporting this research and seeing it through the very end. Many people have helped me become a better worker these past three years, and I think I'm ready for whatever is next.

TABLE OF CONTENTS

1 Transport into the stratosphere

Most tropospheric air enters the stratosphere through the tropics. This transport is strongly guided by the slow-moving part of the Brewer Dobson Circulation (BDC), yet recent studies have brought attention to the importance of vertical and horizontal mixing on the overall transport (*Flannaghan and Fueglistaler* (2014); *Fueglistaler et al.* (2009a); *Konopka et al.* (2007); *Randel and Jensen* (2014); *Sargent et al.* (2014)). The BDC is the combined result of transports on all spatial and temporal scales that act together to move constituents from the upper troposphere into the stratosphere. In the tropics, the distinction between the troposphere and stratosphere does not occur as a sharp boundary. Instead, this region can be thought of as a transition layer possessing dynamical and chemical characteristics from both regimes. Spanning several kilometers in the vertical, this region is known as the tropical tropopause layer (TTL) and it plays a regulating role for certain tracers entering the stratosphere (*Fueglistaler et al.*, 2009a) .

Stratospheric climate depends on tracers such as water vapor and very short lived species containing bromine. Bromine and water vapor concentrations can decrease stratospheric ozone as long as they are able to pass through the TTL. Dehydration in the TTL, associated with or without overshooting clouds, is critical for stratospheric chemistry and surface climate. In the stratosphere, water vapor can lead to the formation of polar stratospheric clouds which allow for heterogeneous chemical reactions that lead to large ozone loses in the polar stratospheric vortexes (*Fueglistaler et al.*, 2009a). Dehydration of water vapor in the TTL also affects the surface climate as changes of concentration in the stratosphere result in changes of longwave and (to a lesser extent) shortwave fluxes which

then influence temperature in both the stratosphere and troposphere (*Solomon et al.*, 2010). Therefore understanding the dynamics within this region is important from scientific and everyday perspectives as the energy reaching earth cannot be without TTL influence.

The purpose of this study is to quantify the strengths of the major transports in the TTL and the lower stratosphere in hopes of better understanding the large-scale influence of multiscale dynamics—from quick, small-scale vertical mixing to slow, large-scale vertical advection. Models show a large (10K) spread in the annual mean tropical cold point tropopause (CPT) temperatures and these discrepancies have been associated with their differing transports (*Gettelman et al.*, 2009). As mentioned above, these temperatures control the amount of water vapor entering the stratosphere, where they then play a larger role in shaping the radiation budget. With a better understanding and implementation of total transport on varying scales, the temperature spread may narrow. Consequently, accurate modeling in the TTL would result in improved calculations of the global radiation balance which is crucial for future climate predictions (*Gettelman et al.*, 2004). To accurately simulate TTL transport, we must first understand the dynamics of the region.

1.1 The tropical tropopause layer

The TTL rests between convective outflow in the upper troposphere (up to altitudes of 12-14 km) and stable air of the stratosphere (above about 18 km). It therefore features a mix of chemical and dynamical properties from both regions and is controlled by complex interactions involving small- and large-scale dynamics, convection, and radiation (*Randel and Jensen*, 2014). Although *Bjerknes and Palmén* (1937) hinted at the TTL's existence,

Highwood and Hoskins (1998) first highlighted its nature as a transition layer while *Folkins et al.* (1999) laid foundation for TTL transport. Currently there are no direct measurements of the magnitude or variability of tropical upwelling, despite its controlling role for tracers moving into the stratosphere (*Abalos et al.*, 2013). And although a plethora of TTL studies have surfaced in the past decade and its global impact has been noted, the roles of vertical and horizontal mixing on the overall transport require further discussion.

Horizontal mixing and slow upwelling in the TTL are closely related because both are driven by Rossby wave breaking occurring between the tropics and extratropics. On the other hand, vertical mixing is connected with gravity wave activity associated with overshooting clouds and latent heat anomalies (*Alexander et al.*, 2006). Overshooting convection can influence water vapor concentrations in the TTL through indirect dehydration and direct lofting of the tracer. Upper-level clouds have cooling aloft (*Paulik and Birner*, 2012) which then results in condensation at the expense of water vapor (indirect dehydration). Convection can increase water vapor concentrations in the TTL if ice particles are sublimated (direct lofting). Finally, convection and latent heating anomalies also lead to gravity wave generation. When the gravity waves break, they can also indirectly affect the water vapor concentration through vertical mixing. These three processes—slow upwelling, horizontal mixing, and vertical mixing—are represented in Figure 1, originally from *Fueglistaler et al.* (2009a).

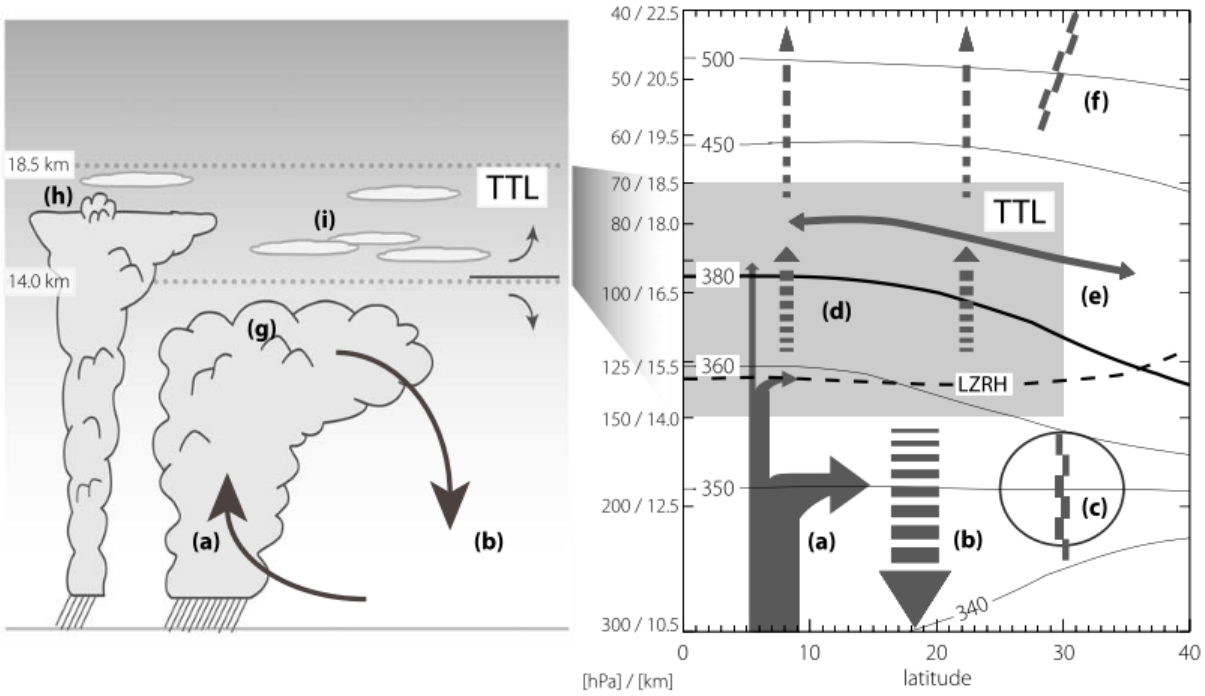

Figure 1: A schematic from *Fueglistaler et al.* (2009a). "The left picture shows cloud processes and transport and the right picture shows the zonal mean circulation. Arrows indicate circulation, black dashed line is clear-sky level of zero net radiative heating, and the black solid lines show isentropes (in K). Letter (a) indicates deep convection: main outflow around 200 hPa, rapid decay of outflow with height in tropical tropopause layer (TTL), and rare penetrations of tropopause with fast vertical transport (mixing) of tracers from boundary layer into the TTL. The letter (b) indicates radiative cooling (subsidence). The letter (c) indicates subtropical jets, which limit quasi-isentropic exchange between the troposphere and stratosphere (transport barrier). The letter (d) indicates radiative heating, which balances forced diabatic ascent. The letter (e) indicates rapid meridional transport of tracers over extratropics ("the surf zone"). The letter (g) indicates deep convective cloud. The letter (h) indicates the convective core overshooting its level of neutral buoyancy. The letter (i) indicates ubiquitous optically (and geometrically) thin, horizontally extensive cirrus clouds, often formed in situ. Note that the height-pressure-potential temperature relations shown are based on tropical annual mean temperature fields, with height values rounded to the nearest 0.5 km."

This study examines the relationships between these three transports within observations. We also analyze reanalysis data and a chemistry-climate model (CCM) to further support our conclusions on the interconnected roles of the transports, and to also simplify the factors controlled by dynamics versus those controlled by data assimilation. As

it remains a struggle for most models to accurately simulate TTL transport (*Gettelman et al.*, 2009), this work will be important to modeling and theoretical work. Extended focus is given to understanding and quantifying mixing in relation to the slow vertical advection. Branching out from previous studies, we also test the seasonal cycle of vertical mixing because its temporal characteristics remain ambiguous (*Flannaghan and Fueglistaler*, 2014). Simulations and analyses occur in pressure and isentropic coordinates. It is beneficial to use pressure coordinates to understand the transports in global circulation models. Isentropic coordinates are helpful for realistic modeling of quasi-adiabatic motion, such as transport by Rossby waves, and to better quantify vertical mixing which is partially included in the heating rate term. To analyze these transports, we use the tape recorder signal of water vapor because this gas is quasi-conserved in the upper TTL and lowermost stratosphere.

1.2 Tape recorder characteristics

The tropical tape recorder is the name given to the signal created by certain zonally-averaged trace gases, like carbon monoxide and water vapor, when they are plotted in height and time. The name was coined because as certain tracers leave the TTL and slowly ascend through the stratosphere, their characteristics remain more or less constant at the value first seen at the cold point tropopause (*Highwood and Hoskins*, 1998).

The tropical pipe refers to the upwelling region bounded by the surf zones on either side. Beyond the subtropical jets are the surf zones where mixing is relatively fast compared to mixing between the surf zones and the tropical pipe. The tropical pipe label

was modified by *Neu and Plumb* (1999) to include detrainment of surf zone air into the tropics and thereafter became the tropical "leaky" pipe. With this model in mind, *Garny et al.* (2014) found that the age of air in the tropical lower stratosphere was increased due to the transport of older air from the extratropics, through the subtropical barrier, and back into the tropics. This mixing is quasi-horizontal and leads to recirculation of air parcels along the residual circulation.

Without mixing in the horizontal or vertical, the BDC would rely only on the residual circulation. Using an idealized model (based on *Mote et al.* (1998)) to advect air with the residual circulation alone, we found that the amplitude of water vapor is underestimated by about 40% at only 80 hPa. This is shown by Figure 2 which also highlights how the synthetic signal has shifted forward in time, particularly for the moist part of the signal. The reason it is shifted forward is because it takes much longer for the water vapor to be transported when only the residual circulation is active and horizontal and vertical mixing are shut off. The amplitudes are underestimated even more at higher altitudes (lower pressures) and this is because of the shallow branch of the BDC near 80 hPa which marks the decreasing strength in the residual circulation with height (however a seasonal cycle remains). With increased horizontal motion in the shallow branch, continuity requires the vertical advection by the residual circulation to reduce in magnitude. Figure 2 shows that consequence of decreased vertical advection and hints that some other transport(s) may be necessary to advect the water vapor signal.

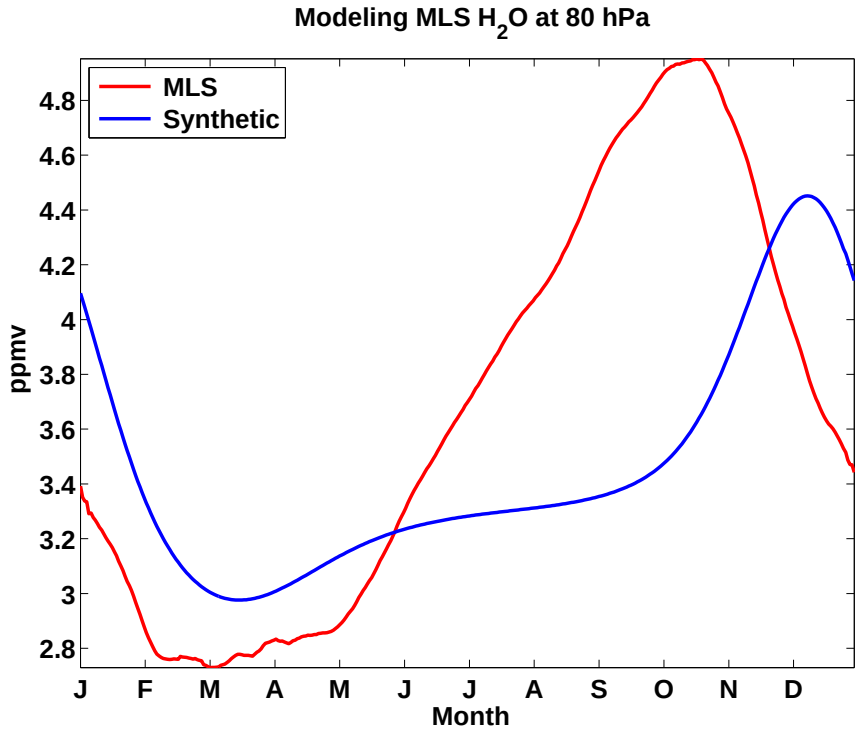

Figure 2: Water vapor from MLS observations (red) and the synthetic model (blue) at 80 hPa where the synthetic values were created using only the vertical advection by the residual circulation and no types of mixing. Note that the vertical advection was modified by including a seasonal cycle based on the effective velocity results in Figure 8 and findings from *Rosenlof* (1995).

The tape recorder moniker relies on the conservative trait of gases as they rise through the stratosphere. For water vapor, its concentration cannot increase or decrease as it enters the stratosphere where temperatures increase with height. Upward from the level with the coldest temperature, water vapor cannot increase or decrease where there is no source. Such a source, however, could be methane which oxidates at and above 20 km to form water vapor (*Mote et al.*, 1996). For this study, we are interested in the region below 20 km where water vapor does not have a significant source or sink. Within this region, between 16 and 20 km, the signal is attenuated with an e-folding time of about 8 months (*Mote et al.*, 1996). This implies that the tape recorder is dominated by the slow, large-scale vertical

advection of the residual circulation and deemphasizes the effects of horizontal and vertical mixing.

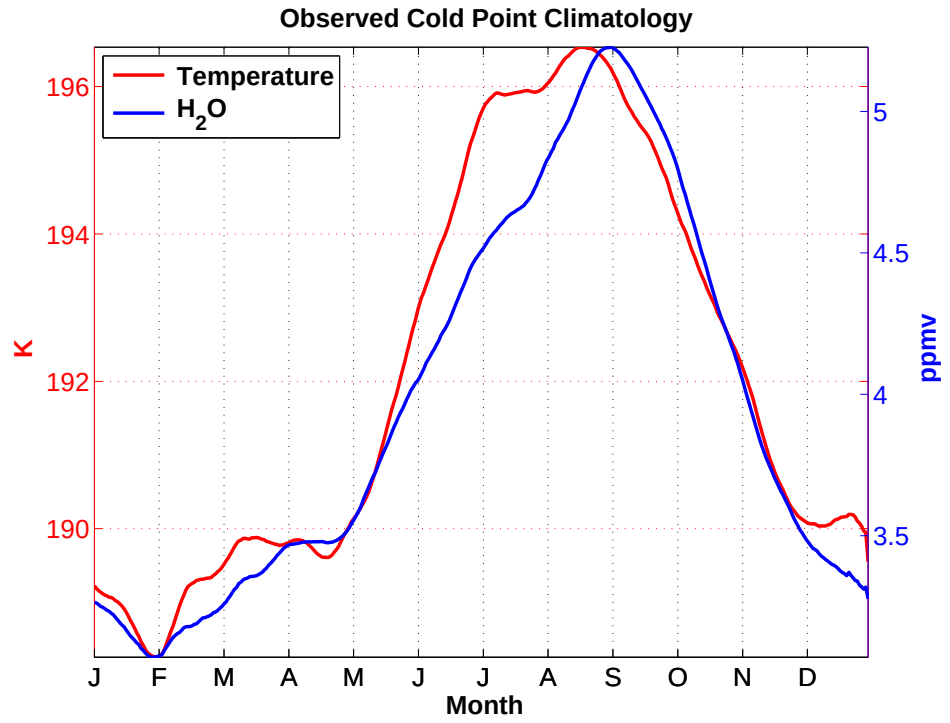

Figure 3: The zonal-mean, climatological-mean cold point tropopause temperature (K) and water vapor mixing ratio (ppmv) at the corresponding altitude in MLS observations.

At the tape head, water vapor has a strong seasonal cycle with anomalously wet (dry) values during boreal summer (winter). This is a direct result of the cold point tropopause (CPT) temperature being anomalously warm (cold) during the summer (winter) which affects the amount of water vapor existing in the air through the process of freeze-drying (dehydration). This relationship can be seen in Figure 3 where CPT temperatures (K) are shown by the red line and water vapor mixing ratios (ppmv) are shown by the blue line. All tape recorder data used in this study shows a phase lag between the base signal and the signal at higher altitudes, as seen in Figure 4 which shows the observed tape recorder from the MLS satellite (more discussion on the satellite data in Chapter 2). A similar structure

is seen the seasonal cycle of carbon monoxide, but the tracer anomalies are reversed with positive anomalies during the boreal winter when agricultural burning, a large source of carbon monoxide, maximizes (*Liu et al.*, 2007). Interannual variability associated with the phases of the quasi-biennial and the El Niño Southern oscillations also impact the phase and amplitude of water vapor in the TTL and stratosphere. For example, *Davis* (2013) found extreme 2-7 year variability in the zonal-mean TTL cloud occurrence tied to QBO and ENSO with impacts for the temperature, relative humidity, and therefore the water vapor at the base of the tape recorder.

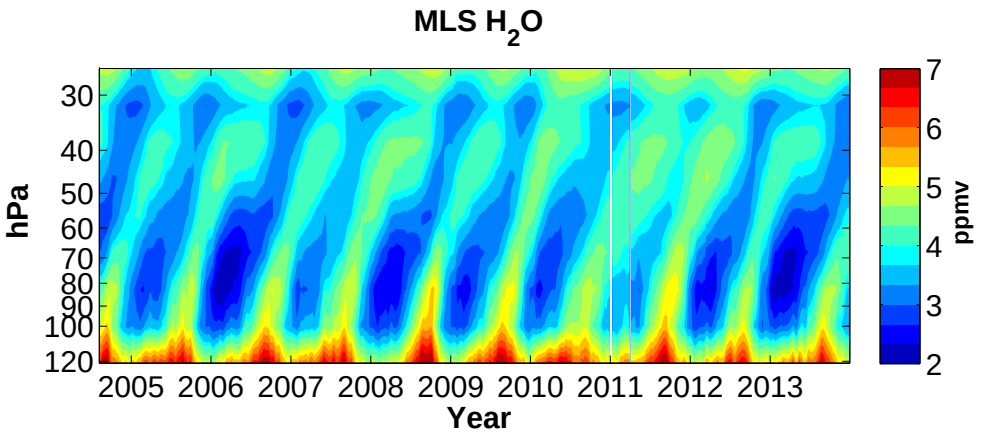

Figure 4: The zonal-mean (10°S-10°N) tropical tape recorder of water vapor from MLS observations. Colored contours indicates the mixing ratio of water vapor in ppmv.

The slope near the base of the tape recorder is a direct consequence of the multiscale transports within the TTL. This study is about separating the individual transports and quantifying their seasonally-varying strengths. The model used here is a modification of the one introduced by *Mote et al.* (1998). Uniqueness comes from testing many combinations of transports—like a parameter sweep—and understanding the influence of seasonally-varying transports on the BDC. Although the foundation of this work is built on

using seasonally-varying transports, it is also worth discussing the impact of removing transport seasonality.

Schoeberl et al. (2008b) and *Mote et al.* (1998) used the water vapor tape recorder to understand the total and individual transports, respectively. To view total transport in the time mean, *Schoeberl et al.* (2008b) used a lag correlation method while *Mote et al.* (1998) used a simple model that individually represented the three types of transport (the method and model are discussed in Chapter 3). This work builds upon these two studies by introducing seasonally-dependent total and individual transports. Comparing the total transport in *Schoeberl et al.* (2008b) to the vertical velocity in *Mote et al.* (1998), it is clear that the total transport is larger than the transport due soley to vertical advection. Using these two methods, we identify the strengths of transports and how much they add to the overall speed in the TTL and above. We view water vapor in MLS observations, the ECMWF Reanalysis-Interim (ERA-i), and the Goddard Earth Observing System (GEOS) chemistry-climate model (CCM).

Ascent of the water vapor tape recorder has become more realistic in reanalyses as they improved (e.g., from ERA-40 to ERA-i). However, in ERA-i, there is now an apparent moist bias (*Dee et al.*, 2011). This bias is contradictory because it is paired with a cold bias CPT which would be expected to be associated with drier air. This may be due to a variety of reasons. Firstly, it could be due to how the CPT temperature is measured. The zonal mean cold point may not be representative of the coldest temperature at which parcels pass through. The Lagrangian cold point, in which parcels are followed through their coldest point, could be more physically appropriate. Secondly, the bias in ERA-i could be due to how the BDC is modeled. Lastly, the bias could be associated with data

assimilation if the ingested observations misplace important features such as the CPT (*Fueglistaler et al.*, 2009b). Besides analyzing observations, this study also evaluates the ability of ERA-i to reproduce the seasonal cycle of water vapor in both amplitude and phase throughout the TTL and lower stratosphere. The transports that make up the total motion in ERA-i are also compared to those that best simulate the observed tape recorder.

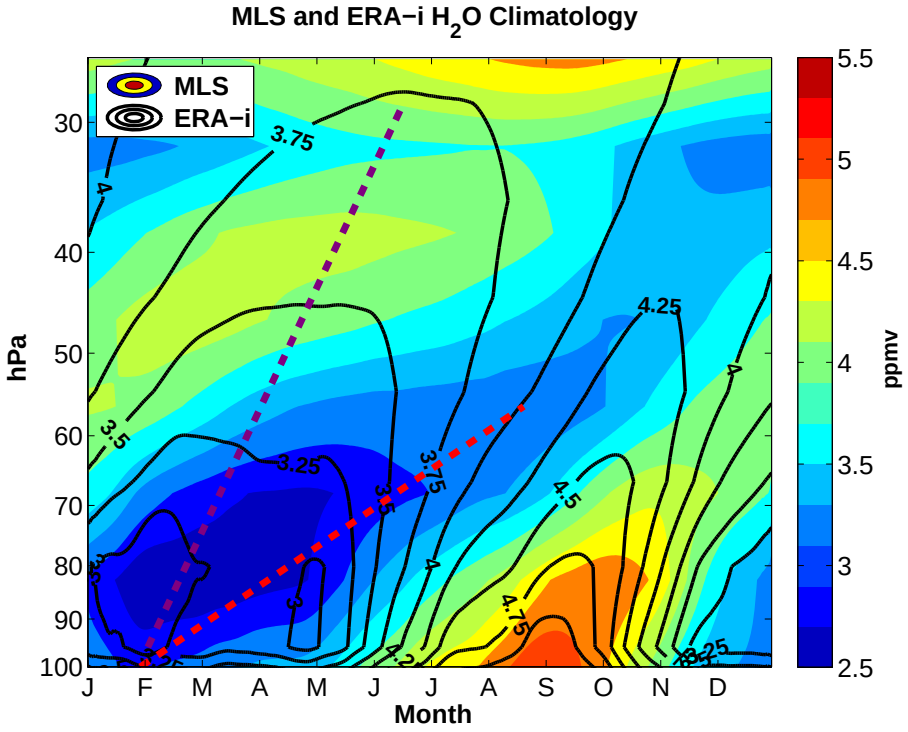

Figure 5: The zonal-mean (10°S-10°N), climatological-mean MLS (colored contours) and ERA-i reanalysis (black contours) tape recorder of water vapor in ppmv. The purple dotted line connects the dry minimums with time for ERA-i while the red dotted line connects the dry minimums for MLS.

Figure 5 shows that the tape recorder in ERA-i slopes upward much more with height compared to observations, and therefore the phase at each height leads those in observations. A cold bias in CPT temperatures has been linked to this increased tropical upwelling in ERA-i (*Dee et al.*, 2011). Overall the contradictions between temperature and water vapor in ERA-i hint that some other dynamics may be at work in the TTL. In

simulations of water vapor, *Plöger et al.* (2011) found that freeze-drying plays a first order role. Perhaps there is not enough dehydration by freeze-drying occurring in ERA-i or perhaps the increased speeds are associated with increased mixing vertically or horizontally. It should be noted that even though ERA-i does not ingest MLS water vapor, both datasets closely agree on the longitudinal structure and amplitude at 100 hPa (*Dee et al.*, 2011).

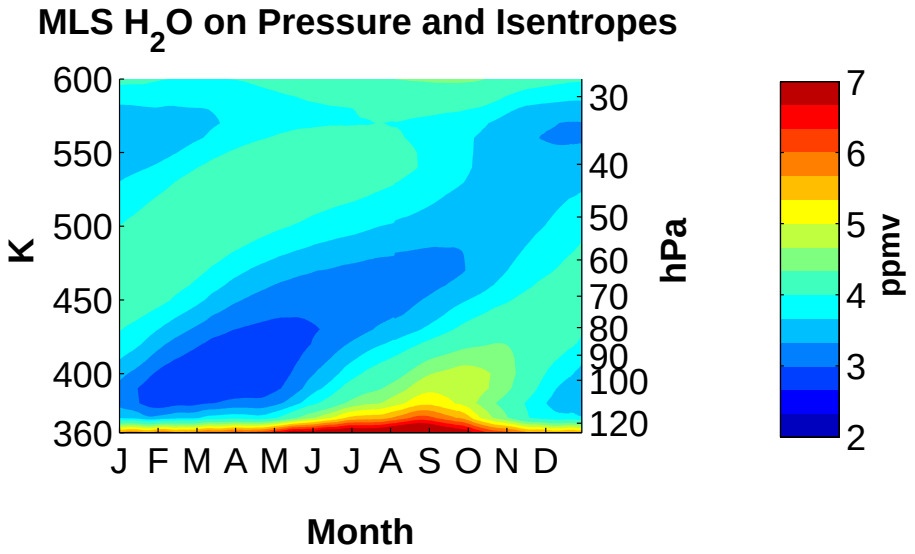

Figure 6: The zonal-mean (10°S-10°N), climatological-mean observed MLS water vapor (ppmv) tape recorder in isentropic coordinates with the their associated time mean pressure surfaces.

A large part of this study relies on using isentropic coordinates to better explain horizontal mixing driven by Rossby wave breaking. In observations, the dry minimum occurs near 90 hPa or 380 K, as seen in Figure 6. Because potential temperature is conserved for adiabatic processes, plotting the signal in isentropic coordinates allows us to look at water vapor in a quasi-Lagrangian framework. By averaging along isentropic surfaces which may have zonally asymmetric features (e.g., the warm pool), one follows the natural parcel surfaces. In contrast, parcels are not confined to pressure surfaces as strictly. Since horizontal motion on isentropic surfaces is entirely adiabatic, it is similar to following

parcel motion unless diabatic heating is involved in which case the motion is vertical. It is not completely Lagrangian because individual parcels are not followed.

1.3 Modeling transports by way of the tape recorder

This study is not the first to try to quantify transports in the TTL. However it is the first to largely test each parameter in order to answer the question: is there only one optimal solution or does a continuous range of solutions exist? The model used in this study is based on that from *Mote et al.* (1998). However instead of defining the tape recorder with a wave solution and solving for time-independent unknowns, we vary the strengths of those unknowns (now seasonally-dependent) to find that a well-defined optimal solution does not exist, or rather that a range of solutions can exist.

Three transports are paramount in this model: vertical advection, vertical mixing, and horizontal mixing. Firstly, vertical advection refers to the slow ascent part of the BDC. It is defined by the transformed Eulerian-mean residual circulation which is used to study the zonally-averaged transport of mass in the stratosphere (*Andrews and McIntyre*, 1976). Therefore, it is the transport remaining after the conservative "wiggling" effects of eddies on pressure surfaces are removed. Past studies have noted a seasonal cycle in this transport with larger net upward mass flux across pressure surfaces during boreal winter than boreal summer (*Rosenlof*, 1995). The speeds of this transport are controlled by the amount of wave breaking occurring in the midlatitude stratosphere, which is larger during the boreal winter due to stronger planetary wave generation in the northern hemisphere (*Plumb*, 2002).

Secondly, vertical mixing can be physically thought of as mixing caused by gravity wave breaking initially created by overshooting cloud tops or latent heat anomalies. This type of mixing can be identified by looking at the distance between surfaces of potential temperature. Surfaces spread apart at the level where mixing occurs; above and below that level, the gradients in potential temperature become stronger. In steady state, this mixing has to be compensated by dibatic heating. *Flannaghan and Fueglistaler* (2014) found that vertical mixing can lead to large changes in climatological zonal wind in the TTL with a temperature perturbation of approximately 4 K in some parts of the tropics (e.g., the warm pool).

Thirdly, horizontal mixing represents meridional exchange of water vapor between the tropical and extratropical stratospheres. Physically, this simulates the effect of Rossby wave breaking. Because Rossby waves drive the tropical upwelling, this transport is somewhat related to the residual circulation. However, this term is also tied to the strength of the jet—the "mixing barrier" between the tropics and extratropics (*Richard et al.*, 2003). During boreal winter, the jet is strongest as seen by the thermal wind balance. The jet is relatively weaker in boreal summer and that is when this transport peaks. The mathematical representation of this transport is done by a relaxation constant.

The relaxation term may be a weakness in the model. When there is more water vapor in one zonal band, it is forced to move over to the other zonal band at a certain rate. In this study, the rate is seasonally-dependent and maximizes during boreal summer when the jet is relatively weak. The vertical mixing term is better represented; it is based on the tracer gradient and follows Fick's first law of diffusion. Since this model is one-dimensional and in the vertical direction, this is perhaps more physical. The vertical advection term is also well represented.

Taking into account its weaknesses, the workings of the model are relatively simple. The water vapor data at the base of the tape recorder is fed into the model, and it is then transported upward via the transports discussed above. Therefore this is accomplished in an Eulerian framework. Modeling is done in pressure and isentropic coordinates, where the latter is more physically appropriate for understanding horizontal motion as adiabatic parcels slide along surfaces of potential temperature. Another advantage to using isentropic coordinates is that vertical mixing is partially implicit in the framework itself. When vertical mixing causes potential temperature surfaces to separate, a part of the changes are seen in the adjacent heating rates. Therefore the strength of vertical mixing in the two coordinate systems do not need to equal.

This study is also unique in implementing seasonally-dependent transports. Wave breaking and tropical convection possess seasonality and this leads us to wonder if the transports they influence should also have seasonal cycles. Each transport is given a seasonal cycle based on past literature, and their annual means also reflect past literature (*Mote et al.*, 1998). The seasonal cycles of the residual advection and horizontal mixing are well described (*Rosenlof*, 1995 and *Konopka et al.*, 2009) however the seasonal cycle of

vertical mixing is not completely understood. Therefore that seasonal cycle is manipulated until the best time-dependency is found. The simulated tape recorder with seasonally-dependent transports is compared to the tape recorder created with time-constant transports.

Although a simple model is used for this study, it physically represents three of the most important transports in the TTL. The terms are simple but not unrealistic; the simplicity allows for better interpretation. Each one has some amount of control on the water vapor that enters the stratosphere. And even though the amounts are seemingly small (average 4 ppmv), being unable to simulate a 0.5 ppmv change can equate to 50% error in water vapor concentrations (*Sargent et al.*, 2014). Therefore quantifying the strengths of these transports is paramount to understanding stratospheric chemistry and the global radiation balance.

1.4 Outline for this study

The data used in this study is described in Chapter 2. Chapter 3 discusses the methods and model. In Chapter 4, the optimal solutions of motion in the TTL are discussed for each dataset with a focus on being able to replicate the seasonal cycle and annual mean. We also look at the influence of the individual transports on the time tendency of the tape recorder as well as the influence of seasonality in the dynamics. Chapter 5 summarizes the results and their implications with a look into future work.

2 Water vapor data

This study uses data from observations and compares them with a reanalysis and a chemistry-climate model (CCM). All data is retrieved on pressure coordinates, and the zonal average from 10°S to 10°N is used to create the plots of the tape recorder. Data from both the observations and the reanalysis are also analyzed in isentropic coordinates. In order to get the water vapor from pressure coordinates onto isentropic coordinates, the potential temperature at each grid point and each time is calculated. These values are interpolated onto a suitable range of isentropic values. In isentropic coordinates, the values of water vapor are also mass-weighted using pseudo-density $\sigma = -\frac{1}{g\partial_p\theta}$ where g is gravity, p is pressure, and θ is the potential temperature.

2.1 Observations from the MLS instrument

For tracing the speed of upwelling in the TTL, this study focuses on the tropical tape recorder of water vapor. For observations of water vapor in the TTL, this study uses data from the Earth Observing System (EOS) Microwave Limb Sounder (MLS) which is onboard the National Aeronautics and Space Administration (NASA) Aura satellite. The satellite, which has been almost continuously recording since 15 July 2004, gathers data from the upper troposphere through the mesosphere by measuring radiation in the GHz and THz frequency range (*Waters et al.*, 2006). Essentially the Aura MLS is a limb-scanning emission microwave radiometer that retrieves daily vertical profiles every 165 km along the suborbital track, spanning 82°S to 82°N on each orbit (*Waters et al.*, 2006).

Unlike the other instruments on Aura, the MLS is a forward looking limb. The limb scans the surface to ∼95 km every 24.7 seconds. These vertical profiles have a cross-track width of ∼7 km measured every ∼160 km along the orbital track. The vertical resolution varies from 1.5 km to 5 km depending on the product. For MLS water vapor, the vertical resolution is ∼3.5 km (within the tape recorder) and it is only observed at pressures of 316 hPa and smaller. The satellite is in a near polar, sun-synchronous orbit at an attitude of ∼705 km (*Livesey et al.*, 2007). Aura does 233 revolutions per cycle and repeats its ground track every 16 days. The same latitude is scanned for each orbit.

This paper utilizes the MLS version 3.3 (v3.3) files downloadable from the Aura website (http://mls.jpl.nasa.gov/index-eos-mls.php). The quality screening given in the MLS data quality document (*Livesey et al.*, 2007) is followed by using stats flags, quality flags, and precision and convergence values. With flagged data removed, there are many advantages to using this MLS v3.3 data. The measurements are reliable in the presence of aerosol or cirrus clouds which can be degraded by other forms of measurement. Also, cloud ice and ice particle size are calculated. As mentioned before, the measurements are performed at all times of day and night with nearly global coverage. Finally, the MLS is able to spectrally resolve weak emission lines in the presence of nearby strong ones (*Waters et al.*, 2006).

The one disadvantage to MLS may be a large one if unaccounted for. Past studies have found a statistically significant moist (high) bias in MLS v3.3 retrievals of water vapor after comparing the satellite measurements to ground- and balloon-based instruments (*Vömel et al.* (2007); *Barnes et al.* (2008); *Hurst et al.* (2014)). Studies involving MLS v3.3 found a moist bias between 83 and 100 hPa. However a bias has not been found in the spatial gradients of water vapor, so these findings have little to no effect on understanding

the movement of water vapor (*Hurst et al.*, 2014). It remains important, however, from a global radiation perspective as *Solomon et al.* (2010) showed that rapid drying in the upper troposphere/lower stratosphere (UTLS) near the end of 2000 reduced global surface warming by 25% between 2000-2009. Therefore if v3.3 water vapor data is used to look at surface radiation trends, this bias needs to be accounted for.

2.2 The ERA-interim reanalysis

To enhance our understanding of transport processes and to test our methods, the study also employs the European Centre for Medium-Range Weather Forecasts (ECMWF) Interim Reanalysis, hereafter ERA-i. This reanalysis outputs global atmospheric and surface parameters on a Gaussian grid at T255 spectral resolution ($\sim$80 km or $\sim$0.7°) on 60 vertical levels. The available data spans from 1 January 1979 to present with 6-hourly temporal resolution. This reanalysis version made many improvements to the previous (ERA-40) including a more realistic stratospheric circulation (*Dee et al.*, 2011).

This study focuses on water vapor in the pressure range between 95 hPa and 21 hPa (or the isentropic range between 380 K and 600 K). The vertical resolution is comparable to those given for MLS data. Past studies have found that ERA-i accurately models the water vapor in the tropical lower stratosphere, particularly above 370 K. However the reanalysis has large errors in representing water vapor in the tropical upper troposphere from 310K to 370K when compared to in situ observations (*Kunz et al.*, 2014). These errors are both over- and underestimations of the observed water vapor on scale with time mean value of water vapor at the CPT. *Kunz et al.* (2014) suggest that convective processes may be

creating the discrepancy. This is interesting because other studies have remarked on the cold bias of CPT in ERA-i coupled with the opposing moist bias in its stratospheric water vapor (*Plöger et al.*, 2011).

ERA-i uses a 12-hourly 4D-Var data assimilation scheme which is a way of saying that it ingests available observations and combines them with forecast model information to aid in estimating a short-range forecast of the atmosphere (*Dee et al.*, 2011). The observations help to keep the model from straying away from reality. Between 1989 and 2010, the number of assimilated observations have increased by an order of magnitude; thus this increases constraint on the model output while decreasing parameters that have to be extrapolated by the model. Overall, better forecasts mean that smaller nudges will be made to keep consistency with observations. Even though ERA-i ingests UTLS water vapor from a small number of sources—radiosondes, pilot balloons, and aircraft—instead of MLS, their spatial gradients in the tropics are largely similar (*Dee et al.*, 2011).

New parameterization in ERA-i allows supersaturation with respect to ice and has resulted in substantial increase in upper tropospheric relative humidity, particularly in the tropics (*Dee et al.*, 2011). Between ERA-40 and ERA-i, tropical cloud cover changed in opposing amounts depending on if the data is over ocean or land. Over ocean, it decreased by up to 15% while it increased by 20-30% over land. The latter can be contributed to improved deep convective triggering. These changes to cloud cover are connected to delayed ice cloud formation and increased high cloud amounts (*Dee et al.*, 2011 and references within), both of which play a role in the amplitude of the tape recorder.

Tropical stratosphere transport in the previous reanalysis, ERA-40, was twice as fast as what now exists in ERA-i. For example, the moist and dry signals reached 30 hPa only

about three months after leaving the 100 hPa level. In ERA-i, the transport between those surfaces takes six months, closer to reality (*Dee et al.*, 2011). Nonetheless, our studies agree with *Schoeberl et al.* (2008b) that this is still at least twice as fast compared to observations. Near the end of their discussion on the stratospheric circulation, *Dee et al.* (2011) show that the mean age of air at 20km in ERA-i agrees well with observations from aircraft measurements of CO_2 and SF_6 at most latitudes, although their paper also mentions again that the prime difficulty is in representing the slow ascent in the BDC.

2.3 The GEOS Chemistry-Climate Model

To better understand the influence of data assimilation in ERA-i, we also analyze the tape recorder in a model that has no data assimilation. For this and other purposes, we chose to work with the Goddard Earth Observing System (GEOS) Chemistry Climate Model (CCM) which was also used by *Schoeberl et al.* (2008b). The GEOS CCM combines atmospheric chemistry and transport modules with the GEOS circulation model, all developed at Goddard. The GEOS CCM took part in the Coupled Chemistry Model Validation round 2 (CCMVal-2) which included other high-top, interactive-chemistry models performing historical (REF-B1) and predictive (REF-B2) runs that include the effects of greenhouse gases.

Compared to all other models in CCMVal-2, GEOS CCM was found to have the best average mean age of air—a measure of transport. In the tropical lower stratosphere, the average phase speed of GEOS CCM compares well to observations although it is variable on short timescales. The residual circulation in the lower stratosphere is somewhat slower

than what is implied through the tape recorder and age gradient ascent rates, however they agree in the middle stratosphere (*Eyring et al.*, 2010). We find this helpful in comparing it to ERA-i which is known for its strong BDC. The barrier to horizontal mixing is also found to be stronger in the tropical middle stratosphere; this keeps older extratropical air from recirculating back into the tropics (*Eyring et al.*, 2010).

This study uses the future REF-B2 projections of water vapor to understand the transport processes. This time range includes January 2000 to December 2100. We use these analyses to better understand the results seen in ERA-i.

3 Methods for determining transport strengths

This section discusses how the effective velocities are calculated and how the one-dimensional tracer transport model works. The effective horizontal and vertical transport are quasi-Lagrangian while the 1-D model uses an Eulerian framework. We also discuss how the simulated results are analyzed by looking at certain measures of the seasonal cycle as well as the annual mean difference between the simulated and actual tape recorder. Finally, we discuss how the time tendency from each transport is calculated and how we alter seasonality to understand its influence.

3.1 Phase-lagged correlation calculation of effective velocity

Relatively small ascent rates and sparse observations make it difficult to actually measure effective (total) vertical velocity in the UTLS. To work around this, effective vertical velocity is calculated in one of two frameworks. Firstly, we discuss here the Lagrangian perspective which focuses on following each parcel in time. The following section discusses the 1-D model and an Eulerian perspective which focuses on a fixed region of space through which air flows. To calculate the effective vertical velocity of all data in this study, a simple phase-lagged correlation method (*Schoeberl et al.* (2008b) and *Niwano et al.* (2003)) is used. Because this method is applied to zonally averaged data, it is not completely Lagrangian. However, this method is somewhat Lagrangian because it tracks the signal of water vapor, which is a conserved tracer in the lowermost stratosphere.

Niwano et al. (2003) introduced this method which was refined by *Schoeberl et al.* (2008b) and it can be described as a phase-lagged correlation which calculates the

time-mean effective vertical velocity in the lower stratosphere. This study modifies their methods to parse out the seasonal cycle. To begin the method, a correlation coefficient is calculated between daily data at level i and level i+1. The data in the upper level are shifted in 1-day increments up to 14 months, until the largest correlation coefficient is found. Strong correlation between the data at the lower level and the phase-shifted data at the upper level is assumed to follow the propagating signal of water vapor. The effective vertical velocity, assigned to midpoints between levels, is simply the distance between the levels divided by the time-shift associated with the largest correlation coefficient (*Niwano et al.*, 2003).

Aspects of the phase-lagged correlation method require detailed attention. In their study, *Schoeberl et al.* (2008b) assume that mixing terms can be neglected and that the resulting velocity represents the residual vertical velocity. However, if this assumption is incorrect and mixing is more important, this method would result in an overestimate of the residual vertical velocity. For example, vertical mixing would spread the signal between two levels and reduce the time lag required for large correlation. In this study, we do not assume mixing to be negligible and therefore the calculation is for an effective transport velocity.

Instead of using a 365 day sample size for calculating the time-mean correlation coefficient (*Schoeberl et al.*, 2008b), this study has found a sample size of 180 days capable of parsing out the seasonal cycle of effective velocity. Tested on a constant vertical advection of -0.5 hPa day^{-1}, this method was found to capture the speed within $\pm$0.05 hPa day^{-1} as shown in Figure 7. Also unlike *Schoeberl et al.* (2008b), this study retains high correlations that occur at lags of less than one month. However, lags of less than seven

days are omitted because that setup produces unrealistic and temporally-unvarying speeds with low correlations.

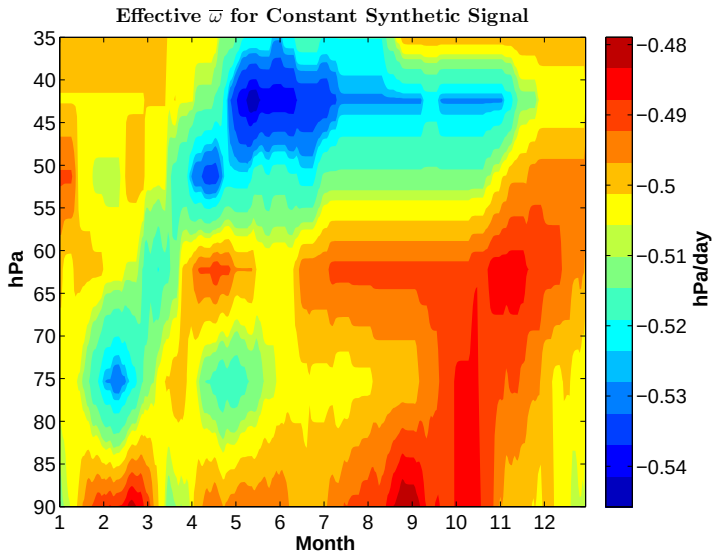

Figure 7: The effective vertical velocity calculated from performing the phase-lagged correlation method on a synthetically-generated tape recorder that was made using spatially- and temporally-constant vertical advection of -0.5 hPa day^{-1}.

The phase-lagged correlation method was also tested on seasonally-dependent velocities as shown in Figure 8. Here we notice that the method can be somewhat noisy, even when the climatological average is taken. We notice that the method is more likely to underestimate by 0.05 hPa day^{-1} below 60 hPa and overestimate by 0.05 hPa day^{-1} above that. It appears that the method has trouble identifying small vertical velocities in the middle stratosphere and it also struggles when the water vapor gradient is strong across time (e.g., in May when the signal goes from dry to moist). Overall, the method appears to successfully capture the seasonality and magnitude of the transport.

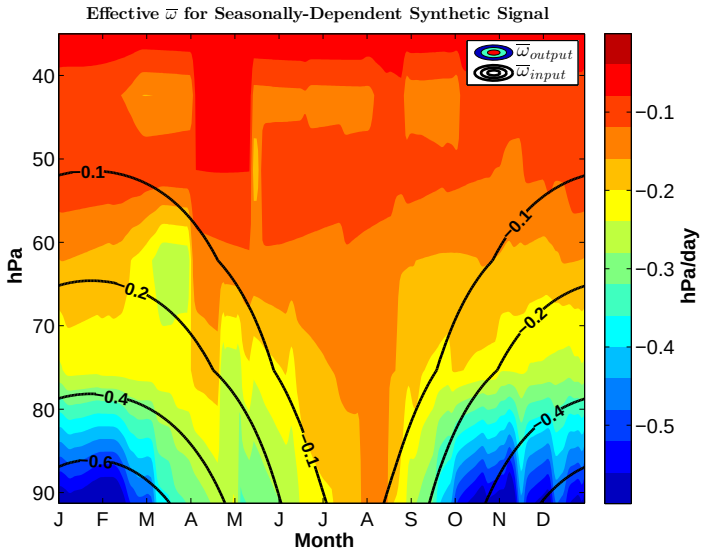

Figure 8: The effective vertical velocity ($\overline{\omega}_{output}$) calculated from performing the phase-lagged correlation method on a synthetically-generated tape recorder that was made using spatially- and temporally-varying vertical advection shown with the black contours ($\overline{\omega}_{input}$). Both contours are plotted in hPa day^{-1}.

This study also adds upon the work of *Schoeberl et al.* (2008b) and *Flury et al.* (2013) by applying the method to isentropic surfaces in order to calculate the effective horizontal velocity. The method is applied to a plot of time versus latitude instead of time versus pressure. By doing this, we are able to calculate the horizontal transport occurring along a surface of potential temperature. It was found that a sample size of 180 days was still able to find a seasonal cycle. Instead of only shifting the sample size forward in time when comparing water vapor at two latitudes, it also must be shifted backwards in time. In the general sense, the sample size should be shifted forward as long as the correlation takes place between equatorward latitudes and time-shifted poleward latitudes. However, because the signal shifts to follow tropical convection—meaning it is not always at the equator—we choose to start the analysis in the southern-most part of the isentropic surface and simply correlate with latitude bands northward of that until reaching the

northern-most part of the surface. Therefore, we must correlate forward and backward in time in order to account for the signal's dispersion in northern and southern hemispheres (respectively) and the latitude-shifting signal. We continue to shift the data day-by-day up to 14 months, now backwards and forwards, until the best correlation coefficient is found.

3.2 One-dimensional modeling of the tape recorder

Eulerian studies are often computationally less expensive than Lagrangian ones (*Zhang and Chen*, 2007). Although Eulerian models have the disadvantage of numerical vertical mixing, they also have the advantage of being able to simulate vertical mixing in space whereas most Lagrangian models are not capable of doing so (Stohl et al., 2005). In order to quantify the strength of each transport factor, a one-dimensional, fourth-order Eulerian model is used to simulate the tape recorder. This study modifies the synthetic model work by *Mote et al.* (1998) which inversed-solved for the three unknowns after defining the tape recorder with a wave solution. Instead of focusing on an average solution for the unknowns, this study explores a range of combinations and introduces seasonal-dependence of each factor.

Thousands of transport combinations (in pressure and isentropic coordinates) are tested in this one-dimensional advection-mixing model. The tape recorder simulated in pressure (eqn. 1a) and isentropic coordinates (eqn. 1b) is calculated using the models

$$\partial_t \overline{\chi} = -\overline{\omega}^* \partial_p \overline{\chi} + \partial_p (K \partial_p \overline{\chi}) - \alpha(\overline{\chi} - \overline{\chi}_{ML}) + S \tag{1a}$$

$$\partial_t \overline{\chi} = -\overline{Q}\partial_\theta \overline{\chi} + \left(\frac{1}{\sigma}\right)\partial_\theta(\sigma K \partial_\theta \overline{\chi}) - \alpha(\overline{\chi} - \overline{\chi}_{ML}) + S \tag{1b}$$

where $\overline{\chi}$ is the tracer mixing ratio, $\overline{\omega}^*$ is the residual vertical velocity, $\overline{Q}$ is the diabatic heating rate, K is the vertical diffusivity, α is the horizontal mixing rate, σ is pseudo-density for isentropic calculations, $\overline{\chi}_{ml}$ is the midlatitude (30°N to 60°N) value of $\overline{\chi}$, and S is a chemical source-sink term. The overbars represent the zonal mean.

This model carries implicit assumptions which are discussed by *Mote et al.* (1998). Firstly, it assumes that tropical air is horizontally well-mixed within the latitude bounds (here, 10°S to 10°N) and is notably different, though not completely isolated, from midlatitude air. Secondly, the values of $\overline{\omega}^*$, K, and α apply to water vapor. Thirdly, horizontal mixing by midlatitude air is modeled by a linear relaxation process in which tropical air is relaxed towards $\overline{\chi}_{ml}$ with rate α. The last assumption regarding horizontal mixing is the most extreme in the lower stratosphere because midlatitude air below 20 km is unlikely homogeneous and horizontal mixing is a more complex process (*Plöger et al.* (2011); *Konopka et al.* (2009)).

Due to their initial definition that the tracer at each level is described by a waveform equation, *Mote et al.* (1998) are able to inverse-solve for the three unknowns. This definition is sensible for sparse observations, however improving coverage has revealed large temporal and spatial variation in the zonal-mean tape recorder signal (*Flannaghan and Fueglistaler*, 2014). A waveform definition of water vapor may no longer be appropriate. This study uses varying combinations of the three unknowns in the one-dimensional model that integrates in time using the Runge-Kutta method.

The fourth-order Runge-Kutta method samples the slope at intermediate points as well as the end points to find a weighted average of the slope across the time interval. Our early modeling used the first-order upwind method which relies on the previous value to predict the next, however this led to large numerical diffusion. This study uses Runge-Kutta because of the very low numerical diffusion compared to the upwind scheme. Also, Runge-Kutta allows for a finer resolution. For this study, 5 hPa (10 K) is used to simulate the tape recorder in pressure (isentropic) coordinates.

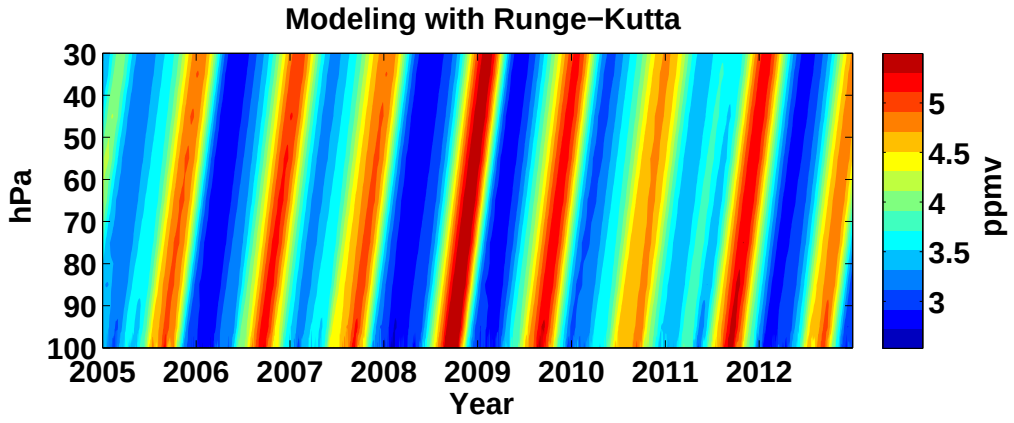

Figure 9: The Runge-Kutta synthetic tape recorder created using spatially- and temporally-constant vertical advection of -0.5 hPa day^{-1} and water vapor at 100 hPa from MLS observations.

Unlike *Mote et al.* (1998), this study allows the three transport factors to vary in time and height instead of height alone, as seen in Figure 10. The profiles from the original study are used as the mean around which each factor oscillates to form a seasonal cycle. Vertical mixing follows a seasonal cycle similar to the vertical advection with a maximum (minimum) in boreal winter (summer). The seasonal cycle of horizontal mixing is opposite from the vertical advection and vertical mixing. Horizontal mixing maximizes during boreal summer when the northern hemisphere jet is relatively weak and horizontal motion

is allowed to intensify (*Gettelman et al.*, 2011). Figure 10 shows the transports magnitudes in pressure coordinates. We transform these into isentropic coordinates by using the stratification (derivative) of potential temperature surfaces with pressure surfaces.

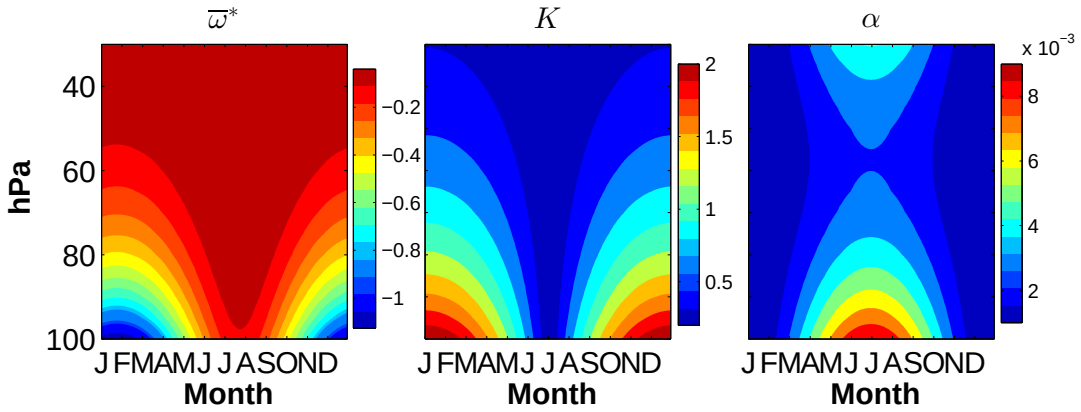

Figure 10: The climatology of the three synthetic transports, at their original strengths following *Mote et al.* (1998). The residual circulation $\overline{\omega}^*$ (hPa day^{-1}) is on the left; K (hPa^2 day^{-1}) is in the middle; and α (day^{-1}) is on the right.

3.3 Analyzing model performance

Following the end of the model runs, we then analyze the simulated results by comparing them to what they are trying to replicate—either the MLS observations, the ERA-i reanalysis, or the GEOS CCM. This study analyzes the performance of the 1-D model in three ways: amplitude, phase, and the annual-mean. Every transport combination is tested using these measures. Amplitudes are compared by way of amplitude ratio and phases are compared by way of a lead or lag. These calculations are carried out at each level, however much of the results focus on 80 hPa (400 K) which is the base of the stratosphere yet still affected by multiscale TTL dynamics.

Amplitude ratio takes the simulated amplitude and divides it by the actual amplitude in each dataset. Therefore when the amplitude ratio is less (greater) than one, the

simulated tape recorder underestimates (overestimates) the amplitude. To calculate the amplitude, the annual mean must first be removed from the data at every level such that the seasonal cycle remains. Then a discrete Fourier transform is performed on this data and the absolute value of the transform gives the power spectrum. The maximum in the power spectrum gives the amplitude, and this result matches the amplitude when it is calculated using the crest and trough values of water vapor.

The phase lag is simply the difference in the phase between the simulated and actual tape recorders where a negative value corresponds to the model lagging behind the actual data. To calculate the phase in each time series, we also needed to remove the annual mean from each level and perform a discrete Fourier transform. Following this step, the phase angles were calculated by multiplying the transform of the simulated data by the conjugate of the transform of the actual data. Next the imaginary part of the result is divided by the real part, the arctan is taken, and the phase angle is found. If the phase angle is greater than zero, then the simulated tape recorder leads the actual data and therefore the simulated effective speed is too large.

The final diagnostic that measures model performance is based on the annual mean and not the seasonal cycle. It is calculated by first taking the annual mean values of water vapor at each level. Then the actual annual mean values are subtracted from the simulated annual mean values. Next that value is divided by the actual mean values and multiplied by 100 such that the resulting measurement is a percent difference in the annual mean. Positive (negative) values of this diagnostic equate to overestimates (underestimates) in the simulated annual mean water vapor at a given level.

Altogether, these measures allow for sturdier conclusions to be made regarding the strengths of each transport. Although much of this study is interested in the seasonal cycle of transports, it is equally important to measure simulation in the annual mean. Studies that only use the annual mean to understand transport could be misrepresenting half of the tape recorder yet still finding good performance within that single diagnostic. Consequences of only using one diagnostic can materialize as larger problems such as having more water vapor enter during the dry part of the signal and resulting in changes to the surface radiation calculation (*Sargent et al.*, 2014). Beyond understanding the strengths of transports seasonally, it is also important to understand how much the optimal transport combinations contribute to shaping the tape recorder of water vapor.

3.4 Water vapor tendency from each transport

Knowing the influence of each transport is important to theoretical TTL studies. During each run, the time tendency of water vapor (in ppmv/day) due to the individual transports is recorded. This means the $\partial_t \chi$ from each of the three terms is logged before the Runge-Kutta integration takes place. These are logged for each day and each level. This allows us a way to see how much of the tape recorder changes (on a seasonal cycle) as a result of vertical advection, horizontal mixing, and vertical mixing. These transports add up to equal the total time tendency of water vapor.

The second method that helps explain the influence of each transport uses the percent variance explained by each term in the 1-D model. Using the time tendencies from each transport in the previous method and the time tendency from the total transport, the

correlation coefficient is calculated between each transport and the total. The resulting correlation coefficient is squared and then multiplied by 100 to result in the percent variance of the total time tendency of water vapor explained by each individual transport. Because the transports are cross-correlated, meaning they do not act independently, the sum of the variances does not need to add to 100% as we will see in Chapter 4.6. Each term depends on the water vapor which, above the tape head, was set by the terms themselves.

The seasonal time tendency calculations as well as the percent variance calculations are performed in both pressure and isentropic coordinate systems. As discussed earlier, there are a few benefits to modeling in both frameworks. Modeling horizontal transport is more physically appropriate in isentropic coordinates as parcels move along surfaces of potential temperature. However modeling in pressure coordinates is also beneficial because many reanalysis models operate in such these coordinates (*Dee et al.*, 2011) and the observational data is provided on pressure surfaces.

3.5 Changing seasonality of transports

A large part of this study is interested in knowing the influence of seasonality. The question is: does seasonality in dynamics matter to TTL transport? To test this question and for comparison with previous work, the annual mean is used for all three transports, following *Mote et al.* (1998). This is performed using the tape head water vapor from MLS observations on pressure coordinates. This test checks the robustness of transport profiles found by *Mote et al.* (1998) and offers insight into the influence of a dynamics with seasonal cycles.

Because the seasonality of the vertical advection and horizontal mixing are well documented (*Plumb* (2002); *Rosenlof* (1995)) while the seasonality of vertical mixing is more ambiguous, we choose to focus on analyzing the latter in more detail. This is done by shifting the phase of the seasonal cycle month-by-month and running the 1-D model for each scenario. This is also performed using MLS observations on pressure coordinates.

4 Transports in the tropical tropopause layer

In this section, we present the results on the effective transport and 1-D simulations. First, the seasonal cycle of the effective transport is discussed from vertical and horizontal viewpoints. Such results were found using the phase-lagged correlation method created by *Niwano et al.* (2003), further explored by *Schoeberl et al.* (2008b), and refined within this work. Following that section, the rest of the results are found by applying a parameter sweep to the 1-D model discussed by *Mote et al.* (1998) and modified here with by allowing realistic seasonal-dependencies of transports. We discuss the results in pressure and isentropic coordinate systems for each dataset. Further investigation on the seasonal cycles of transports occurs near the end.

4.1 Seasonal cycle of the effective transport

Using the phase-lagged correlation method (*Niwano et al.* (2003); *Schoeberl et al.* (2008b)), the vertical and horizontal effective transports are calculated for all datasets. The effective vertical transport was calculated in both pressure and isentropic coordinates, however, the effective horizontal transport is only calculated in isentropic coordinates as horizontal mixing caused by Rossby wave breaking occurs quasi-adiabatically and therefore flows along surfaces of constant potential temperature.

4.1.1 Vertical transport

The seasonal cycle is evident in each coordinate system and in each dataset. Represented with colored contours in Figure 11, MLS pressure velocities (hPa day^{-1}) are

over three times larger in the boreal winter than summer. A similar seasonality is seen in ERA-i, shown by the black contours in Figure 11, however it is not confined to the TTL. The largest difference between the velocities in MLS and ERA-i are in the speeds. Within the TTL, ERA-i has speeds about 2-3 times greater than those calculated within observations. There are also differences in the how far the signal penetrates into the middle stratosphere with the vertical velocities penetrating higher for ERA-i. Figure 8 showed that this method can underestimate if the vertical advection is too small, and that may be the case with MLS observations and it may be associated with the resolution.

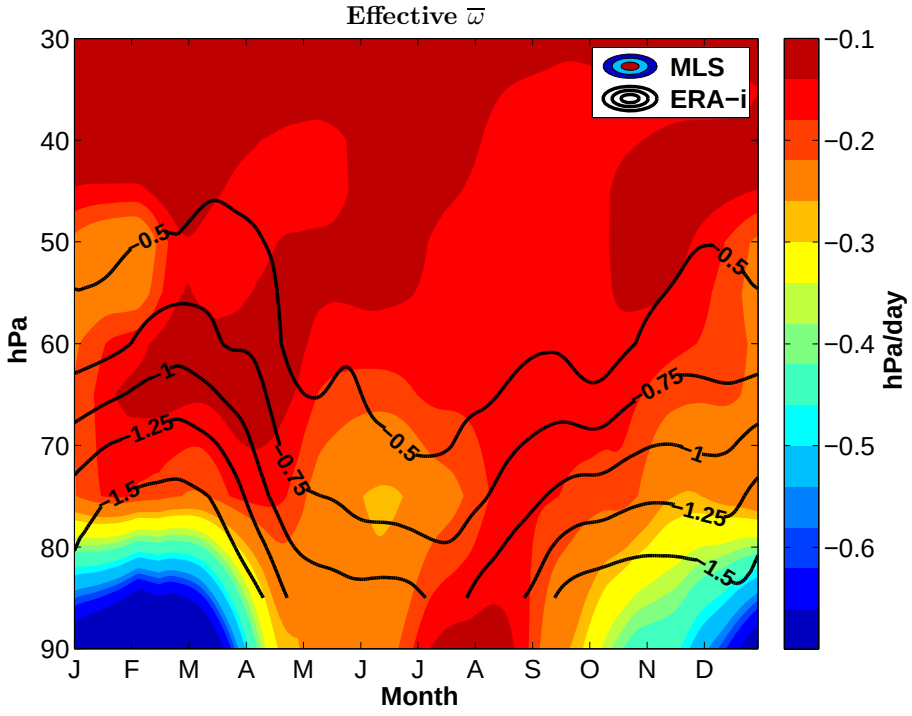

Figure 11: The climatologyof the zonal mean effective vertical velocity (hPa day^{-1}) calculated using the phase-lagged correlation method. The colored contours are for MLS observations and the black contours are for the ERA-i renalysis.

The vertical advection by only the residual circulation in ERA-i is much less than the effective vertical velocity calculated through the phase-lagged correlation method, as seen

in Figure 12. Within the TTL, the effective vertical velocity is 4 times larger than the vertical advection by the residual circulation in boreal winter. Testing the phase-lagged correlation on known velocities showed that this method may miscalculate by only ±0.05 hPa/day (see Figure 7). Therefore most of the transport in the TTL and lower stratosphere still cannot be explained by the residual circulation in the ERA-i reanalysis. This signifies that vertical or horizontal mixing (or both) may be playing a large role in the reanalysis and potentially also in observations.

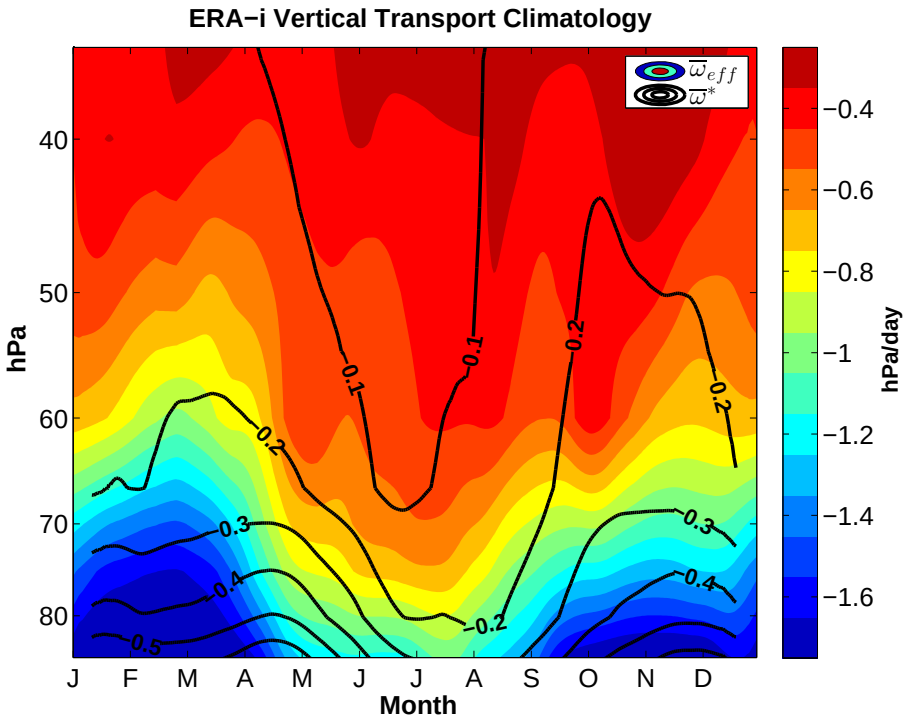

Figure 12: The ERA-i climatologies of the zonal mean effective vertical velocity (colored contours) and the zonal mean residual circulation $\overline{\omega}^*$ (black contours) in hPa day^{-1} for both.

A seasonal cycle is also evident within MLS and ERA-i in isentropic coordinates (see Figure 13) but the magnitude of difference is even larger with diabatic heating nearly 4-5 times larger in the reanalysis than the observations. This result is supported by *Wright and Fueglistaler* (2013) and *Yang et al.* (2010) who found the longwave cloud radiative

heating rates above 200 hPa to be larger in ERA-i compared to other reanalyses and a detailed radiative transfer model. *Wright and Fueglistaler* (2013) note that water vapor contents and therefore treatment of convective anvil clouds in ERA-i could partially explain the anomalous heating rates. There is also a noticeable difference in the level with maximum effective diabatic heating. In ERA-i, the maximum heating occurs at 410 K while in observations it occurs at 390 K. This could be due to the fact that ERA-i has a colder and higher tropopause (*Wright and Fueglistaler*, 2013).

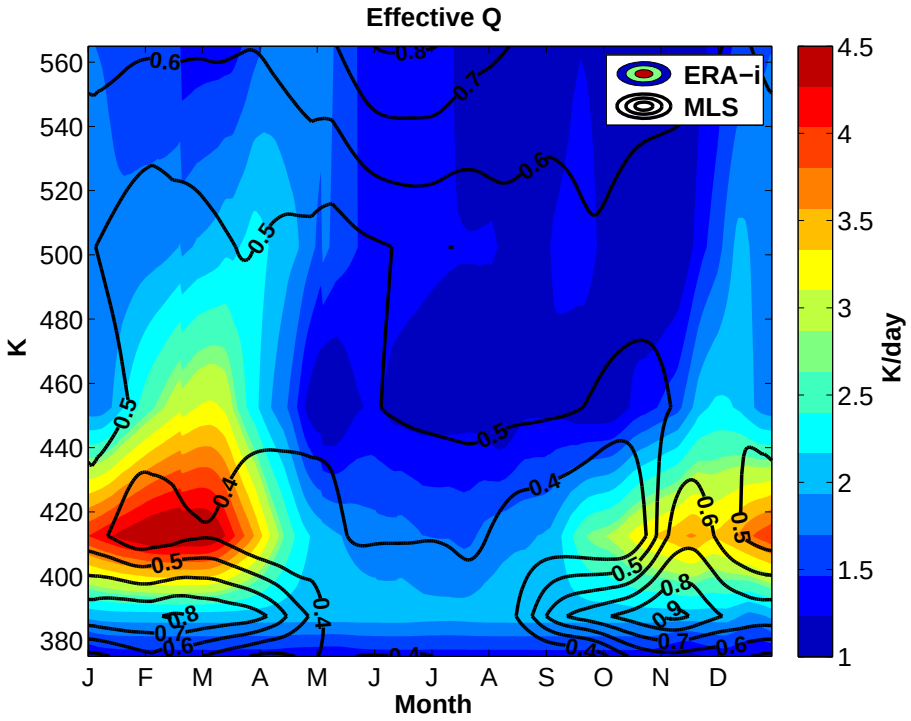

Figure 13: The climatologies of the zonal mean effective diabatic heating rate (in K day^{-1}) for ERA-i (colored contours) and MLS (black contours).

In both pressure and isentropic coordinates, the effective transport velocities in ERA-i are much larger than those seen in observations, especially in the TTL. This leads to a hypothesis that vertical mixing in ERA-i may be too large either in the numerical sense and/or as a byproduct of discordance between the forecast model and data assimilation.

All models have numerical diffusion and it can be physically thought of as vertical mixing of parcels. In regards to the latter, if more water vapor enters the lower stratosphere in the model than in data assimilation, excessive vertical dispersion and/or excessive exchange between the tropics and midlatitudes is a way to resolve the issue. *Schoeberl et al.* (2003) found this to be true for two data assimilation systems and they used it to explain increased stratospheric transport in a chemical transport model driven by the assimilation. By creating a synthetic tape recorder, we work towards understanding how much mixing plays a role in both the observations and the reanalysis. We then use a model that does not use data assimilation in order to understand its influence.

4.1.2 Horizontal transport

Understanding horizontal transport is more physically appropriate in isentropic coordinates, for reasons discussed above, so we will only show such results here. The calculations were performed on 390 K, a surface within the TTL that possess tight gradients of water vapor that highlight the seasonal cycle more than 380 K or lower. Figure 14 shows the effective horizontal transport for MLS, in which a seasonal cycle can be seen with equatorward speeds maximizing during the northern hemisphere summer and bringing air from about 30°N. The southern hemisphere shows little equatorward horizontal transport.

Compared to the meridional part of the residual circulation, the effective horizontal transport is of similar sign and possess similar seasonality at the equator (*Butchart*, 2014). Specifically, the lag correlation method is able to capture the poleward movement as well as the seasonality of the circulation as it overshoots the equator and bends into the

summer hemisphere before turning poleward towards the winter hemisphere. The latter is most visible during boreal summer while it is less evident during the winter, and this is true for both MLS and ERA-i.

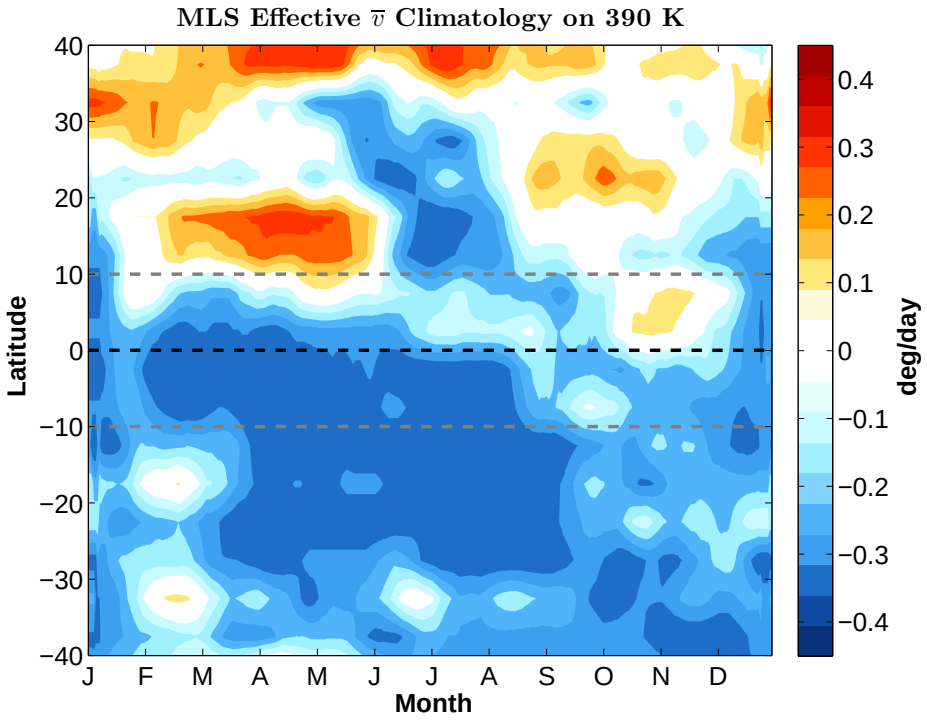

Figure 14: The climatology of the zonal mean effective horizontal velocity (in degree day^{-1}) on the 390 K surface for MLS. The lines mark the equator and tropical boundaries used in this study.

The horizontal transport in ERA-i is 2-3 times larger than those in MLS as seen in Figure 15. However, the seasonal and latitudinal structures are very similar and again this method shows transport originating near 30°N and moving equatorward during the boreal summer. During the winter, there is a strong barrier to mixing in ERA-i that is less apparent in MLS. This can be seen in Figure 15 which shows strong northward transport north of 10°N with apparent absent horizontal transport south of that (as shown by the white contours). MLS shows more available southward transport at this location, and therefore possible mixing, as seen in Figure 14.

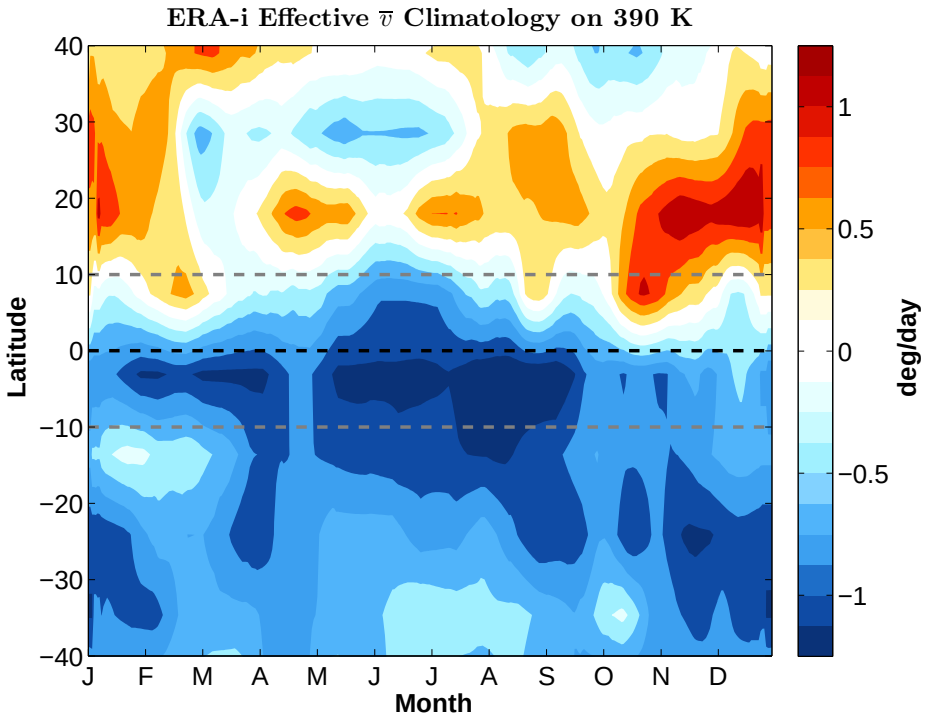

Figure 15: The climatology of the zonal mean effective horizontal velocity (in degree day^{-1}) on the 390 K surface for ERA-i. The lines mark the equator and tropical boundaries used in this study.

The shallow branches of the BDC operate in both the winter and summer hemispheres. This is why ERA-i and MLS generally show poleward motion away from the equator. As

mentioned in Chapter 3, most of the water vapor moves outward from the equator however the maximum water vapor occurs slightly northward of the equator during the boreal summer. From that maximum, it spreads towards both poles and this partially explains why this method calculates southward transport within the northern hemisphere. This is supported by the structure of the BDC during the boreal summer in which it somewhat overshoots the equator before bending towards the south pole.

Flury et al. (2013) performed a similar correlation method using water vapor on 100 hPa. Because we are interested in adiabatic transport which occurs along isentropic surfaces, we chose to focus on the 390 K surface instead. The speed of the meridional transport toward the northern hemisphere found by *Flury et al.* (2013) was twice as fast as what was found in this study. However the speeds of the meridional transport toward the southern hemisphere were found to be nearly identical. The discrepancy with the northern hemisphere could be due to the fact that 100 hPa is at a higher altitude than the 390 K surface in the middle latitudes. Therefore, 100 hPa actually sees a seasonal cycle of water vapor pushed forward in time (e.g., the water vapor maximum is in September instead of July). Our effective horizontal velocity results agree more with *Konopka et al.* (2015) who found the northward and southward transports to be of comparable magnitude when working in isentropic coordinates.

The stronger speeds seen in ERA-i may be interpreted as increased horizontal mixing associated with the extratropical wave forcing. These results suggest that the vertical and horizontal transport in the ERA-i reanalysis may be overestimated. The next results look into understanding the strengths of each transport.

4.2 Summary of transport simulations

This study follows in the footsteps of *Mote et al.* (1998) who solved their simple 1-D transport model for an optimal solution. Here, a parameter sweep is performed where the strengths of the individual transport components are varied such that the best combinations may be discovered. Unlike the original study, this work allows for the transport variables to vary in time. The time-dependence for each transport component is based on past literature (*Rosenlof*, 1995; *Richard et al.*, 2003) and the seasonalities of the effective velocities. Further analysis of the time-dependencies are discussed in Chapter 4.7. Following the parameter sweep, every transport combination is tested on its ability to reproduce the seasonal cycle and annual mean of the tape recorder. First, we discuss the characteristics of the successful (and unsuccessful) transport combinations for each MLS and ERA-i in each coordinate system. The way in which these results were reached are discussed later, in Chapter 4.3 and 4.4.

4.2.1 Optimal solutions

This section discusses the optimal solutions that best replicate the tape recorder. The ways in which these solutions were reached are discussed in the following chapters.

A range of combinations was found to successfully simulate the observed tape recorder in pressure coordinates. Reproducing the amplitude of the seasonal cycle requires at least doubling the strength of vertical mixing, but changing by an order of magnitude was not found necessary. A similar message was seen in the annual mean, with vertical mixing strengthened by a factor of 3-7 resulting in an accurate annual mean. However the strength

of vertical mixing was found to play a small role in shaping the phase of the tape recorder and actually a range of factors were able to produce the correct phase. Therefore, the best combination is not one, but a range where vertical mixing varies and the vertical velocity and horizontal mixing variables remain near their original values. To highlight one possible solution, Figure 16 shows the synthetic model (black contours) that uses the original values of vertical advection and horizontal mixing, with vertical mixing increased by a factor of 4. This figure also shows the synthetic tape recorder created using the strengths prescribed by *Mote et al.* (1998) with the pink dashed contours. Between the pink and colored contours, the phases are relatively similar with height however the amplitudes are much weaker when the original values from *Mote et al.* (1998) are used.

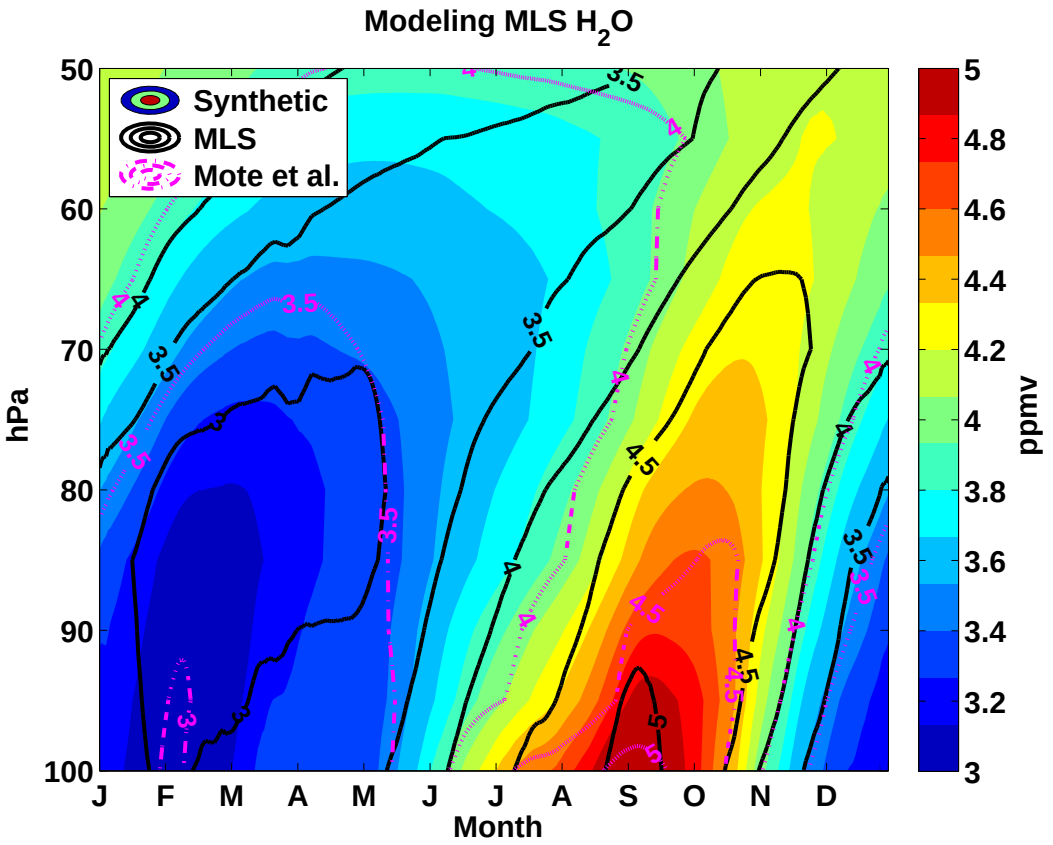

Figure 16: The climatology of one of the best synthetic solutions, $1\overline{\omega}^*$—$4K$—1α, for MLS water vapor in pressure coordinates. The colored contours represent the synthetic tape recorder, the black contours represent the observed MLS tape recorder, and the pink dashed contours represent the synthetic tape recorder using the original values form *Mote et al.* (1998).

Simulating the ERA-i reanalysis in pressure coordinates requires even greater amounts of vertical mixing than seen in observations. Based on all the measurements, vertical mixing is at least an order of magnitude larger than the original values prescribed by *Mote et al.* (1998). The horizontal mixing also needs to at least be tripled, but a swath of factors 3-7 times the original amount are able to replicate different characteristics of the transport. Again, the vertical advection by the residual circulation must remain near its original value. If the residual circulation deviates away from the original amount, strong increases in the both types of mixing are required to compensate for the change. Shown in Figure 17

is the solution that uses the original value of the residual circulation, vertical mixing increased by a factor of 10, and horizontal mixing increased by a factor of 5.

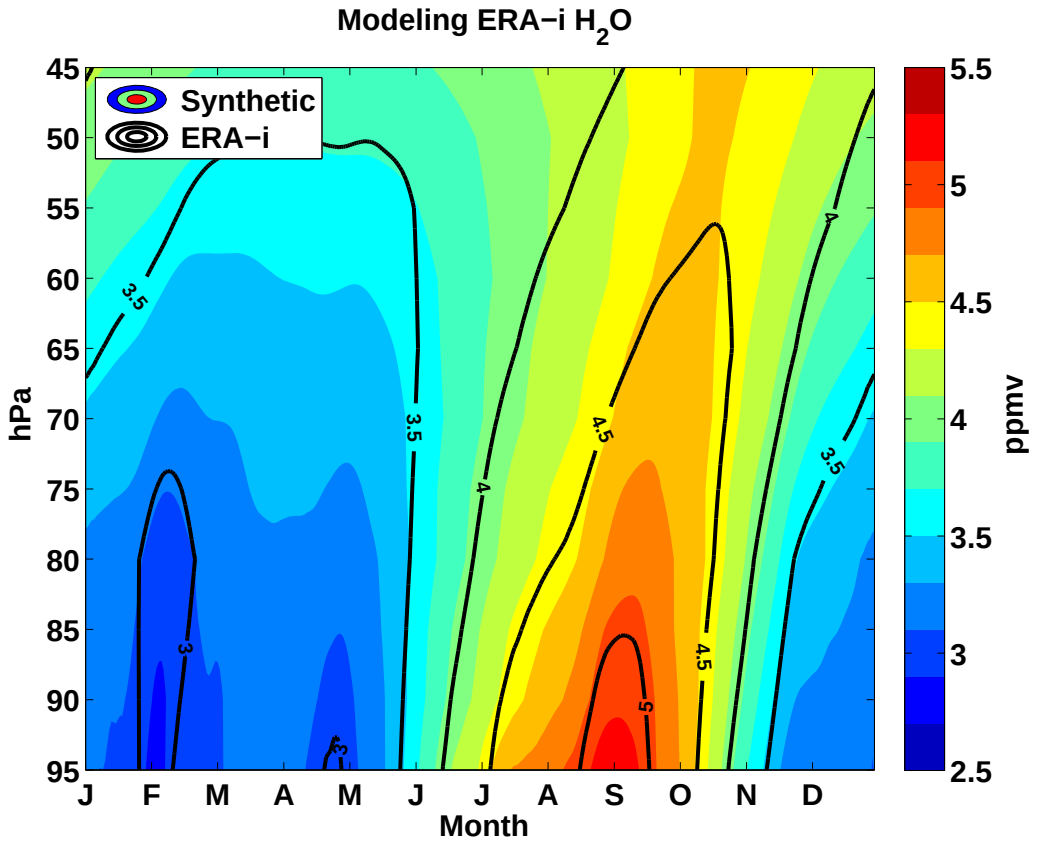

Figure 17: The climatology of one of the best synthetic solutions, $1\overline{\omega}^*$—$10K$—5α, for ERA-i water vapor in pressure coordinates. The colored contours represent the synthetic tape recorder and the black contours represent the ERA-i tape recorder.

A different story emerges when simulating the tape recorder of water vapor in isentropic coordinates. The original values of each transport, translated into isentropic units, are able to reproduce the observed signal. The range of solutions is narrower in these coordinates. Overall the results show that diabatic heating must be 1-3 times its original value; vertical mixing can be a range of values; and horizontal mixing must be close to its original value. Compared to vertical advection and horizontal mixing in the TTL, vertical mixing plays a small role in isentropic coordinates. Vertical mixing acts on the curvature of water vapor,

and within the TTL, this value is relatively small (more discussed below). Shown in Figure 18 is one of the range of solutions that uses the original strength of each transport.

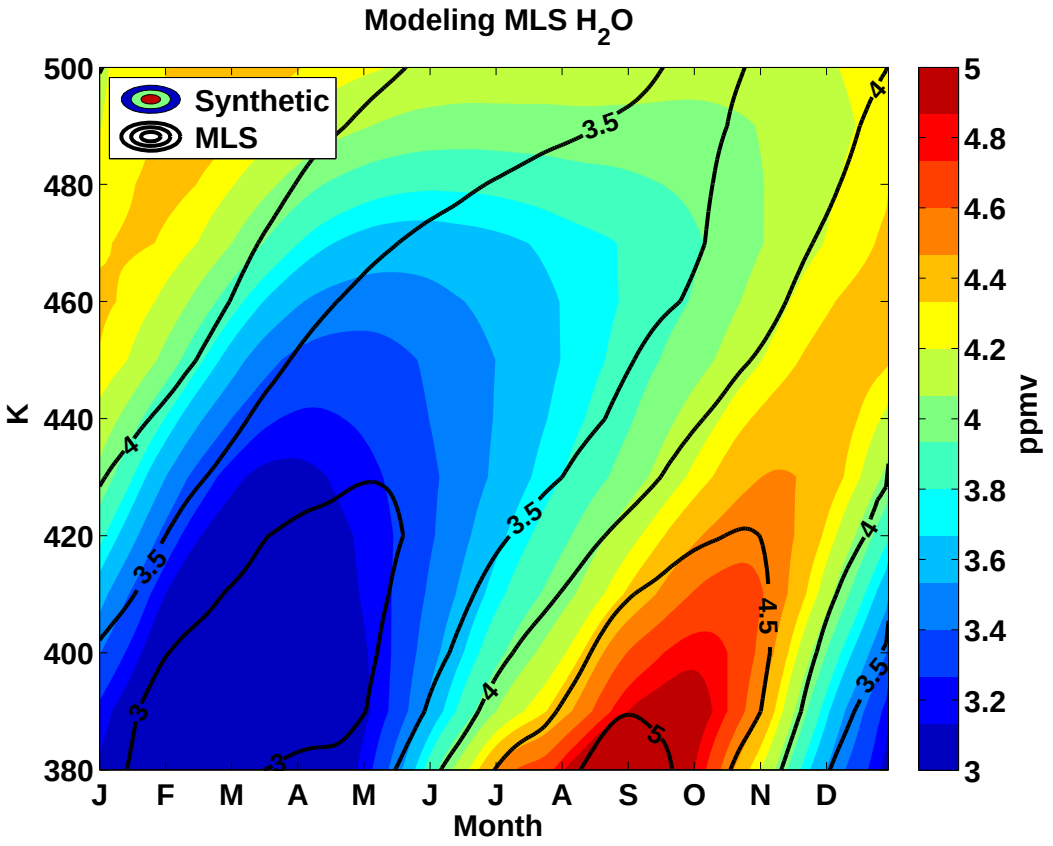

Figure 18: The climatology of one of the best synthetic solutions, $1\overline{Q}$—$1K$—1α, for MLS water vapor in isentropic coordinates. The colored contours represent the synthetic tape recorder and the black contours represent the observed MLS tape recorder.

Simulating the ERA-i tape recorder in isentropic coordinates requires similar strengths of transports, except the heating rate must be increased by a factor of 2-3. The value of horizontal mixing in isentropic coordinates must be around 1-3 times its original value. Again, vertical mixing can take on a range of values because it has small effects on the signal in isentropic coordinates. Shown in Figure 19 is a solution using the combination $3\overline{Q}$—$4K$—2α. There is a relationship between diabatic heating and horizontal mixing similar to that in MLS observations, but overall the diabatic heating must be increased by about three times its original amount.

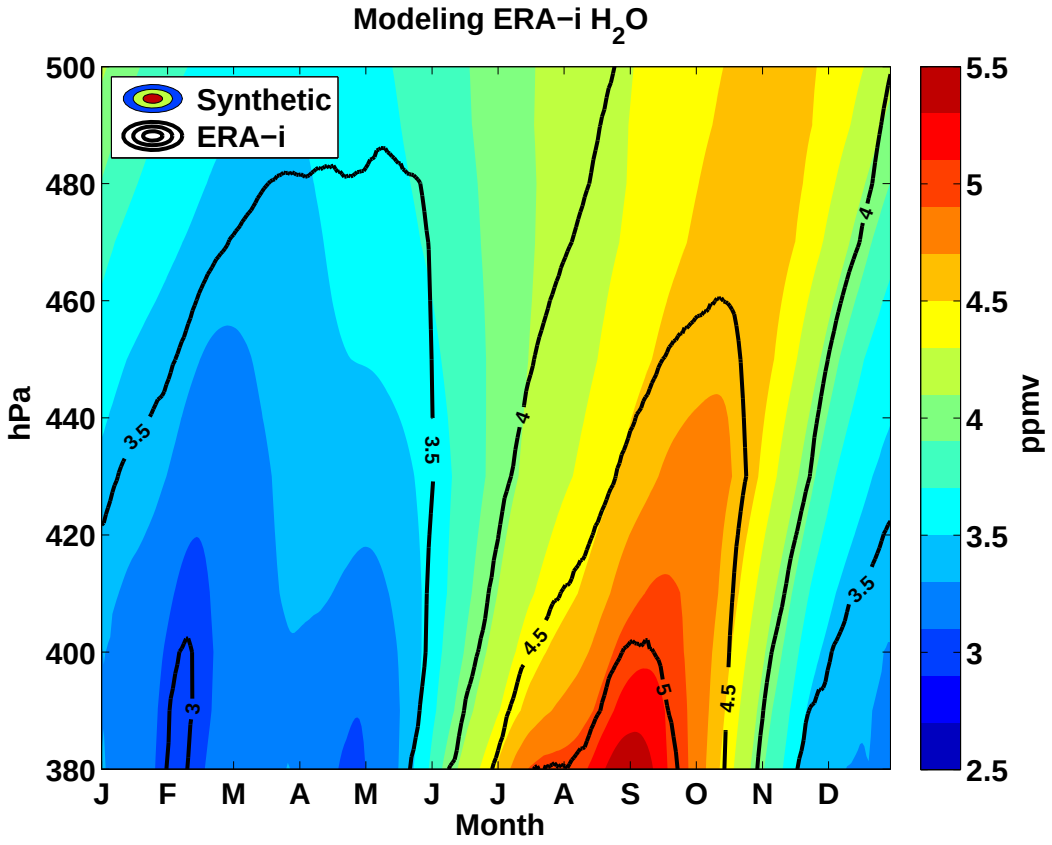

Figure 19: The climatology of one of the best synthetic solutions, $3\overline{Q}$—$4K$—2α, for ERA-i water vapor in isentropic coordinates. The colored contours represent the synthetic tape recorder and the black contours represent the ERA-i tape recorder.

4.2.2 Upper bounds of transports

It is important to understand how much of one transport is needed in order to simulate the tape recorder signal on its own (without any other transports). This is done simply by "turning off" the other two transports and increasing the strength of the remaining transport until it best simulates the phase and amplitude of the seasonal cycle as well as the annual mean water vapor at each level within the TTL and the lower stratosphere.

It is possible to simulate the observed tape recorder using only individual terms while turning off the others. Simulating MLS observations in pressure coordinates requires the transport to be three times its original value. Running the simple model with only vertical mixing at play requires it to be over twenty times its original value. With only horizontal mixing, the tape recorder signal cannot be replicated, even when the transport is strengthened beyond realistic values. In isentropic coordinates, the upper bound for vertical mixing occurs at much smaller strengths; it must be five times its original value. Diabatic heating must be near three times its original value again.

Nearly fifty times the original value of vertical mixing is required to simulate ERA-i data in pressure coordinates. Vertical advection must be increased by a factor of ten in order to accurately model amplitude and phase. Again, horizontal mixing can never replicate the tape recorder on its own. Modeling the ERA-i signal in isentropic coordinates requires less vertical mixing, qualitatively similar to MLS. Nearly ten times the original value of vertical mixing is required to simulate ERA-i in isentropic coordinates. The take-away point is that vertical advection and mixing can successfully produce tape recorders on their own. The strength the vertical advection needed to replicate the tape

recorder does not change much between coordinates, however the strength of vertical mixing changes by an order of magnitude depending on the coordinate system.

4.2.3 Combinations with large error

Important insights can also be gained when the setup produces large error. When simulating MLS observations in pressure coordinates, the signal's amplitude decreases by 50% when vertical velocity is increased to compensate for reduced horizontal or vertical mixing. This coincided with the synthetic tape recorder leading the observed one. The opposite occurred when vertical velocity was decreased when either horizontal or vertical mixing were overly strong. In such case, water vapor was overestimated by 75% and the synthetic signal lagged behind observations.

These results tell us that the dynamics are more complicated than they are simple. If mixing in a model is too weak, amplifying the residual circulation will not solve the problem. Instead it will lead to less water vapor in the stratosphere. On the other hand, if mixing in a model is too strong and vertical velocity is mistakenly lowered, even more water vapor is allowed to pass into the stratosphere. Strong mixing in either direction plays a large role in increasing stratospheric water vapor. Together, their roles are nearly as large as the residual circulation when looking at the top of the TTL (80 hPa).

When the observed tape recorder is simulated in isentropic coordinates, we see that it takes very large vertical mixing ($K > 20$) before the diabatic heating rate is overwhelmed and the amplitude is overestimated. On the other hand, if weak diabatic heating is compensated with increased horizontal mixing, this actually leads to underestimation of amplitude and annual mean water vapor values. This latter result is opposite from what

was seen in pressure coordinates. In the case where horizontal mixing is weak and diabatic heating is increased to attempt a balance, this leads to overestimation of the annual mean. Again, this result opposes those observed in the pressure framework. Similar to the pressure coordinate results, the synthetic tape recorder will lead the phase of the observed tape recorder when Q was increased to compensate for a weak strength of K. Qualitatively similar relationships were seen in simulations of the ERA-i reanalysis.

4.3 Simulating MLS observations

In order to discover the range of solutions, this study calculated amplitude ratio, phase lag, and percent difference in the annual mean between the synthetic and actual tape recorders of water vapor. For ease of the reader, we show plots where two of the transports are varied in strength and the third is held at the original value. The comparisons were calculated for each level, however the plots shown here focus near the base (80 hPa or 400 K) of the tape recorder where multiscale dynamics are involved.

4.3.1 The annual mean

Figure 20 shows the percent difference in the annual mean at 80 hPa for various strengths of each transport. For example, panel (a) varies the strengths of vertical mixing (K) and horizontal mixing (α) while the vertical advection ($\overline{\omega}^*$) is held constant at the original value. Therefore the original transport combination found by *Mote et al.* (1998), which are $1\overline{\omega}^*$—$1K$—1α, can be seen in every plot. It is important to note that the white contours in Figure 20 correspond to a synthetic annual mean that matches observations within $\pm 1\%$. Warm contours indicate overestimation and cool contours indicate

underestimation. In the upper-right corner of panel (c), the synthetic model becomes numerically unstable because the vertical velocities are too large for the timestep. This numerical instability can also be seen in the other plots below.

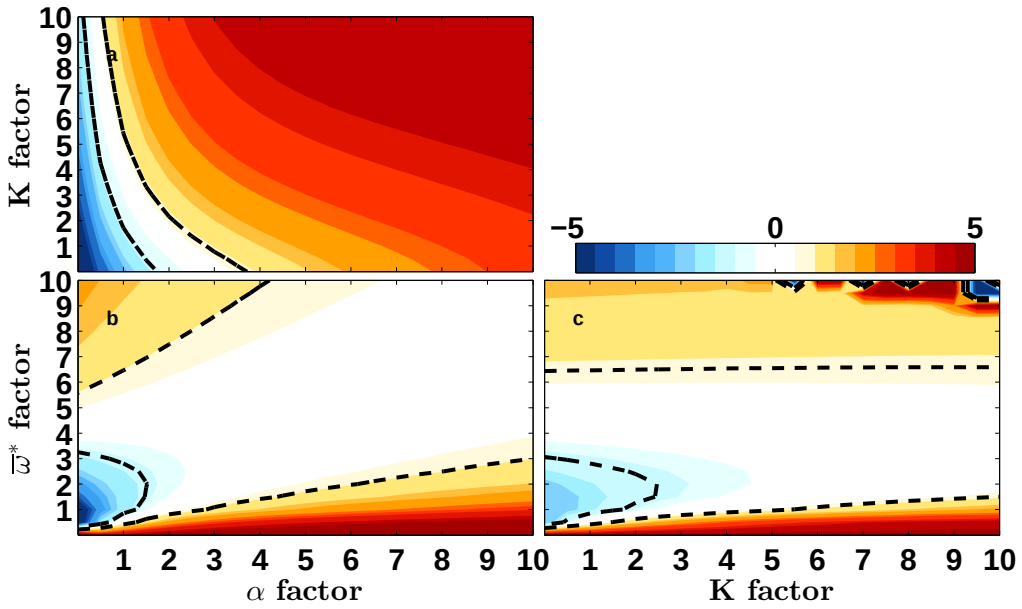

Figure 20: The annual mean difference (%) between the synthetic and observed tape recorders at 80 hPa for varying combinations of strengths. In each subplot, there are two independent variables that are allowed to vary while the third (invisible) one remains constant at the original value prescribed by *Mote et al.* (1998). The dotted lines indicate ±1%.

Figure 20 shows that a range of transport strengths can reproduce the annual mean water vapor at 80 hPa, however the original strengths underestimate the annual mean by 2-3%. A range of vertical mixing strengths appear to work well. In panel (b), vertical mixing is held at its original value and we notice that this setup has little restraint on α or $\overline{\omega}^*$. The only real constraint that the annual mean requires is upon the horizontal mixing, which needs to be near its original value because if it's too large, then less K is required and that leads to underestimation in panel (c). From the upper bound results, we know that vertical advection is able to produce a tape recorder without any mixing as long as the

transport is strengthened to 3 times its original value. This tells us that anything above that is probably unrealistic and we can focus below that factor in panels (b) and (c). It's necessary to look at the other measures to minimize the range of K and $\overline{\omega}^*$.

Overall the annual mean difference tells us much about relationships between the three transports. If vertical mixing is too weak (near its original value), it will not benefit the model if vertical advection and horizontal mixing are strengthened equally. And since they are tied to one another through Rossby wave breaking, this may not be an obvious result. In fact, the idealistic model finds that strengthening horizontal mixing over the residual circulation will compensate for any weakness in vertical mixing. If horizontal mixing is increased too much, this can result annual mean overestimation of water vapor near 5% which is associated with an increase in cold point temperature of about 1 K. If the original values of each transport are used, the associated cold point temperature would be decreased by about 0.5 K.

In isentropic coordinates, the annual mean is decided by a considerably smaller range of combinations. Figure 21 shows the results similar to Figure 20 but modeled in potential temperature coordinates. The only panel that looks the same as before is panel (a) where we see that horizontal mixing is strongly constricted near or below its original strength, depending on the corresponding strength of vertical mixing. Interestingly, all plots show that the annual mean is more likely to be overestimated in these coordinates, rather than underestimated. Panels (b) and (c) show that vertical advection and vertical mixing are strongly constrained near their original values. It is important to highlight that changing the K factor in panel (c) leads to only small increases in the annual mean. However panel (b) shows that changing α can lead to large changes in the mean, up to 10% which is associated with a 2 K increase in temperature at the cold point.

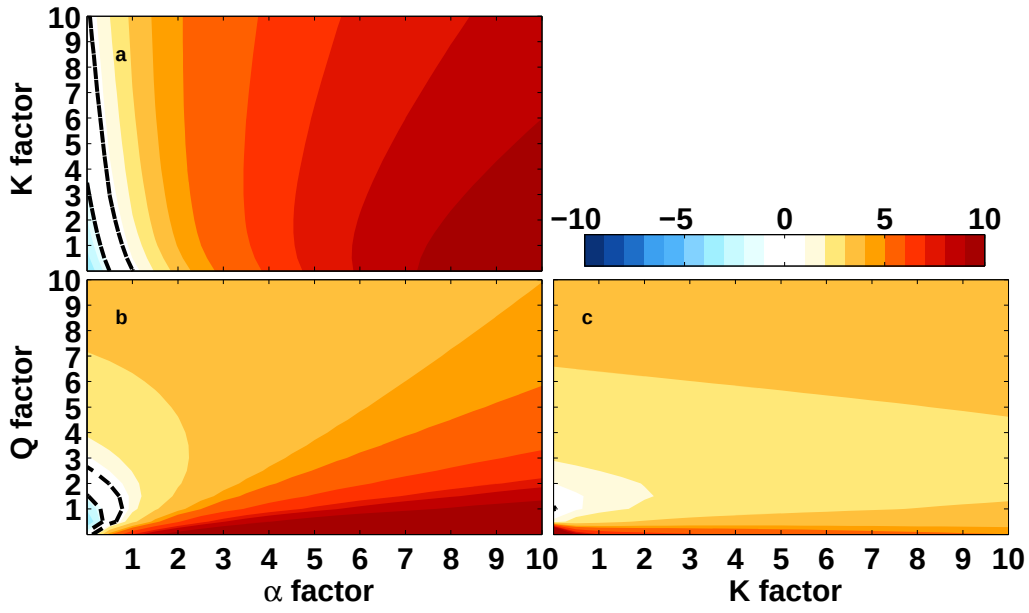

Figure 21: The annual mean difference (%) between the synthetic and observed tape recorders at 400 K for varying combinations of strengths. In each subplot, there are two independent variables that are allowed to vary while the third (invisible) one remains constant at the original value prescribed by *Mote et al.* (1998). The dotted lines indicate ±1%.

4.3.2 The seasonal cycle

In order to narrow the range of transport strengths for the vertical advection and vertical mixing, properties of the seasonal cycle are explored. Figure 22 shows the phase lag (in days) where warm (cool) colors correspond with the synthetic tape recorder leading (lagging) the observations. Again, panel (c) shows numerical instability in the upper-right corner for reasons discussed above. As with the annual mean measurement, this measurement also shows that vertical mixing plays a somewhat small role. When the vertical advection and horizontal mixing are at their original values, however, vertical mixing should be nearly 4-5 times its original strength in order to reproduce the phase at 80 hPa. Again we see that horizontal mixing needs to be near its original value in panel (a). Looking at panel (b) is not completely appropriate because the annual mean measurements and panel (c) show that increased K is required. Nonetheless, panel (b) shows that underestimations in K can be compensated with a combination of vertical advection and horizontal mixing. However, using the original values for each transport results in the tape recorder lagging observations by about 2 weeks. Panel (c) in this figure shows that vertical advection needs to be 1-2 times its original value.

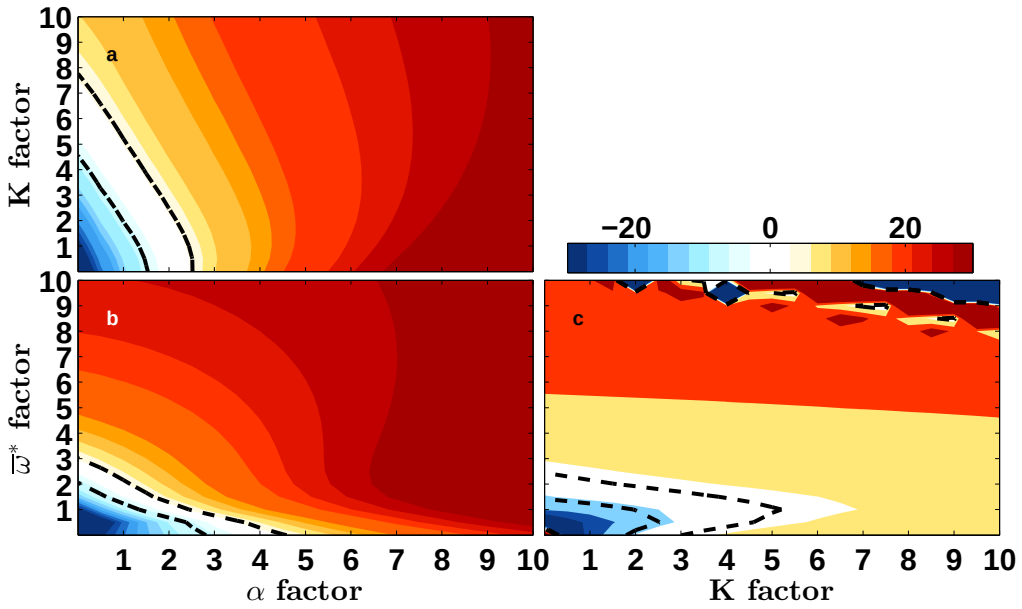

Figure 22: The phase lag (days) between the synthetic and observed tape recorders at 80 hPa for varying combinations of strengths. In each subplot, there are two independent variables that are allowed to vary while the third (invisible) one remains constant at the original value prescribed by *Mote et al.* (1998). The dotted lines indicate ±5 days.

Figure 23 shows the phase difference at 400 K and it looks very similar to the annual mean results in Figure 21. Again, we see that each transport is constrained near their original strengths. If horizontal mixing or vertical advection are too large, the synthetic tape recorder will lead the observations (warm contours) by up to one month. If vertical mixing is strengthened, the phase will not change by much, but may cause the synthetic results to lead by about 10 days. This result strengthens the findings in Figure 21.

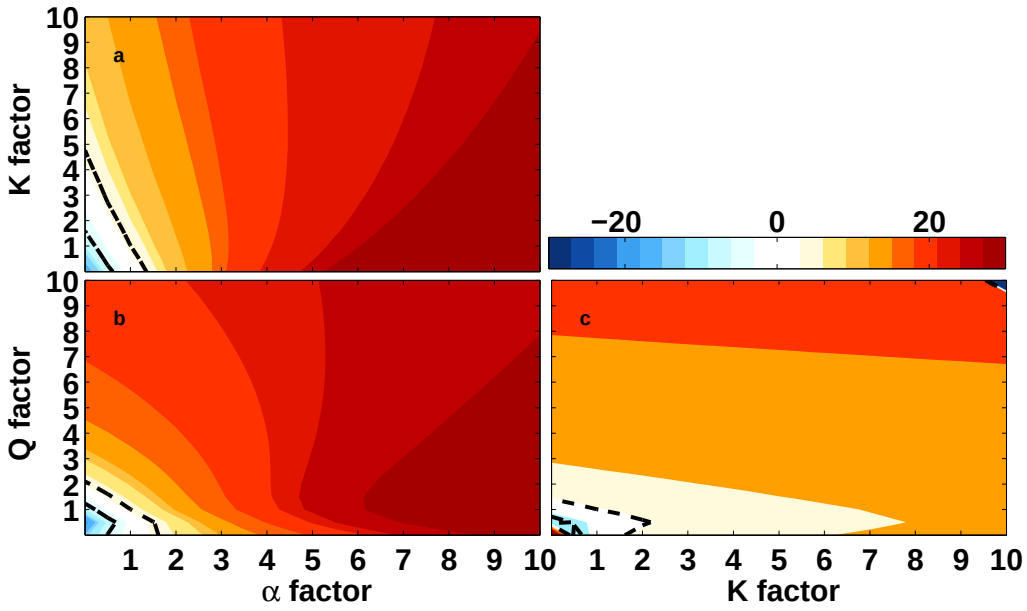

Figure 23: The phase lag (days) between the synthetic and observed tape recorders at 400 K for varying combinations of strengths. In each subplot, there are two independent variables that are allowed to vary while the third (invisible) one remains constant at the original value prescribed by *Mote et al.* (1998). The dotted lines indicate ±5 days.

The amplitude ratio is a ratio between the synthetic and real amplitudes where values greater than one correspond to the synthetic tape recorder having a larger amplitude and vice versa. Figure 25 shows this measurement at 80 hPa where yellow contours represent successful modeling, cool colors represent underestimated amplitude, and warm colors represent overestimated amplitude. Panel (a) again shows that if horizontal mixing is near its original value then vertical mixing must be increased by a factor of 4. If horizontal mixing is increased, the vertical mixing must also increase. From the phase and annual mean, however, we know that increased horizontal mixing is not beneficial. Panel (b) shows that horizontal mixing and vertical advection do not act independently of each other, a result also found by *Garny et al.* (2014). Taking into account previous results that α must remain near its original value, we again conclude that $\overline{\omega}^*$ should be about 1-2 times greater

than its original value assuming K is held constant. As with the earlier measurements on 80 hPa, panel (b) is less appropriate since it holds vertical mixing constant at its original value (and we know we need at least a doubling). However, it is important to note the range of combinations in this panel that show a quasi-linear relationship between vertical advection and horizontal transport. Panel (c) again shows a range of vertical mixing is appropriate, and it reinforces the range of $\overline{\omega}^*$.

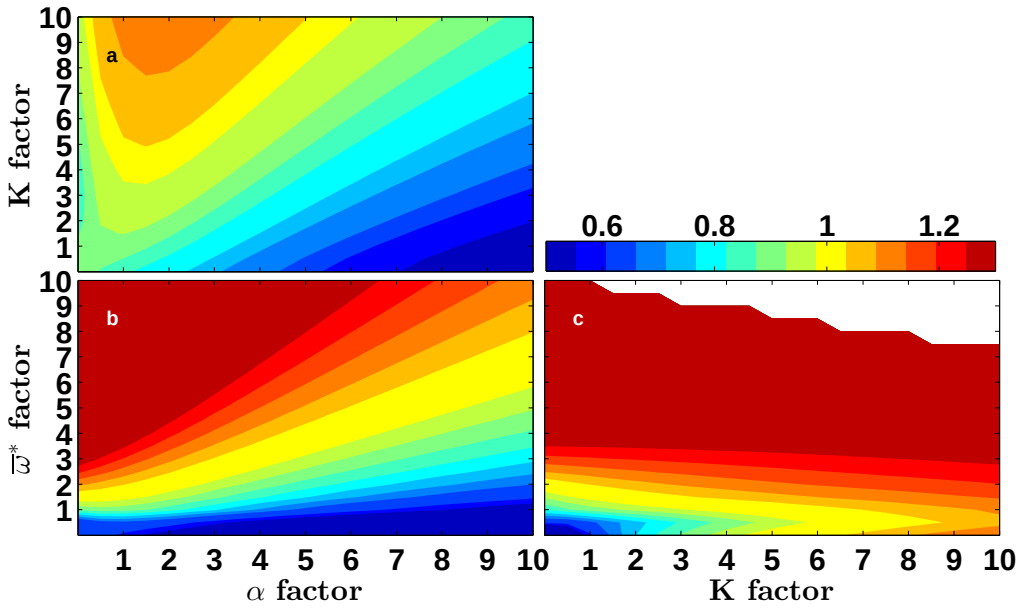

Figure 24: The amplitude ratio (ppmv/ppmv) between the synthetic and observed tape recorders at 80 hPa for varying combinations of strengths. In each subplot, there are two independent variables that are allowed to vary while the third (invisible) one remains constant at the original value prescribed by *Mote et al.* (1998).

Figure 25 shows the amplitude ratio results at 400 K. Unlike the results on pressure coordinates, vertical mixing is less constricted by this measurement. The reasoning behind its ambiguity is due to its small role in deciding the overall time tendency of the signal in isentropic coordinates (see Chapter 4.6 for further discussion). The best overall amplitude can be seen when diabatic heating is 1-2 times greater than its original value (as seen in

panels (b) and (c)). Overall this measurement agrees with earlier results in isentropic coordinates. Although it accepts a range of K strengths, we know from the annual mean and phase lag measurements that the original strength works best. Most notable is that the amplitude can be easily overestimated in isentropic coordinates except in the case of increased horizontal mixing which results in underestimation.

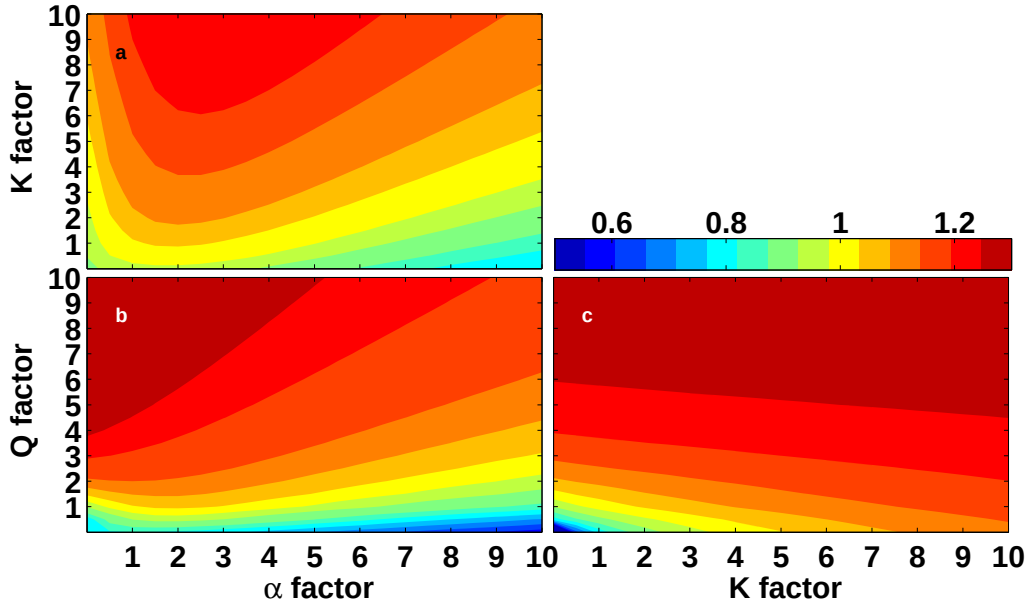

Figure 25: The amplitude ratio (ppmv/ppmv) between the synthetic and observed tape recorders at 400 K for varying combinations of strengths. In each subplot, there are two independent variables that are allowed to vary while the third (invisible) one remains constant at the original value prescribed by *Mote et al.* (1998).

4.3.3 Summary

A range of solutions exists for the idealistic transport model in pressure coordinates while the solutions are more constrained in isentropic coordinates. In both coordinate systems, the original strength of the vertical advection (diabatic heating rate) is sufficient when taking into account all measurements. The pressure framework shows that a relationship exists between vertical and horizontal mixing, but overall a larger K is more

desired across all measurements (especially the amplitude ratio). Interestingly, the phase is largely independent of the vertical mixing in pressure coordinates but this mixing type is strongly constrained near 1-2 times its original value in isentropic coordinates. In pressure coordinates, vertical mixing influences the amount of water vapor at a given level but not the speed at which the water vapor moves. In isentropic coordinates, vertical mixing has less influence on the water vapor amount and instead diabatic heating and horizontal mixing becomes more important to the amplitude. These measurements led us to use $1\overline{\omega}^*$—$4K$—1α for pressure coordinates and $1\overline{\omega}^*$—$1K$—1α for isentropic coordinates when highlighting results in Chapter 4.2 above.

In order to show all three measures together, we introduce a score (out of 100%) that depends on vertical mixing K and a new term G which can be described as the effects of subtropical wave breaking which include horizontal mixing and vertical advection. As mentioned earlier, those two terms are not independent of each other (*Garny et al.*, 2014) and often panels (a) and (c) look similar because they compare K with a wave-driven dynamic (horizontal mixing or vertical advection). The score calculation is

$$score = \frac{100}{1 + \frac{|A_s - A_r|}{|A_r|} + \frac{|\phi_s - \phi_r|}{|\phi_r|} + \frac{|q_s - q_r|}{|q_r|}} \tag{2}$$

where A is the amplitude, ϕ is the phase, and q is the water vapor mixing ratio. The s and r subscripts refer to the synthetic and real tape recorders, respectively. This score is calculated for each panel, and panels (a) and (c) are averaged such that the final plot shows the score for combinations of K and G. The value of G always denotes the strength of vertical advection. In many cases, the optimal solution requires equal strengths of

vertical advection and horizontal mixing. For cases in which $\overline{\omega}^*$ and α are not of equal strength, we interpolate the scores associated with α (panel a) onto the corresponding range for scores associated with $\overline{\omega}^*$ (panel c) such that the relationship is implicit, and we again average these two panels. For example, if the optimal solution requires three times more horizontal mixing than vertical advection, then G=1 corresponds to $\overline{\omega}^*$=1 and α=3 while G=2 corresponds to $\overline{\omega}^*$=2 and α=6 and so on. A star is plotted signifying the optimal solution discussed in Chapter 4.2.1

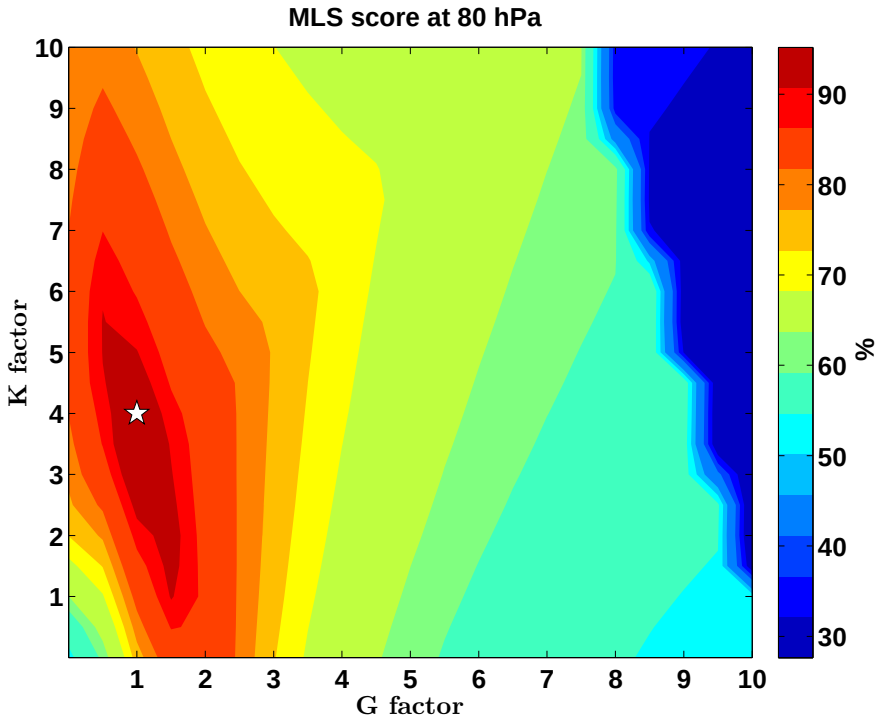

Figure 26: The score (%) of the synthetic MLS tape recorder at 80 hPa for varying combinations of K and G.

Figure 26 shows the score for the synthetic tape recorder at 80 hPa. The optimal solution we showcased in Chapter 4.2.1 is marked with the white star. It is very apparent that there is not one optimal solution and instead a range of successful combinations exist. Using the original combination prescribed by *Mote et al.* (1998) would result in a 85%

score. The dark red represents scores at and above 97%. In isentropic coordinates, the range of optimal solutions is smaller, however the original *Mote et al.* (1998) combination now resides in the successful area as shown by the white star in Figure 27. In both figures, there is a range of successful scores that encompasses many strengths of K.

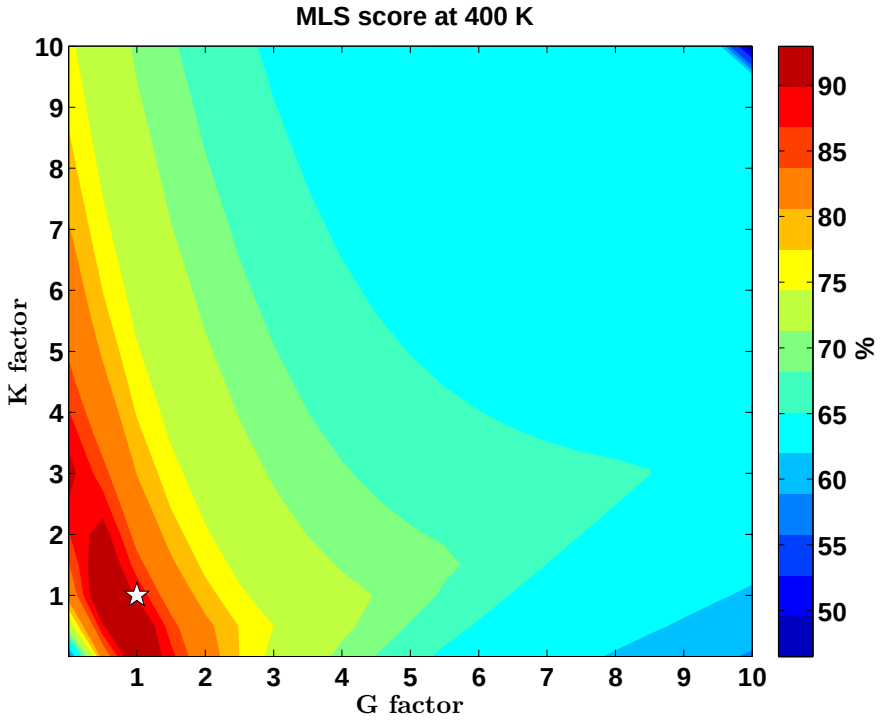

Figure 27: The score (%) of the synthetic MLS tape recorder at 400 K for varying combinations of K and G.

4.4 Simulating the ERA-i reanalysis

This section discusses how we reached the range of optimal solutions for simulating the ERA-i tape recorder in pressure and isentropic coordinates. As mentioned earlier, much more vertical mixing was required along with increased horizontal mixing. As above, we discuss the results in the seasonal cycle and annual mean.

4.4.1 The annual mean

Similar to MLS observations, Figure 28 shows that reproducing the annual mean in ERA-i at 80 hPa requires a relationship between the two types of mixing. Panel (a) shows that a larger K or a larger α is necessary. However, both transports need to be strengthened above their original values. Panel (b) and (c) highlight the drastic increases necessary to horizontal and vertical mixing when vertical advection is increased by just small amounts. When the strength of vertical advection is doubled, it underestimates the annual mean value of water vapor unless the mixing transports are increased. Even when considering the annual mean, Figure 28 shows that mixing transports cannot be neglected, a finding also supported by *Flannaghan and Fueglistaler* (2014). Using the original strengths by *Mote et al.* (1998) to simulate ERA-i in pressure coordinates would result in a 5% underestimation in the annual mean or a 0.25 ppmv underestimation which would be associated with at 1 K change in the cold point temperature.

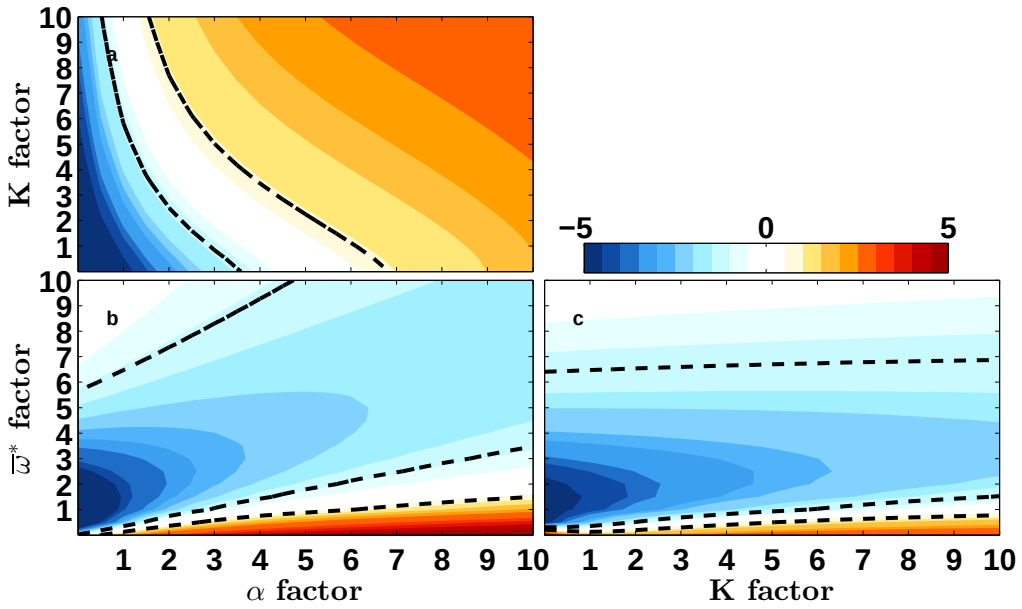

Figure 28: The annual mean difference (%) between the synthetic and ERA-i tape recorders at 80 hPa for varying combinations of strengths. In each subplot, there are two independent variables that are allowed to vary while the third (invisible) one remains constant at the original value prescribed by *Mote et al.* (1998). The dotted lines indicate ±1%.

Figure 29 shows the annual mean difference (%) at 400 K. This figure is useful for understanding relationships between the transports in isentropic coordinates, but it is important to note that the optimal solution shown in Section 4.2.1 used $3Q$—$4K$—2α so none of the panels would be appropriate for that solution. Nonetheless, a range of solutions were able to reproduce the annual mean in ERA-i at 400 K and some can be discussed within this figure. It may not become obvious why we chose the solution $3Q$—$4K$—2α until seeing later results concerning the seasonal cycle.

Panel (a) shows that α is strongly constricted about its original strength. Knowing this, panel (b) then shows a small range of Q values that satisfy the α constraint. Generally, this shows that the diabatic heating rate must be somewhere between 2-5 times stronger than normal. Panel (c) shows a range of vertical mixing strengths satisfy the results from

panels (a) and (b), but the strength should not exceed by an order of magnitude, unlike the results in pressure coordinates. An interesting result is visible in panels (b) and (c) showing that the annual mean can be successfully simulated with nearly nonexistent diabatic heating but some combination of horizontal and vertical mixing. This region of high accuracy is extremely small and unlikely to exist, yet is important to note. Although the next measurements will show that vertical mixing plays a small role, in the annual mean, it can work with horizontal mixing to simulate the water vapor values. If horizontal mixing is too strong, it can lead to an annual mean difference of 0.5 ppmv or a 2 K change in cold point temperature.

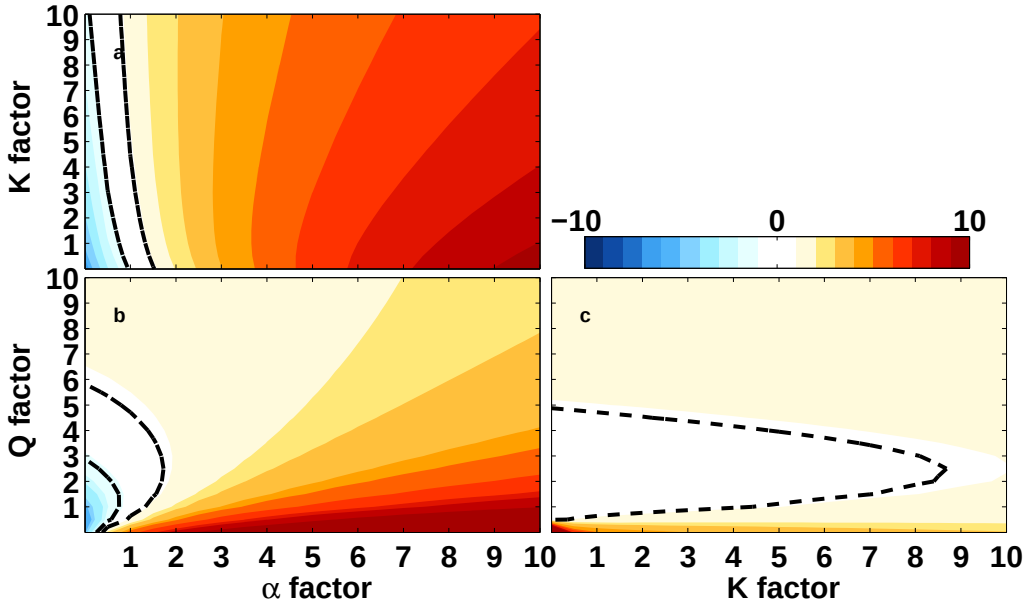

Figure 29: The annual mean difference (%) between the synthetic and ERA-i tape recorders at 400 K for varying combinations of strengths. In each subplot, there are two independent variables that are allowed to vary while the third (invisible) one remains constant at the original value prescribed by *Mote et al.* (1998). The dotted lines indicate ±1%.

4.4.2 The seasonal cycle

Vertical mixing in pressure coordinates is not constrained by the phase as shown in Figure 30 in panels (a) and (c). However, panel (a) shows that the range of solutions is wider when vertical mixing is increased beyond 5 times its original amount. If the original strengths of each transport are used, the phase of the synthetic tape recorder lags by at least one month by only 20 hPa above the tape head. Panel (b) in Figure 30 is not physically appropriate because we know from the annual mean measurement that increased vertical mixing is necessary. Nonetheless panel (b) shows that increasing $\overline{\omega}^*$ leads to a wider range of solutions than increasing α as far as the phase is concerned. Panel (c) is similar to panel (b) in being less appropriate for analyses since the annual mean required increased α and this panel has α fixed at its original strength. With that in mind, panel (c) tells us that if horizontal mixing is underestimated, then $\overline{\omega}^*$ must be increased beyond the upper bound for MLS but perhaps realistic strengths for ERA-i. Overall, a large range of combinations exist if the phase of the tape recorder is the only focus. We continue to narrow the range by looking at the amplitude below.

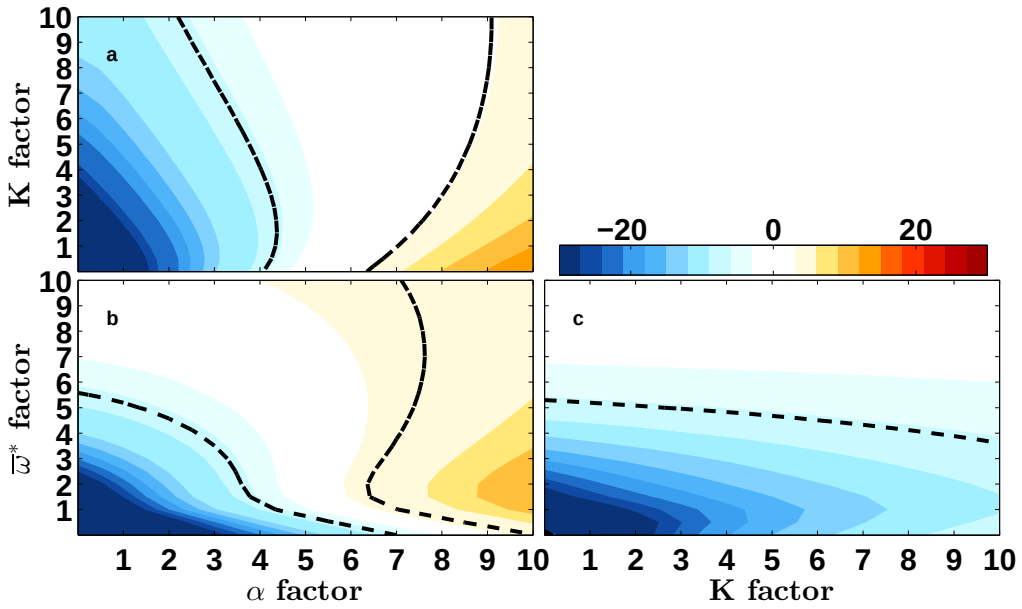

Figure 30: The phase lag (days) between the synthetic and ERA-i tape recorders at 80 hPa for varying combinations of strengths. In each subplot, there are two independent variables that are allowed to vary while the third (invisible) one remains constant at the original value prescribed by *Mote et al.* (1998). The dotted lines indicate ±5 days.

Measuring the phase lag at 400 K, Figure 31 shows that a narrower range of solutions exist. Panel (a) holds Q constant at its original value, however it shows that α is again restricted. This panel shows that horizontal mixing should be 1-3 times stronger than normal and it also shows that vertical mixing can take on a range of values. Panel (b) is more appropriate than the other panels because K is largely unrestricted by these measurements. This panel highlights the importance of increasing Q and α beyond their normal strengths. The range is widest when Q is increased by a factor of 3 and α is increased by a factor of 1-3. Panel (c) shows that vertical mixing can again take on a range of values, but a lag of about 5 days will be seen for the successful range of Q. This panel would be improved and show zero lag if α was held constant at a higher strength. Overall, Figure 31 highlights the importance of increasing both the vertical advection and horizontal mixing as far as the phase is concerned.

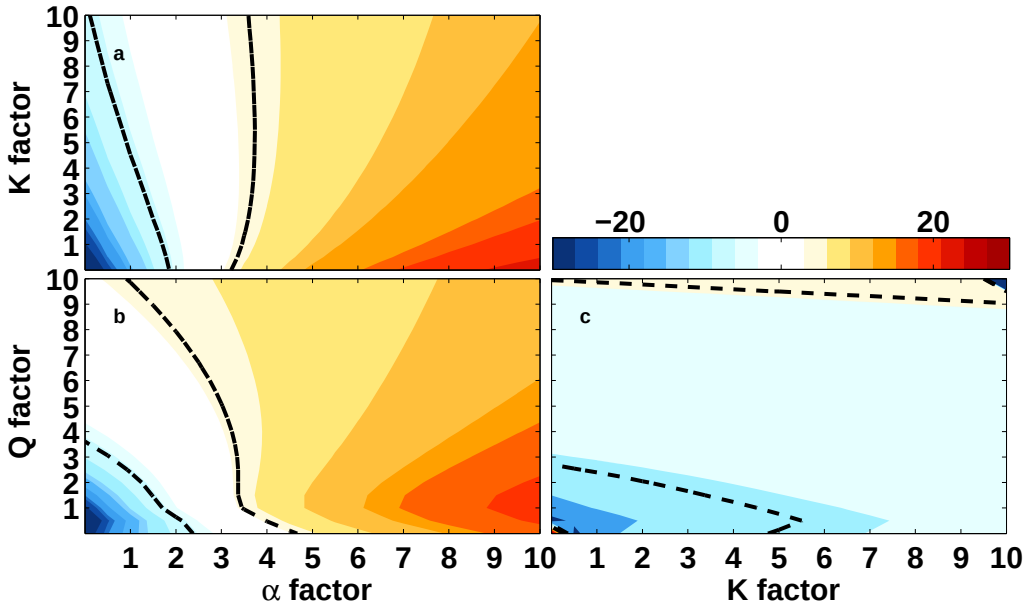

Figure 31: The phase lag (days) between the synthetic and ERA-i tape recorders at 400 K for varying combinations of strengths. In each subplot, there are two independent variables that are allowed to vary while the third (invisible) one remains constant at the original value prescribed by *Mote et al.* (1998). The dotted lines indicate ±5 days.

The amplitude ratio at 80 hPa, shown in Figure 32, helps to narrow the range of solutions. This figure looks very similar to Figure 25 which shows the amplitude ratio for the MLS results however it is much harder to reach a good ratio for the same range of strengths in ERA-i. Panel (a) shows that vertical mixing must be increased by an order of magnitude while horizontal mixing must be increased by a factor between 1-5 for in order to simulate the correct amplitude (warm contours). Panel (b) is not appropriate since it uses a value of K that is far too small. However, panel (b) does show the strengths needed to compensate for small vertical mixing. In that case, the vertical advection should be increased by at least a factor of 3 in order to simulate 80% of the amplitude. Panel (b) shows a range of solutions is possible in that situation. Panel (c) is somewhat unphysical since the previous measurements required increased α and this panel holds α constant at a small value. Nonetheless this panel shows warm contours bend down after K is increased by a factor of 5 such that $\overline{\omega}^*$ may remain near its original strength which is included in the solution ranges in panel (b) of Figures 28 and 30.

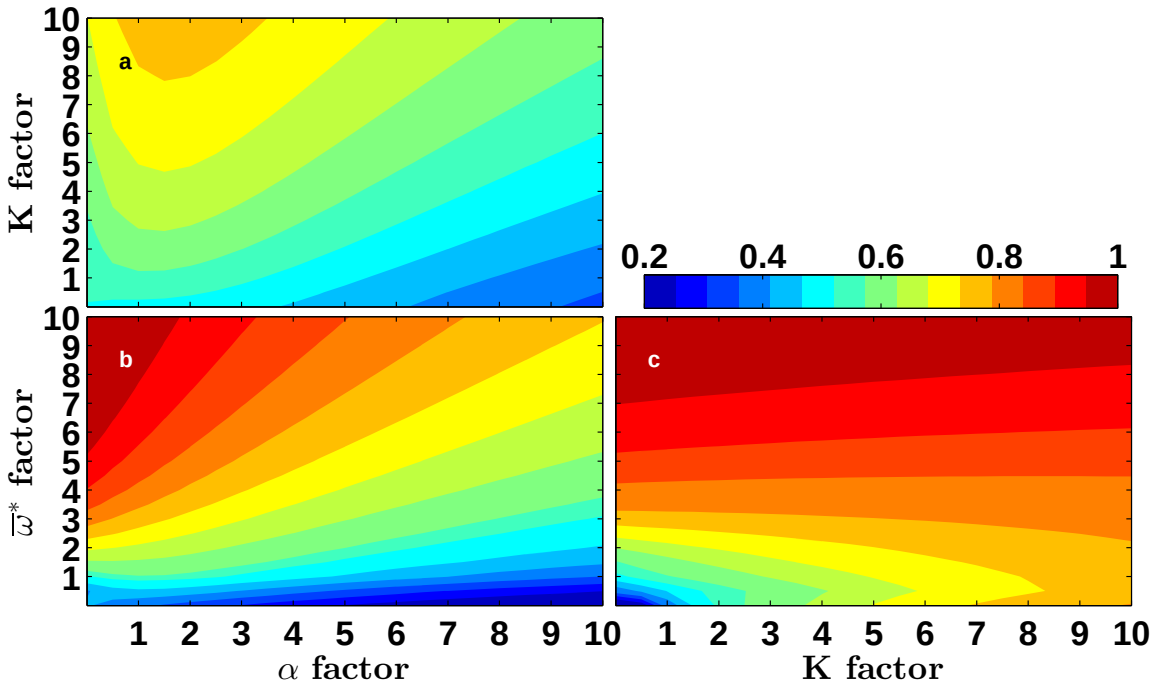

Figure 32: The amplitude ratio (ppmv/ppmv) between the synthetic and ERA-i tape recorders at 80 hPa for varying combinations of strengths. In each subplot, there are two independent variables that are allowed to vary while the third (invisible) one remains constant at the original value prescribed by *Mote et al.* (1998).

Unlike in pressure coordinates, any value of vertical mixing is able to simulate the water vapor in isentropic coordinates as shown in panel (c) of Figure 33. Replicating the amplitude is more reliant on having diabatic heating strengthened to at least three times its original value as seen in panels (b) and (c). The smaller the diabatic heating, the larger vertical mixing must be to force more water vapor through 400 K. As for the horizontal mixing, it must be between 1-3 times larger than its original value to reproduce the signal. Panel (b) shows that increasing horizontal mixing will not benefit weak diabatic heating. In fact, increasing horizontal mixing when the diabatic heating is weak will only decrease the amplitude. Such a situation is unlikely since the two transports are not independent of each other (*Garny et al.*, 2014). Overall this measurement shows that Q and α must be

increased, but K can take on a range of values. If K remains at its original strength, as in panel (b), a range of combinations exists in the other transports and they will satisfy the amplitude.

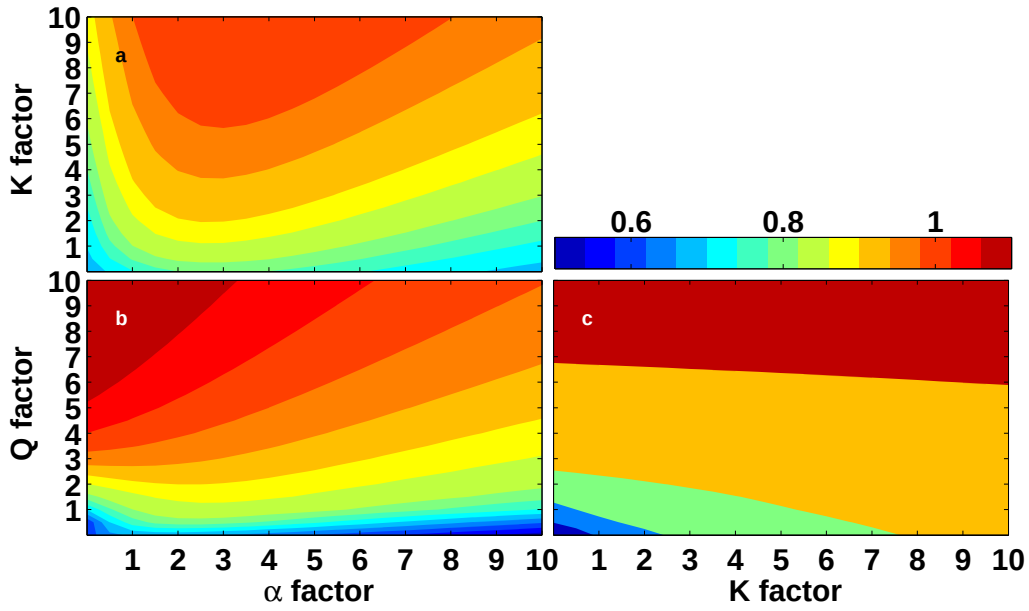

Figure 33: The amplitude ratio (ppmv/ppmv) between the synthetic and ERA-i tape recorders at 400 K for varying combinations of strengths. In each subplot, there are two independent variables that are allowed to vary while the third (invisible) one remains constant at the original value prescribed by *Mote et al.* (1998).

4.4.3 Summary

ERA-i has more vertical and horizontal mixing than MLS. It is interesting that increasing the vertical advection is unhelpful to the annual mean and phase. Overall there are a range of solutions possible in each measure, but we are able to narrow them by aggregating the results. The strength of vertical mixing should be increased by a factor of 7-12 while horizontal mixing should be increased by a factor of 2-6. In all measures, the vertical advection should remain at its original strength unless one or both of the mixing types are weak. Vertical mixing needed in ERA-i could exist as a result of data assimilation

(*Schoeberl et al.*, 2003) or it could exist for numerical reasons. Less of this diffusion is required in isentropic coordinates and instead diabatic heating plays a larger role.

Oddly, both the phase and amplitude of the tape recorder are mostly independent of vertical mixing when in isentropic coordinates. Because this type of mixing provides little change to the total water vapor tendency in isentropic coordinates, almost any strength of it will work. Nevertheless, based on the other transports, it appears that a value of vertical mixing near 4 times its original amount is especially sufficient. Horizontal mixing must be near its original amount; we used a factor of 2 in Chapter 4.2.1. Most notably, the diabatic heating must be increased (by at least a factor of 3) in order to simulate the tape recorder in this framework. This is most likely because of a reason stated earlier: the longwave cloud radiative heating rates above 200 hPa are larger in ERA-i compared to observations and other reanalyses (*Wright and Fueglistaler*, 2013). This could be attributed to large amounts of thin cirrus which have the ability to block longwave from escaping to space (*Yang et al.*, 2010).

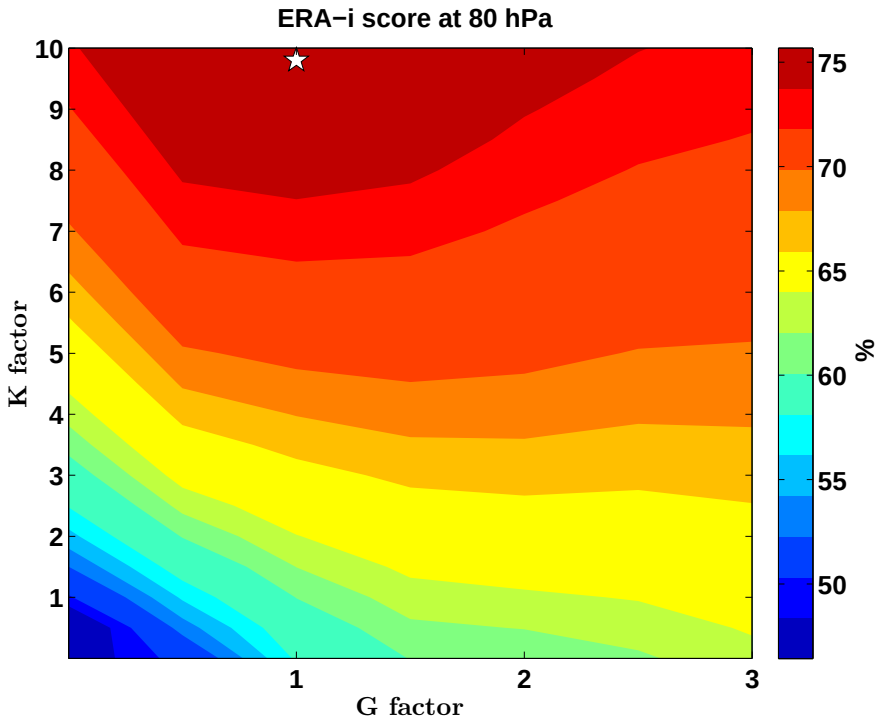

Figure 34: The score (%) of the synthetic ERA-i tape recorder at 80 hPa for varying combinations of K and G.

The range of high scores is somewhat wider for ERA-i than MLS, however they are not as high in percentage. Figure 34 shows the scores in for 80 hPa and the star is located at K=10 and G=1 where the latter represents the vertical advection at its original strength and horizontal mixing strengthened to three times its original value in order to match the optimal solution discussed in Chapter 4.2.1. The G axis stops at a factor of 3 because any higher than that would require α to be increased beyond a factor of 10 (corresponding with the relationship just discussed). Figure 35 shows the range of scores in isentropic coordinates and this looks different from the earlier figure as large G factors are no longer viable. Instead, a wide range of K strengths are able to reproduce the isentropic tape recorder at low strengths of G, but increasing horizontal mixing or the diabatic heating by too much can result in lower scores. Note that in this plot, there is a relationship between

vertical advection and horizontal mixing which is imbedded in G. The optimal solution we chose was $3Q$—$4K$—2α therefore G=3 corresponds with Q=3 and α=2 and the overall relationship is $\frac{2}{3}\alpha = Q$.

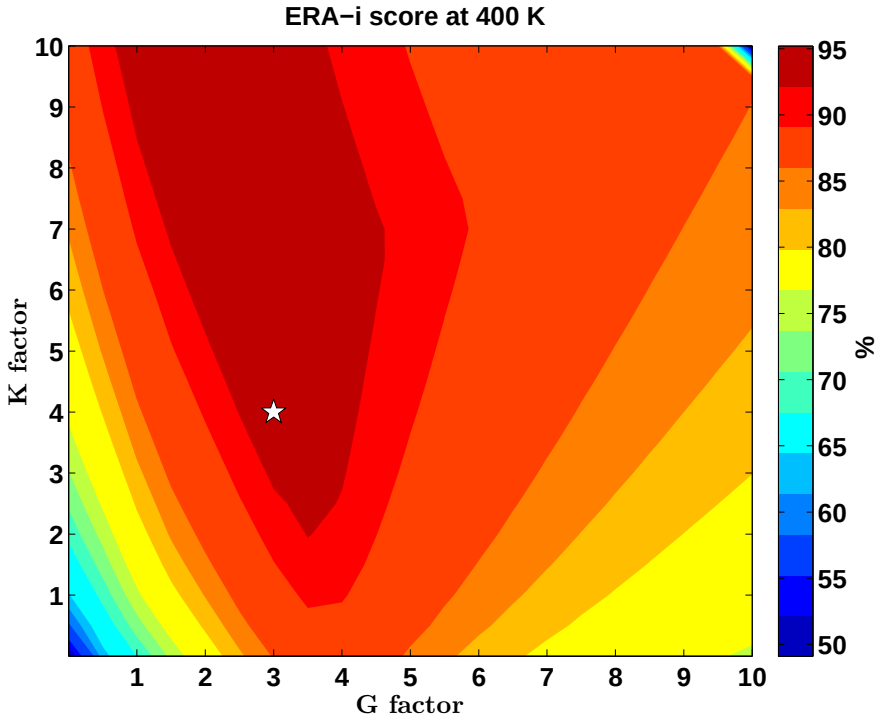

Figure 35: The score (%) of the synthetic ERA-i tape recorder at 400 K for varying combinations of K and G.

4.5 Transports in the GEOS CCM

Transport in the GEOS CCM is useful for studying because it has shares characteristics with the ERA-i tape recorder of water vapor and because it does not use data assimilation. The tape recorder implies that GEOS CCM transport is faster than observations in the lower stratosphere (*Eyring et al.*, 2010) however it matches well in the middle stratosphere. This former point is useful because ERA-i has shown similar traits. A strong barrier to horizontal mixing was identified in GEOSCCM by *Eyring et al.* (2010) and will be

important to keep in mind since our previous results showed increased horizontal exchange in ERA-i.

The fast transport is very evident between 80 and 100 hPa in Figure 36 where almost each part of the signal takes less than a month to move across a 20 hPa depth. This is very similar to the lower stratosphere transport in ERA-i shown in Figure 5.

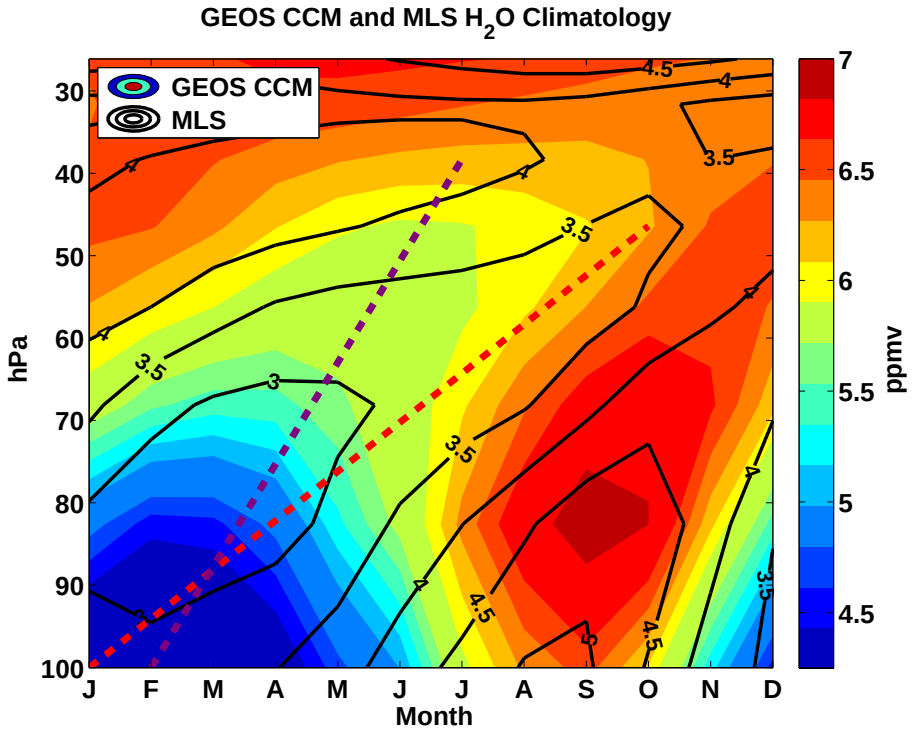

Figure 36: The climatological mean water vapor (ppmv) tape recorder of GEOS CCM (colored contours) and MLS (black contours) where the purple line connects two dry minima for GEOSCCM and the red line connects the dry minima for MLS.

4.5.1 Effective vertical transport

The effective vertical transport calculated for GEOS CCM is shown in Figure 37. The previous Figure 36 shows that there is small seasonality in the vertical speed at 80 hPa; the dry and moist parts of the signal (in the lower stratosphere) appear to ascend at very similar rates. This is unlike the seasonality evident in MLS and ERA-i. Figure 37 supports

this suspicion and only a small seasonal cycle is seen near 90 hPa with faster transport during the boreal winter. Overall, the resulting speeds are stronger than those seen in MLS (black contours), agreeing with *Eyring et al.* (2010), and they are weaker than those seen in ERA-i. Interestingly, this method is able to pick up the fast transport of the dry signal in May between the 70 and 50 hPa.

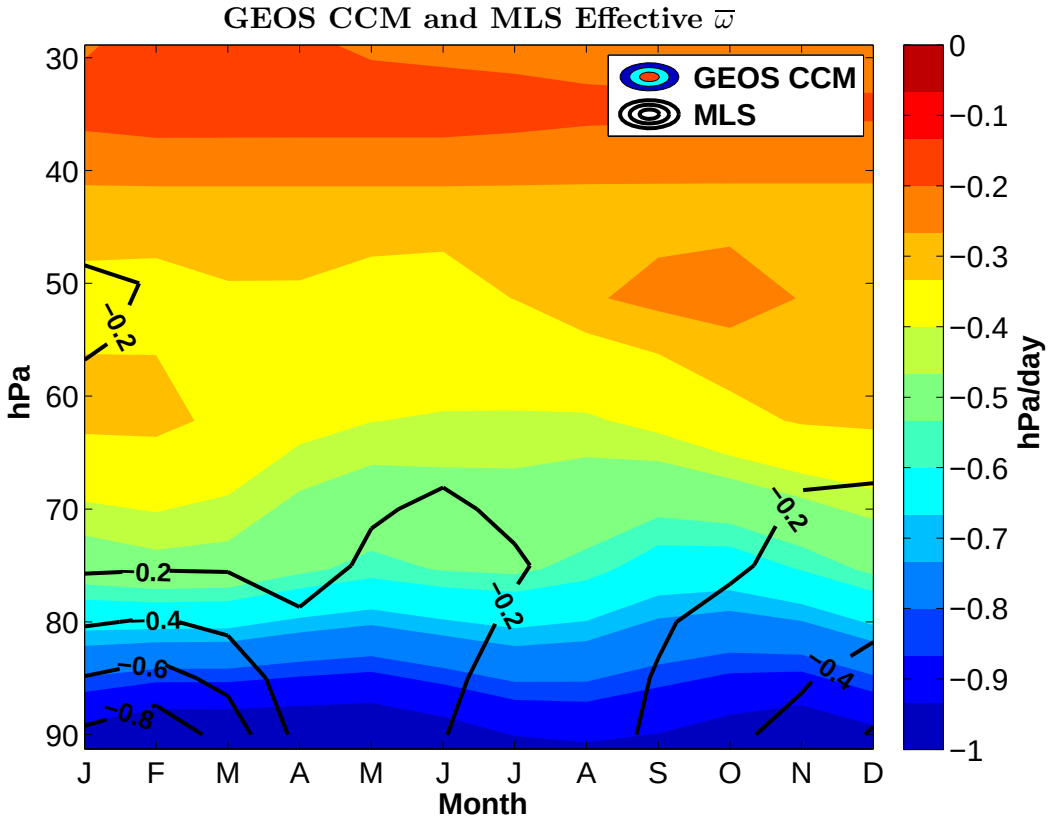

Figure 37: The climatology of effective vertical velocity (in hPa day^{-1}) for GEOS CCM (colored contours) and MLS (black contours).

4.5.2 Simulations

The idealized model was also used to simulate GEOS CCM. Here we show the simulation, the annual mean and phase measurements, and we discuss the amplitude results. Overall, each measurement agrees that increased vertical advection is of great importance when simulating the tape recorder.

The synthetic tape recorder in GEOS CCM is more sloped with height than observations, as shown earlier. Figure 38 shows the tape recorder up to the middle stratosphere. The black contours represent the actual GEOS CCM water vapor and the colored contours represent the synthetic results. In order to match most measures, the vertical advection was strongly increased. It was strengthened by a factor of 4 in this figure while vertical and horizontal mixing were also strengthened however their roles were more minor as we will see below.

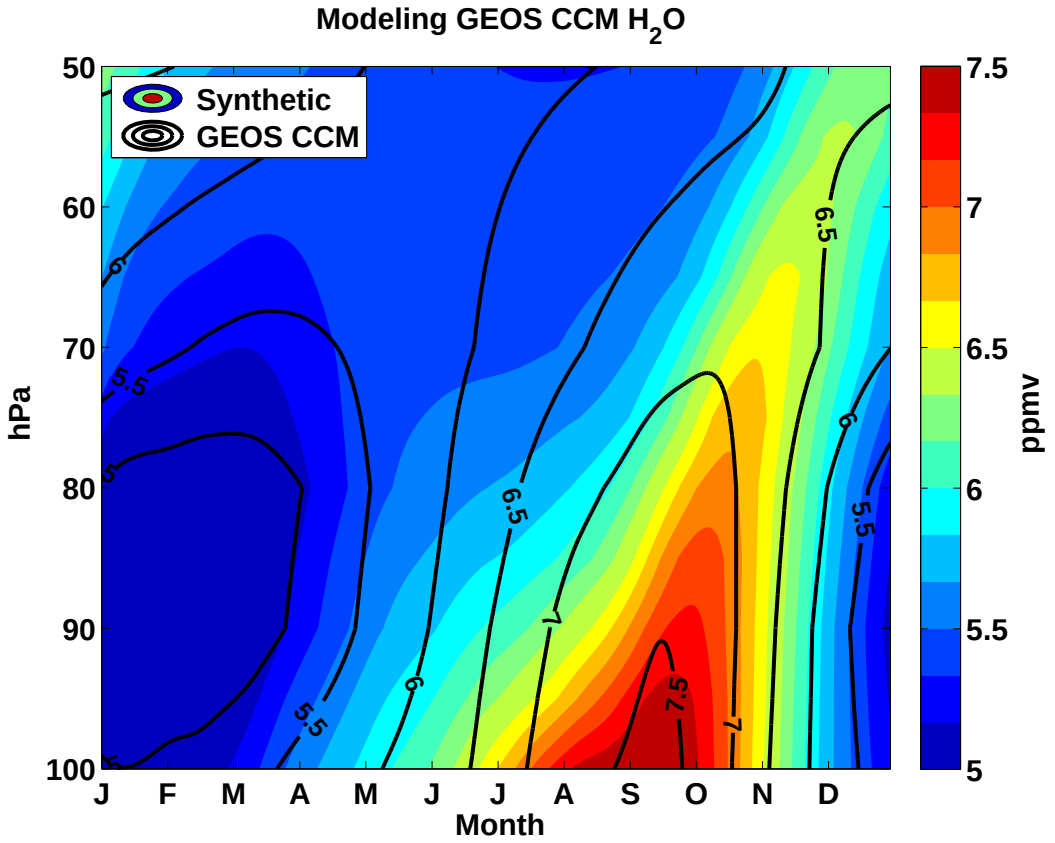

Figure 38: The climatology of one of the best synthetic solutions, $4\overline{\omega}^*$—$3K$—5α, for GEOS CCM water vapor in pressure coordinates. The colored contours represent the synthetic tape recorder and the black contours represent the GEOS CCM tape recorder.

Figure 39 shows that the original combination of variables leads to underestimation of the annual mean by 10% or a cold point temperature change of 2 K. Panel (a) shows a very small range of solutions where α is strongly constricted at 1/3 of its strength while K can assume a range of values. Panel (b) is very important because it again shows some dependence between the vertical advection and horizontal mixing. The range of solutions becomes wide after $\overline{\omega}^*$ is increased by a factor of 3 and horizontal mixing is increased by a factor of 2. The last panel shows again that K is unconstrained, but it also shows that vertical advection must be doubled. Looking closely at panel (c) shows that increasing vertical advection requires small increases in the vertical mixing and that is why we used increased vertical mixing in the simulation shown earlier.

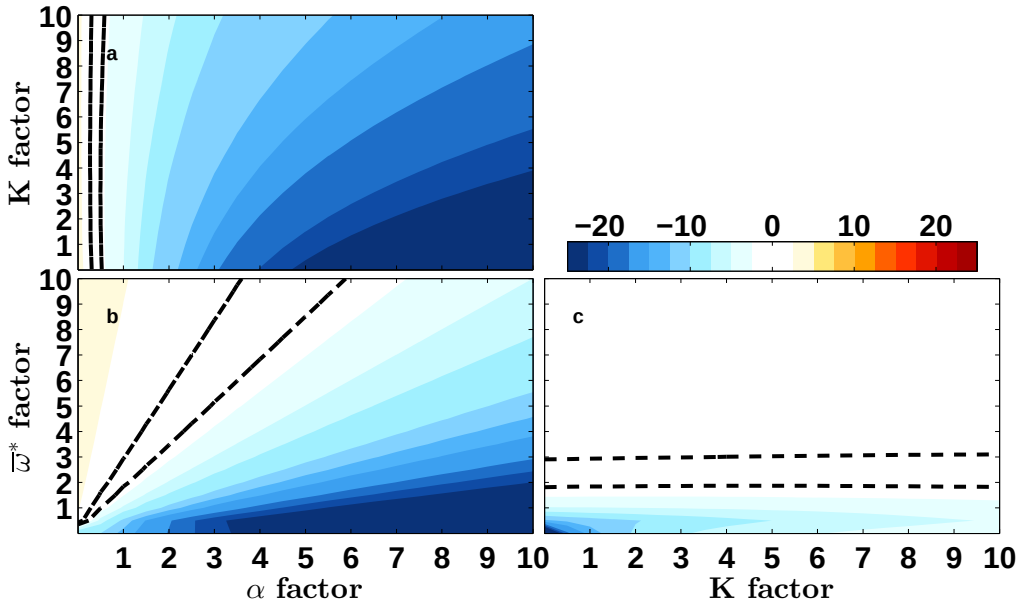

Figure 39: The annual mean difference (%) between the synthetic and GEOS CCM tape recorders at 80 hPa for varying combinations of strengths. In each subplot, there are two independent variables that are allowed to vary while the third (invisible) one remains constant at the original value prescribed by *Mote et al.* (1998). The dotted lines indicate ±1%.

Panels (b) and (c) in Figure 40 show the phase lag results for the simulation, and they look similar to panel (c) in the previous figure. Instead of K being the only free variable, now α is also uninhibited as far as the phase lag is concerned. From these panels, we see that vertical advection must be 2 to 6 times stronger than the values found by *Mote et al.* (1998). Panel (a) represents the case in which vertical advection is too weak and both types of mixing must be strongly increased to keep in phase with the actual tape recorder at 80 hPa. However, this would largely disagree with panel (a) in Figure 39 which showed that increasing both mixing types would result in a large underestimation of the annual mean (associated with a 4 K temperature change to the cold point).

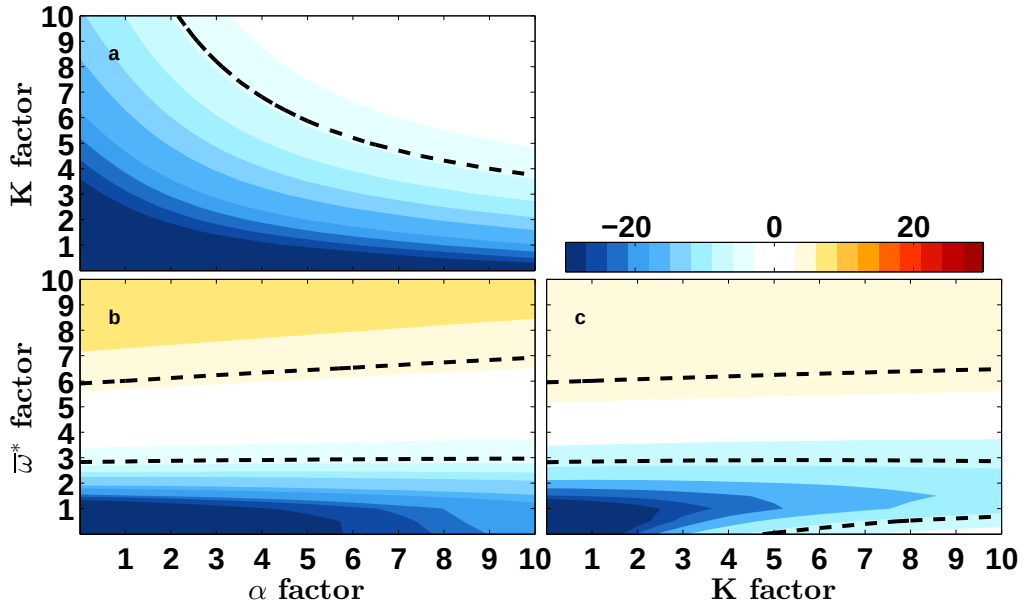

Figure 40: The phase lag (days) between the synthetic and GEOS CCM tape recorders at 80 hPa for varying combinations of strengths. In each subplot, there are two independent variables that are allowed to vary while the third (invisible) one remains constant at the original value prescribed by *Mote et al.* (1998). The dotted lines indicate ±5 days.

The amplitude ratio (not shown here) reiterated the results above; it required the vertical advection to be strengthened by at least a factor of 3. Unlike with the phase

results, increasing both mixing types in the presence of weak vertical advection resulted in a poor tape recorder where the amplitude was underestimated by 60 to 80%. With vertical advection strengthened, vertical mixing was found to play a small role in changing the amplitude further. Increasing horizontal mixing in the same situation, however, led to decreases in the amplitude because it caused the tape recorder to dry. Again, we notice that increases to vertical mixing results in a wider range of vertical mixing factors to choose from.

4.5.3 Summary

Overall, the range of solutions for GEOS CCM is very small after taking into account each measurement. Only the vertical advection needs strengthening. Strengthening vertical mixing would not cause problems, however doing so with horizontal mixing would lead to issues in the annual mean and amplitude (but not the phase).

Knowing that GEOS CCM does not rely on any observations, the results here hint that ERA-i may have strong vertical diffusion because of its data assimilation. This does not mean that ERA-i is clear of numerical diffusion; it could be a combination of both. It is interesting that GEOS CCM can take on a range of vertical mixing strengths without causing a change in the output, but this may be because the change in water vapor concentration with height in GEOSCCM is smaller than that in ERA-i (and MLS). Perhaps the gradient that K works on is too small. It is more likely that vertical mixing (at these strengths) is not enough to carry the signal in GEOSCCM and the vertical advection is left to do the work.

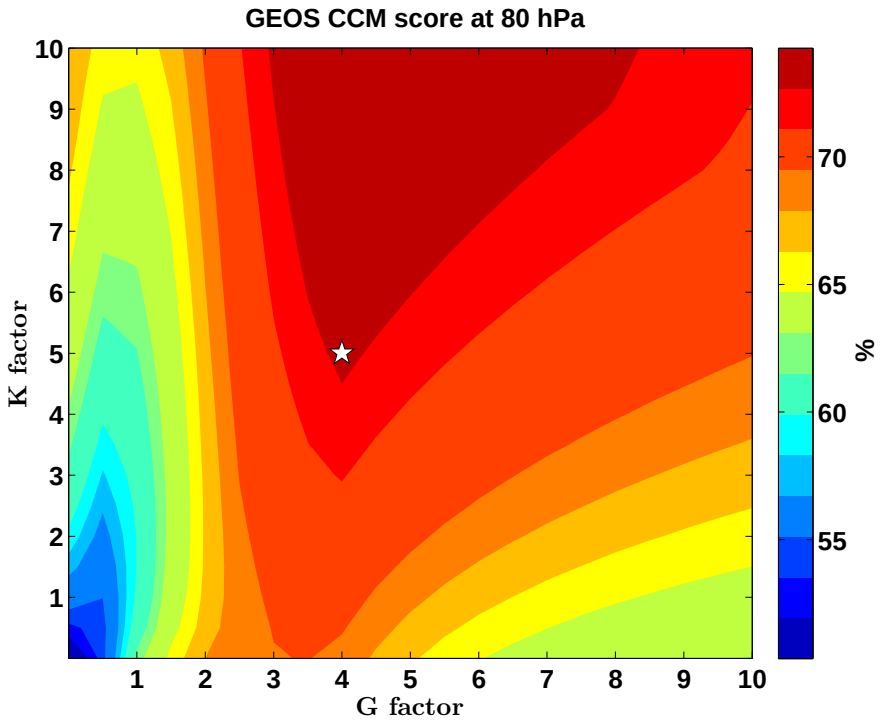

Figure 41: The score (%) between the synthetic and GEOS CCM tape recorders at 80 hPa for varying combinations of K and G.

Figure 41 shows that a range of high scores also exist for GEOS CCM in pressure coordinates. This range is different from that seen in ERA-i (Figure 34) as now G is strongly constrained about 4 times its original value. For a good simulation, 4 times the vertical advection and 3 times the horizontal mixing was used. Overall, GEOS CCM has vertical mixing comparable to that seen in observations, but it is much less than that seen in ERA-i. This supports the argument that diffusion by data assimilation may be important in ERA-i.

4.6 Water vapor tendencies

This chapter investigates changes in water vapor due to the individual transports at 80 hPa and 400K. The strengths used for the transports are based on the optimal solutions

discussed in Chapter 4.2.1. These results are carried out for simulations of the observations and the reanalysis. To further study the influence of the transports, calculations of the variance explained are carried out.

4.6.1 MLS observations

Figure 42 shows that vertical advection (red) and vertical mixing (blue) play equally important roles in forming the tape recorder at 80 hPa (during boreal winter) in MLS observations whereas horizontal mixing (green) plays a small role. The vertical mixing plays a large role in decreasing the water vapor from the fall into the winter. During the summer, vertical mixing plays an extremely large role in carrying the signal from the tape head to 80 hPa. Vertical mixing also adds water vapor to the dry part of the signal from winter to spring. During the late spring and summer, horizontal mixing plays a small yet non-trivial role at increasing the water vapor amplitude at 80 hPa.

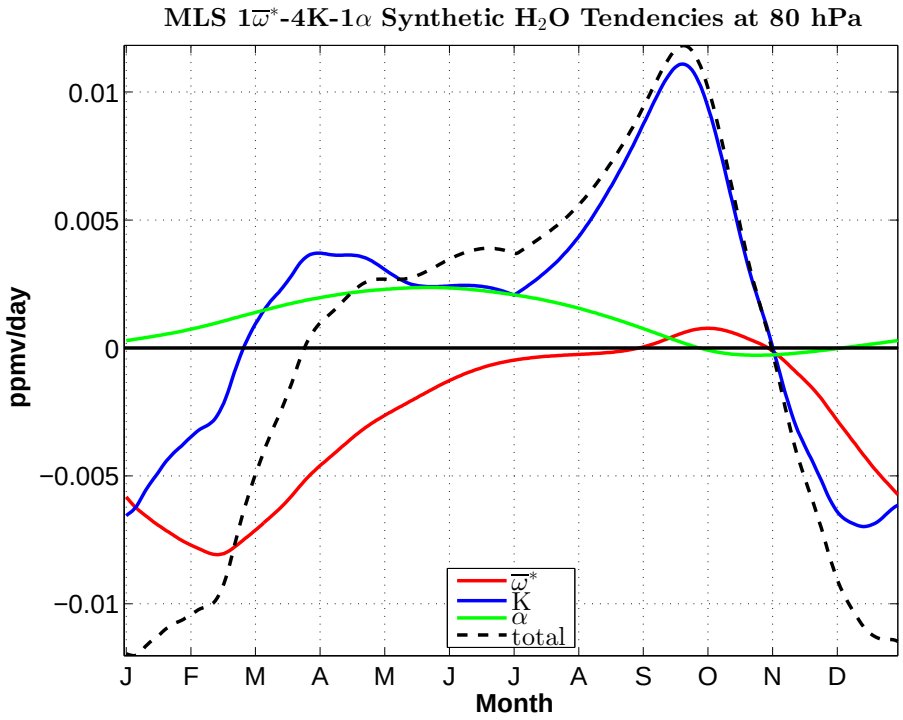

Figure 42: The time tendencies (ppmv/day) of each term and the total for the optimal solution of observed MLS tape recorder at 80 mb.

The time tendencies of observations at 400 K (a level similar to 80 hPa) look quite different in comparison, as shown in Figure 43. In isentropic coordinates, vertical mixing plays a nearly non-existent role in shaping the seasonal cycle of the tape recorder. Instead, horizontal mixing is the transport process moistening the dry part of the signal during the spring to early fall. In all other parts of the seasonal cycle, transport is largely done by diabatic heating, especially during the winter. During the winter, convection frequency is highest in the interior tropics rather than north of them (as during the boreal summer) and this may play a role in the influence of Q.

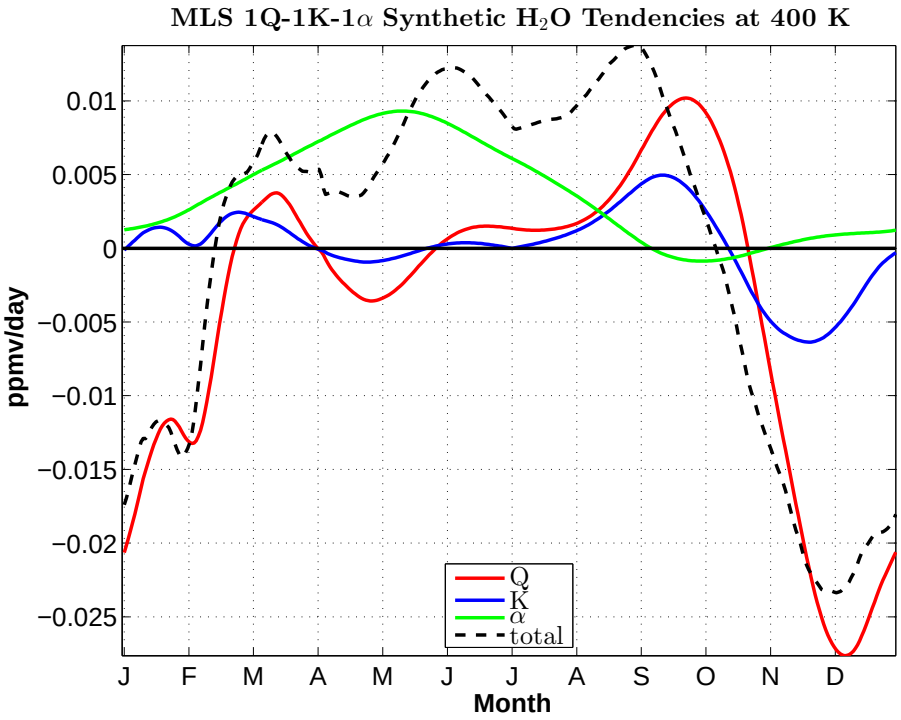

Figure 43: The time tendencies (ppmv/day) of each term and the total for the optimal synthetic solution of the observed MLS tape recorder at 400 K.

The percent variance of the water vapor tendencies explained by each transport is highlighted in Figure 44. Just over 90% of variance in the observed tape recorder in pressure coordinates can be explained by vertical mixing (green); over 60% can be explained by vertical advection (blue); and under 10% can be explained by horizontal mixing (red). Adding up these percentages equals over 100% because the transports do not act as independent predictors. Over 75% of the variance in isentropic coordinates can be explained by diabatic heating; nearly 55% can be explain by vertical mixing; and nearly 25% can be explained by horizontal mixing. In both coordinate systems, the two dominating transports include the residual circulation and vertical mixing. The main difference is that in isentropic coordinates, horizontal mixing plays a larger role while diabatic heating becomes the main transport by a large percentage.

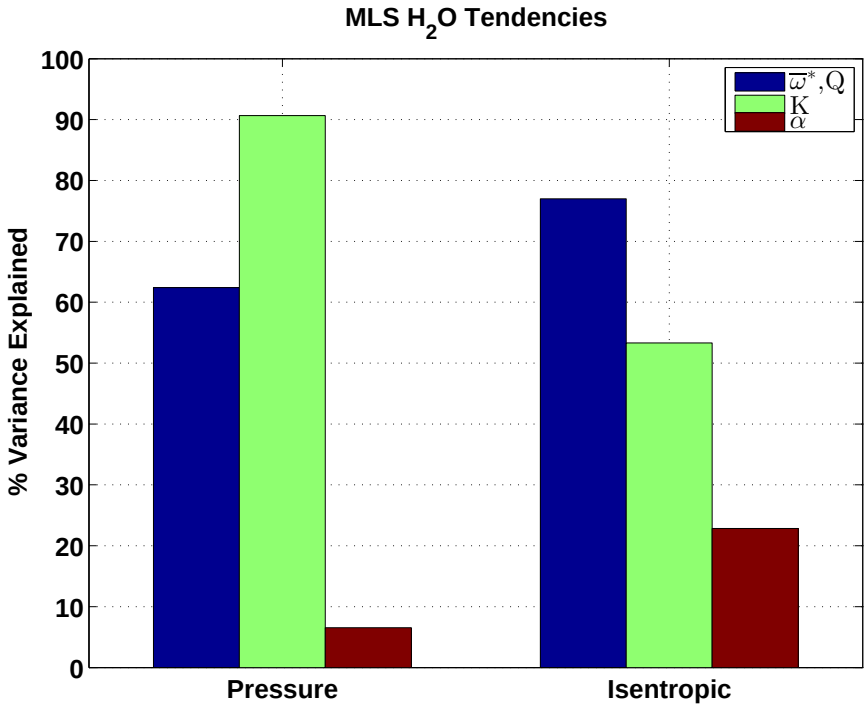

Figure 44: Percent variance in the time tendencies explained by each term in both coordinate systems for the optimal synthetic solution of the observed MLS tape recorder.

4.6.2 ERA-i reanalysis

Figure 45 shows that vertical advection acts to decrease the water vapor with time in the ERA-i simulations. Vertical mixing plays a large role during the boreal fall and spring by adding water vapor to the layer. Horizontal mixing also plays a role in these pressure coordinates. During spring, it moistens the tape recorder while in dries it out during the fall. At other times of the year, it is small. Again we see that vertical mixing and vertical advection play nearly equal roles during the winter.

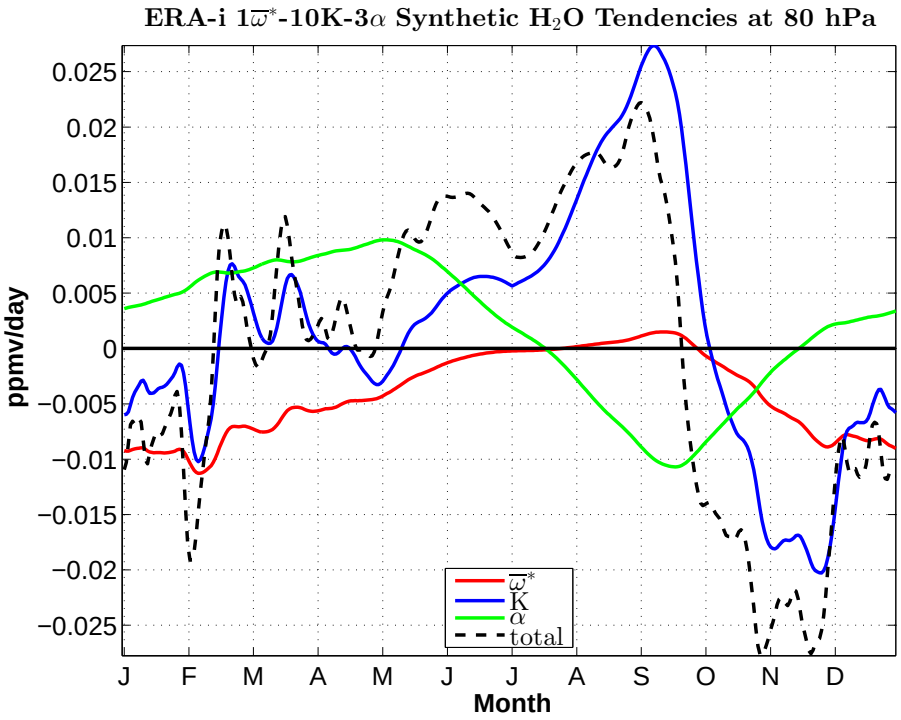

Figure 45: The time tendencies (ppmv/day) of each term and the total for the optimal synthetic solution of ERA-i tape recorder at 80 mb.

At 400 K, the tape recorder in ERA-i is strongly controlled by diabatic heating, with a very strong negative tendency at the end of November and intro December, as evident in Figure 46. Vertical mixing in isentropic coordinates is less important to the time tendencies of water vapor, even though the strength has been increased for this simulation by a factor of 4. Instead of changing sign with season, horizontal mixing now only adds to the water vapor signal and this occurs mainly during the late spring and early summer. Overall, in isentropic coordinates, the tape recorder of the reanalyses is strongly dictated by diabatic heating.

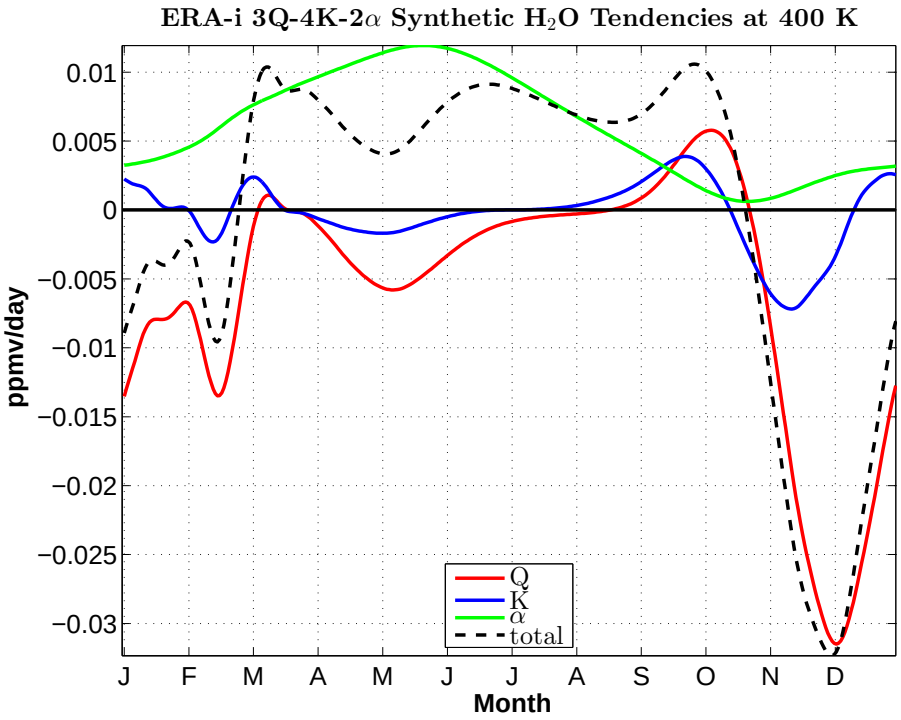

Figure 46: The time tendencies (ppmv/day) of each term and the total for the optimal synthetic solution of ERA-i tape recorder at 400 K.

Figure 47 shows the percent variance explained by each transport for simulations of ERA-i. Compared to simulations of MLS at 80 mb, much less of the water vapor variance can be explained by vertical advection in the reanalysis. Instead, vertical advections only explains about 30%; vertical mixing explains almost 70%; and horizontal mixing explains less than 1% of the variance. In isentropic coordinates, vertical mixing plays a smaller role in the water tendency. Diabatic heating explains over 90%; vertical mixing explains 37%; and horizontal mixing explains 22%. Qualitatively, the variance explained by each coordinate system are similar between MLS and ERA-i

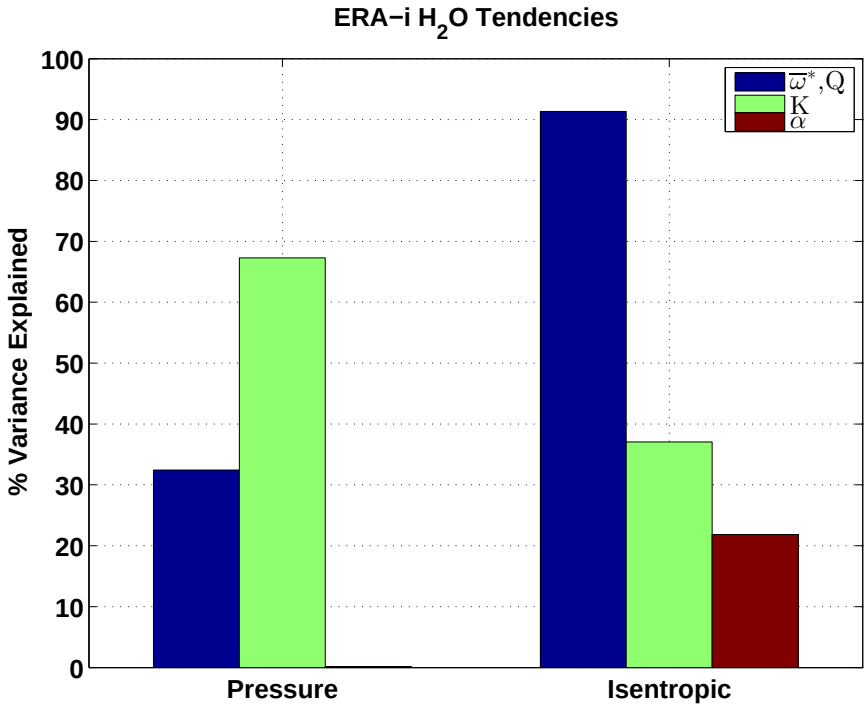

Figure 47: Percent variance in the time tendencies explained by each term in both coordinate systems for the optimal synthetic solution of the ERA-i tape recorder.

4.7 The effect of time-independent transports in MLS observations

This study is also interested in the effect of using time-independent transports in MLS observations. The approach taken by *Mote et al.* (1998) only allowed for time-independent transports to be found, although this seems somewhat unrealistic because of the seasonal cycles apparent in vertical advection and horizontal mixing (*Plumb*, 2002; *Rosenlof*, 1995). This chapter identifies any differences between using time-independent transports or seasonally-dependent transports (which have been studied above). This chapter also looks at the seasonality of vertical mixing.

4.7.1 The annual mean

Figure 48 shows the annual mean difference (%) between the simulations (using time-independent transports) and the MLS observations where warm (cool) contours represent overestimation (underestimation) and the white contours represent a successful annual mean. Qualitatively, this is not too different from Figure 20 which showed the same results for simulations with seasonally-varying transports. The main difference is that there is a wider range of solutions and less variability in the annual mean, even outside of the optimal range (notice the range on the color scale). Interestingly, the vertical advection in this simulation can be increased between factors of 2 and 3 and result in a good annual mean; this result was not possible in the previous simulations. Also, this simulation shows that the two types of mixing are mostly unconstrained when the annual mean is involved. This explains why *Mote et al.* (1998) believed increasing vertical advection was of upmost importance when simulating the aspects of the tape recorder. Without a seasonal cycle, vertical advection is able to increase in strength without underestimating the annual mean water vapor at 80 hPa. A noticeable change in the annual mean will only be seen in the case where horizontal mixing is increased by an order of magnitude and vertical advection remains small. This scenario would be associated with a cold point temperature change of less than 0.5 K.

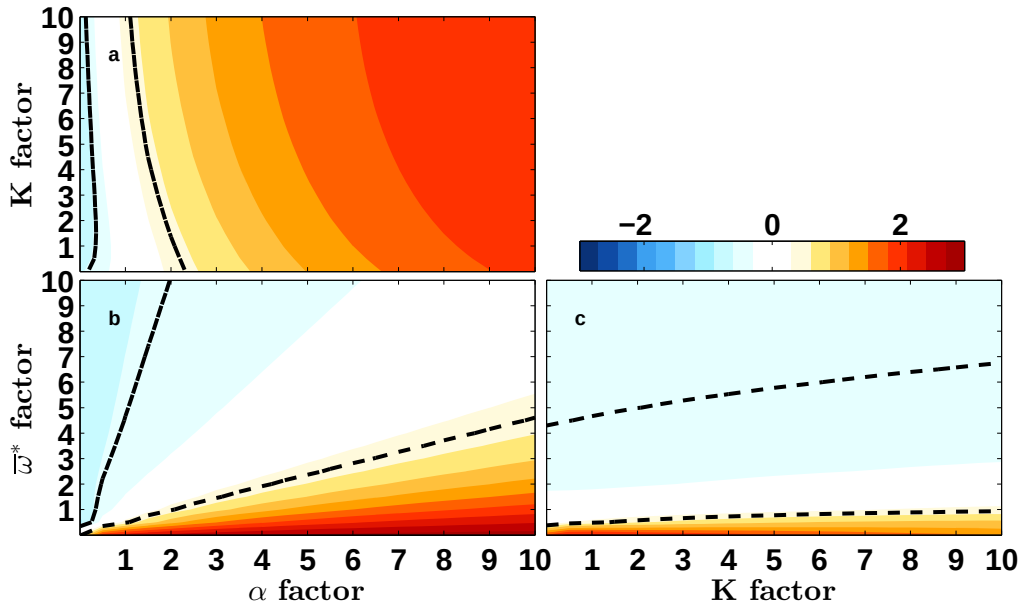

Figure 48: The annual mean difference (%) between the synthetic and observed tape recorders at 80 hPa for varying combinations of strengths of transports, however none of the transports have seasonality.

4.7.2 The seasonal cycle

Horizontal mixing is again unconstrained when looking at the phase lag in simulations without time-varying transports, as shown in Figure 49. These results look similar to Figure 22 especially for panel (c). Panel (a) looks the most different as now a range of horizontal mixing strengths are able to replicate the phase of the tape recorder. The $1\overline{\omega}^*$—$1K$—1α shows the simulations lagging observations by about 15 days. This is an odd result because that is where the phase should be almost perfect, as it matches the strengths of the transports found by *Mote et al.* (1998). The reasons for this discrepancy are described by *Mote et al.* (1998) as 80 hPa is where their interpolation onto finer grids would suffer the most oversampling errors. The observations are about 3.5 km resolution at 80 hPa and their interpolation was for 50 m resolution. *Mote et al.* (1998) states that,

"Below 18 km the solution often differs substantially from the input values, a problem that is exacerbated at higher resolution." When testing their method on synthetically-made data, it rarely calculated the correct transport strengths at the altitudes we consider. Nonetheless, the time-independent transports appeared to work well for the annual mean.

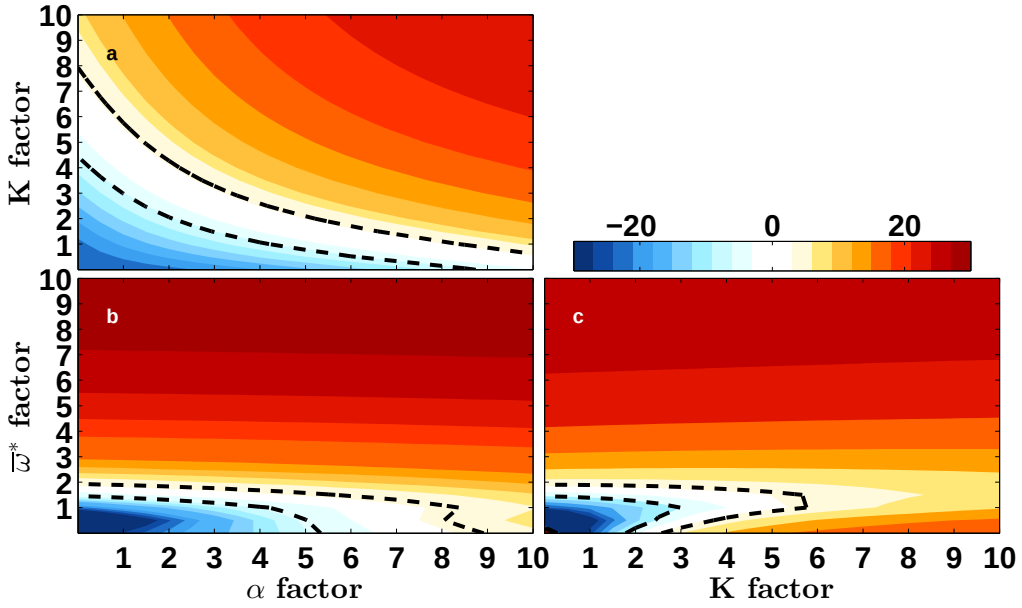

Figure 49: The phase lag (days) between the synthetic and observed tape recorders at 80 hPa for varying combinations of strengths of transports, however none of the transports have seasonality.

The *Mote et al.* (1998) approach also worked well at simulating the amplitude. Figure 50 shows that the time-independent transport simulations produced over 90% of the amplitude for the $1\overline{\omega}^*$—$1K$—1α combination. It's also apparent that a range of combinations satisfy the amplitude, as can be seen by the yellow contours. Panels (b) and (c) are comparable to Figure 25 which shows the amplitude results for time-varying transport simulations. Panel (a) is very different between the two figures since much more vertical mixing was required to simulate the amplitude in Figure 25. These time-independent transports support the findings by *Mote et al.* (1998) but they also

emphasize an earlier point: more than one solution exists. The approach made by *Mote et al.* (1998) only allowed the ability to find one optimal time-independent solution, but we can see from these results that there is more than one. Overall, even using time-independent transports to simulate observations requires increased strengths in either horizontal or vertical mixing for the phase measurement.

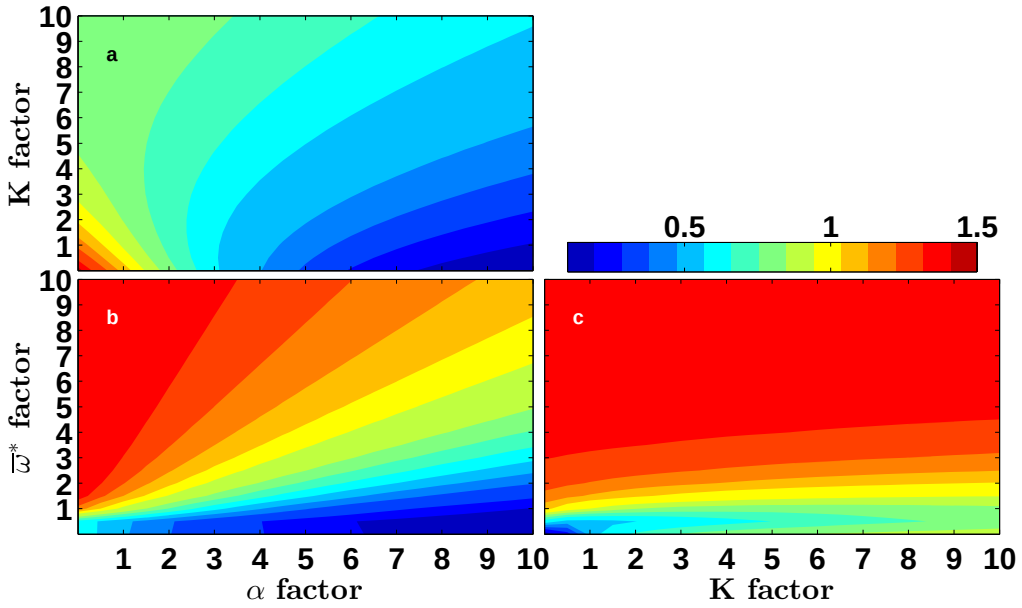

Figure 50: The amplitude ratio (ppmv/ppmv) between the synthetic and observed tape recorders at 80 hPa for varying combinations of strengths of transports, however none of the transports have seasonality.

Figure 51 shows the score for a tape recorder created without seasonally-dependent transports. The white star now lies on the $1\overline{\omega}^*$—$1K$—1α combination and this combination overlaps with a score of about 65% however it close to two separate maximums. This figure supports findings by *Mote et al.* (1998) that increases to vertical advection can be favorable to improving transport, however it does not discredit our earlier findings that amplifying vertical mixing can be advantageous. Overall, using seasonally-independent transport offers a wider range of solutions and bimodality.

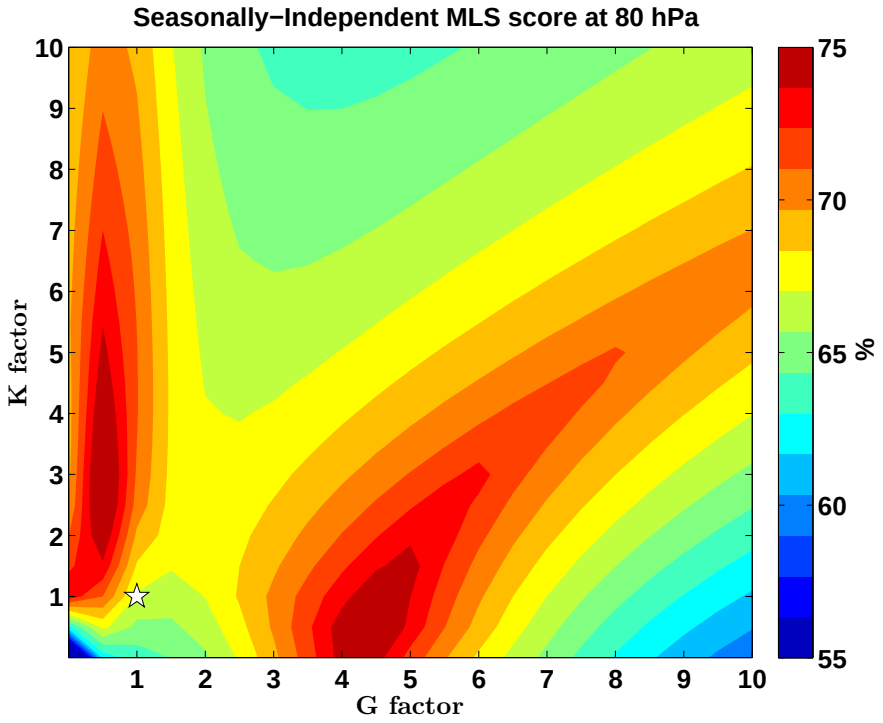

Figure 51: The score (%) between the synthetic and MLS tape recorders at 80 hPa for varying combinations of K and G, however none of the transports have seasonality.

4.7.3 The seasonality of vertical mixing

Because the seasonal cycles of the residual circulation and horizontal mixing have been researched thoroughly (*Plumb* (2002); *Rosenlof* (1995)), this study pays special attention

to the time-dependence of transport by vertical mixing. This is done by shifting one wavelength of a sinusoidal throughout the entire year in order to find which phase produces the best simulation. This is performed with seasonal cycles still imbedded in the other two transports. Therefore every transport has seasonality, but we are shifting the seasonality in vertical mixing until the best phase of it is found.

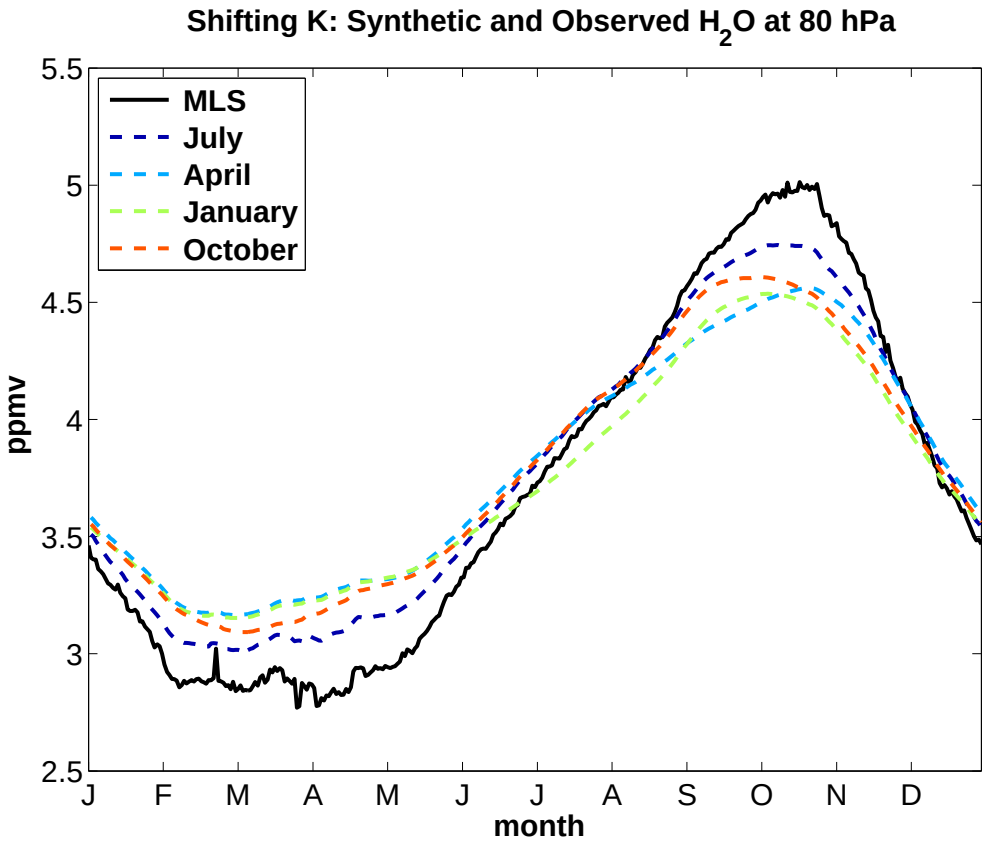

Figure 52: The observed (black) and synthetic (colors) water vapor concentrations at 80 hPa for different seasonal cycles of vertical mixing. The months represent when vertical mixing is at its maximum.

Figure 52 shows the resulting water vapor at 80 hPa for different seasonal cycles of vertical mixing K. Overall K appears to perform best when it peaks in July, however, the differences between all scenarios are small and this should have only small consequences on our earlier simulation setups. During the northern hemisphere summer, the curvature is

very strong and the residual circulation is weak therefore vertical mixing can have profound effects on the water vapor. In the northern hemisphere winter, strong vertical mixing cannot strongly influence the tape recorder for two reasons: (1) vertical advection is already acting and (2) the curvature is weaker. In fact, having strong vertical mixing during the northern hemisphere winter can weaken the transport. It should also be noted that the vertical level where the mixing peaks is important. Even if the peak is just 10 mb lower (higher in altitude), vertical mixing can play a different role because of the change in the curvature of water vapor.

5 Discussion

5.1 Summary and implications

The overarching result is that there is not one optimal solution for the transports occurring within the TTL and the tropical lower stratosphere. It is very possible to implement one set of strengths that approximately simulates the tape recorder for perhaps the wrong reason. By measuring three characteristics of the water vapor signal, we were able to reach stronger conclusions that narrowed the large amount of transport combinations into a smaller set. Compared to *Mote et al.* (1998), each simulation in pressure coordinates required increased vertical diffusion yet these results also showed that the residual circulation should remain constrained at strengths described by past studies (*Mote et al.*, 1998; *Schoeberl et al.*, 2008; *Rosenlof, 1995*; *Plumb*, 2002) in both the observations and the reanalysis. Horizontal transport, on the other hand, must be different strengths depending on if the simulation is for MLS observations or the ERA-i reanalysis.

The stratospheric circulation in ERA-i is at least twice as fast as observations vertically and also horizontally (when viewed on the 390 K surface). This was first noticed by using the lag-correlation method which produced effective velocities. That velocity difference was further supported by the need for largely increased vertical mixing as well and somewhat increased horizontal mixing. Both of these transports can change the phase of the tape recorder with height, and therefore the speed. Vertical mixing is particularly good at simulating the amplitude. Yet in isentropic coordinates, less vertical mixing was required in the simulations due to the fact that a part of this transport is implicit with the heating rate when operating with surfaces of potential temperature. For example, vertical mixing

causes a surface to bulge which results in changes to the stratification and thusly the diabatic circulation. Simulating MLS observations in isentropic coordinates required the original factors of each transport while simulating the ERA-i reanalysis required increased diabatic heating. As expected, horizontal mixing played a larger role in the time tendency of the water vapor signal in these coordinates versus in pressure coordinates.

This study found that increasing the residual circulation in ERA-i by small amounts in either coordinate system required simultaneous increases in vertical and horizontal mixing towards unrealistic values. It was discovered that strong vertical advection was poor at carrying the amplitude upward during the northern hemisphere winter, and therefore vertical mixing played a comparable role at dispersing the signal. Interestingly, all simulations—in the seasonal cycle and annual mean—pointed towards highly constrained values of the residual circulation. However, such strengths of vertical advection were not as large as the effective vertical velocities in observations and the models. In ERA-i, vertical mixing needed to be increased by an order of magnitude beyond the strengths found by *Mote et al.* (1998). Compared to the vertical mixing this study found in MLS observations, ERA-i required over double the amount. Horizontal mixing also needed increase by half an order of magnitude. A part of this study was interested in the influence of seasonally-varying transports. We found that without a seasonal cycle, more solutions exist for the transports. The effective velocity results showed that time-independent transports is probably unrealistic. Therefore, narrowing down the seasonality will only help towards understanding TTL dynamics.

It is important to note that ERA-i assimilates stratospheric water from mostly radiosonde observations which have also been used to suggest that MLS exhibits a moist

bias (*Hurst et al.*, 2014). This means that ERA-i is being nudged toward a drier signal but the outputs are ending up even wetter than the moist-biased MLS, which it doesn't assimilate (*Dee et al.*, 2011). This would mean that if ERA-i did assimilate MLS observations, it would probably be even wetter than it is now. Comparing the ERA-i simulation results to those in GEOS CCM, we found that less vertical mixing was needed in the latter. Knowing that the CCM does not use data assimilation, this hints at the possibility that ERA-i has too much vertical diffusion as a result of its assimilation system. It is important to remember than MLS is not perfect and that its coarse resolution may actually underestimate the effective transport.

Together, the methods used in this study showed us that using annual mean transports, as in *Mote et al.* (1998), is not a robust route for a few reasons. The tape recorder signal is nonlinear, especially at the TTL, and therefore cannot be described using linear transports. This approach appears successful when looking at the annual mean measurement, however it leads to problems in the seasonal cycle specifically in the phase of the synthetic tape recorder which lags observations by about 15 days. Beyond difficulties in the speed of transport, this method also introduces a much wider range of solutions. It was discussed earlier that such seasonally-independent transports are unrealistic because their associated dynamics possess seasonality. Using the annual mean results in a wide range of solutions because the amplitude is constantly underestimated and results in a "successful" annual mean measurement. This however will lead to problems in stratospheric chemistry and the global radiation balance as the minimum and maximum water vapor entering the stratosphere is no longer accurate. The seasonal cycle of the BDC will be slower using this method, which could also lead to problems regarding the temperature of the stratosphere.

Using these seasonally-independent transports in a GCM would result in a misunderstanding that was seen in this study and in *Mote et al.* (1998) where the vertical advection term dominates in the TTL, when the more realistic seasonally-dependent results actually showed that they were of equal importance in shaping the tape recorder signal.

In particular, vertical mixing can have a profound impact on TTL temperature and therefore the water vapor entering the stratosphere, as discussed by *Flannaghan and Fueglistaler* (2014). In their work, they discovered that mixing leads to changes in diabatic heating and zonal acceleration most strongly during the northern hemisphere summer over the Indian Ocean. Further analysis found that these forcings produce a 4 K temperature response in local regions, increasing water vapor concentration by 2 ppmv (*Flannaghan and Fueglistaler*, 2014). Our results agree with those of (*Flannaghan and Fueglistaler*, 2014) that the seasonality of vertical mixing peaks during the northern hemisphere summer, and we build further onto this. When vertical mixing was forced to peak in the northern hemisphere winter, it actually resulted in more water vapor within the dry part of the signal.

If a range of solutions are able to simulate the tape recorder, what does this mean for TTL theory? It probably means that more work needs to be done to understand the seasonality and profiles of transports. In order to narrow the range of solutions, it is important to look at all characteristic of the tape recorder. The range of solutions has a wider spread in ERA-i and this may be due to the differing, yet similar effects of data assimilation and numerical diffusion. If the influence of data assimilation can be quantified, this will help towards understanding the strength of numerical diffusion. Overall the story of vertical mixing, its strength, and its seasonal cycle, are still unclear yet the results are

quickly narrowing down what isn't correct. Either way, vertical mixing has been observed in the TTL (*Flannaghan and Fueglistaler* (2014); *Fujiwara et al.* (1998); *Fujiwara and Takahashi* (2001); *Fujiwara et al.* (2003); *Mote et al.* (1998)), it requires an imbedded seasonal cycle for successful modeling, and more of it appears to exist than previously thought

5.2 Future work

This research opens many new avenues. Firstly, the model can be improved. The vertical profiles were the only factor that went untested in each of the transports. For these, we relied on the study by *Mote et al.* (1998), however it would be interesting for these profiles to change in steepness and it would also be interesting to see what the simulations would look like if the transports sloped with height (similar to the tape recorder). Also, instead of multiplying the entire transport time series by a factor, it would be interesting to only change the factors of certain seasons. It's also very important to test the validity of the horizontal mixing term by comparing it with outputs of vertical mixing from the ERA-i reanalysis, for example.

Secondly, a cloud resolving model (CRM) would benefit this study by introducing non-parameterized processes like gravity waves and cloud features. With fine temporal and spatial resolutions, time filtering could be performed on perturbations of temperature and water vapor to see the direct effects of gravity waves and overshooting cloud tops. A parameter sweep could be useful again. Instead of varying dynamics, we would vary the amounts of water vapor, convective available potential energy at the surface, and other

constituents until heating rates are found that closely resemble reanalyses in order to find a control scenario. This test would identify the sensitivity of vertical mixing to changes on seasonal and longer timescales. Using water vapor budgeting in the CRM, we would be able to quantify the amount of water vapor that enters the vapor phase from overshooting cloud tops.

Last of all, creating (or modifying) a mixing scheme that accounts for unresolved small gravity waves would be powerful. The most recently used mixing scheme in ERA-i, the Monin-Obukhov (MO) scheme, features a Richardson number component that requires low static stability or large increases in the zonal wind with height. The weakness with this scheme occurs when gravity waves are not resolved, and therefore not included in the calculation. A previously-used mixing scheme, the revised Louis scheme (rL), has non-zero diffusivity even when the Richardson number goes to infinity. If gravity waves are resolved, then the MO scheme will have increased mixing. Mixing by the MO scheme was found to maximize in the northern hemisphere winter and be much larger than mixing by the rL scheme which maximizes in the northern hemisphere summer (*Flannaghan and Fueglistaler*, 2014). Studies have not discussed which scheme is better, but it's apparent if gravity waves associated with convection are parameterized, their effects would not be in the latest ERA-i results. It would be beneficial to make a scheme that accounts for parameterized convection-induced gravity waves and their breaking within the TTL.

6 References

Abalos, M., Ploeger, F., Konopka, P., Randel, W. J., and E. Serrano (2013), Ozone seasonality above the tropical tropopause: reconciling the Eulerian and Lagrangian perspectives of transport processes, *Atmos. Chem. Phys.*, 13, 10787-10794.

Abalos, M., Randel, W. J., Kinnison, D. E., and Serrano, E. (2013), Quantifying tracer transport in the tropical lower stratosphere using WACCM, *Atmos. Chem. Phys.*, 13, 10591-10607.

Alexander, M. J., Richter, J. H., and Sutherland, B. R. (2006), Generation and trapping of gravity waves from convection with comparison to parameterization, *J. Atmos. Sci.*, 63, 2963-2977.

Andrews, D. G., J. Holton, and C. Leovy (1987), Middle Atmosphere Dynamics. Academic Press.

Andrews, D. G. and McIntyre, M. E. (1976), Planetary waves in horizontal and vertical shear: Asymptotic thetory for equatorial waves in weak shear, *J. Atmos. Sci.*, 33, 2049-2053.

Barnes, J. E., Kaplan, T., Vömel, H. and Read, W. G. (2008), NASA/Aura/Microwave Limb Sounder water vapor validation at Mauna Loa Observatory by Raman lidar, *J. Geophys. Res.*, 113, D15S03, doi:10.1029/2007JD008842.

Barton, N. P. and Ellis, A. W. (2009), Variability in wintertime position and strength of the North Pacific jet stream as represented by re-analysis data, *Int. J. Climatol.*, 29, 851-862, doi:10.1002/joc.1750.

Birner, T. (2010), Residual circulation and tropopause structure, *J. Atmos. Sci.*, 67, 2582-2600.

Bjerknes, J., and Palmén, E. (1937), Investigations of selected European cyclones by means of serial ascents, *Geofys. Publikasjoner, Norske Videnskaps-Akad. Oslo*, 3, No. 6.

Brewer, A. W. (1949), Evidence for a world circulation provided by the measurements of helium and water vapor distribution in the stratosphere, *Quart. J. Roy. Meteor. Soc.*, 75, 351363.

Butchart, N. (2014), Thet Brewer-Dobson circulation, *Rev. Geophys*, 52, 157-184, doi:10.1002/2013RG000448.

Davis, S. M., C. K. Liang, and K. H. Rosenlof (2013), Interannual variability of tropical tropopause layer clouds, *Geophys. Res. Lett.*, 40, 28622866, doi:10.1002/grl.50512.

Day, K. A., Hibbins, R. E., and Mitchell, N. J. (2011), Aura MLS observations of the westward-propagating s=1, 16-day planetary wave in the stratosphere, mesosphere and lower thermosphere, *Atmos. Chem. Phys.*, 11, 4149-4161, doi:10.5194/acp-11-4149-2011.

Dee, D. P. et al. (2011), The ERA-Interim reanalysis: configuration and performance of the data assimilation system, *Q.J.R. Meteorol. Soc.*, 137, 553597, doi:10.1002/qj.828.

Eichinger, R., Jöckel, P., and Lossow, S. (2014), Simulation of the isotopic composition of stratospheric water vapor - Part 2: Investigation of HDO/H2O variations, *Atmos. Chem. Phys. Discuss.*, 14, 29459-29497, doi:10.5194/acpd-14-29459-2014, in review.

SPARC CCMVal (2010), SPARC Report on the Evaluation of Chemistry-Climate Models, V. Eyring, T. G. Shepherd, D. W. Waugh (Eds.), SPARC Report No. 5, WCRP-132, WMO/TD-No. 1526, http://www.atmosp.physics.utoronto.ca/SPARC.

Flannaghan, T. J. and S. Fueglistaler (2014), Vertical mixing and the temperature and wind structure of the tropical tropopause layer, *J. Atmos. Sci.*, 71, 1609-1622, doi:10.1175/JAS-D-13-0321.1.

Flury, T., Wu, D. L., and Read, W. G. (2013), Variability in the speed of the BrewerDobson circulation as observed by Aura/MLS, *Atmos. Chem. Phys.*, 13, 4563-4575, doi:10.5194/acp-13-4563-2013, 2013.

Folkins, I., M. Lowewenstein, J. Podolske, S. Oltmans, and M. Proffit (1999), A barrier to vertical mixing at 14 km in the tropics: Evidence from ozonesondes and aircraft measurements, *J. Geophys. Res.*,104, 22095-22102.

Fueglistaler, S., Dessler, A. E., Dunkerton, T. J., Folkins, I., Fu, Q, and P. W. Mote (2009), Tropical tropopause layer, *Rev. Geophys.*, 47, RG1004, doi:10.1029/2008RG000267.

Fueglistaler, S., Legras, B., Beljaars, A., Morcrette, J.-J., Simmons, A., Tompkins, A. M. and Uppala, S. (2009), The diabatic heat budget of the upper troposphere and lower/mid stratosphere in ECMWF reanalyses, *Q.J.R. Meteorol. Soc.*, 135: 2137. doi: 10.1002/qj.361

Fujiwara, M., Kita, K., and T. Ogawa (1998), Stratosphere-troposphere exchange of ozone associated with the equatorial Kelvin wave as observed with ozonesondes and rawinsondes, *J. Geophys. Res.*, 103, 19173-19182.

Fujiwara, M., and M. Takahashi (2001), Role of the equatorial Kelvin wave in stratosphere-troposphere exchange in a general circulation model, *J. Geophys. Res.*, 106, 22763-22780.

Fujiwara, M., Yamamoto, M. K., Hashiguchi, H., Horinouchi, T., and S. Fukao (2003), Turbulence at the tropopause due to breaking Kelvin waves observed by the Equatorial Atmosphere Radar, *J. Geophys Res. Letters*, 30, 1171.

Garny, H., Dameris, M., Randel, W., Bodeker, G. E., and Deckert, R. (2011), Dynamically forced increase of tropical upwelling in the lower stratosphere, *J. Atmos. Sci.*, 68, 12141233. doi: http://dx.doi.org/10.1175/2011JAS3701.1

Garny, H., Birner, T., Bönisch, H., and Bunzel, F. (2014), The effects of mixing on age of air, *J. Geophys. Res. Atmos*, 119, 7015-7034, doi:10.1002/2013JD021417.

Gettelman, A., and P. M. F. Forster (2002), A climatology of the tropical tropopause layer, *J. Meteorol. Soc. Jpn.*, 80, 911924, doi:10.2151/jmsj.80.911.

Gettelman, A., P. M. de F. Forster, M. Fujiwara, Q. Fu, H. Vömel, L. K. Gohar, C. Johanson, and M. Ammerman (2004), Radiation balance of the tropical tropopause layer, *J. Geophys. Res.*, 109, D07103, doi:10.1029/2003JD004190.

Gettelman, A., Birner, T., Eyring, V., Akiyoshi, H., Bekki, S., Brhl, C., Dameris, M., Kinnison, D. E., Lefevre, F., Lott, F., Mancini, E., Pitari, G., Plummer, D. A., Rozanov, E., Shibata, K., Stenke, A., Struthers, H., and Tian, W. (2009), The Tropical Tropopause Layer 19602100, *Atmos. Chem. Phys.*, 9, 1621-1637, doi:10.5194/acp-9-1621-2009.

Gettelman, A., et al. (2010), Multimodel assessment of the upper troposphere and lower stratosphere: Tropics and global trends, *J. Geophys. Res.*, 115, D00M08, doi:10.1029/2009JD013638.

Gettelman, A., P. Hoor, L. L. Pan, W. J. Randel, M. I. Hegglin, and T. Birner (2011), The extratropical upper troposphere and lower stratosphere, *Rev. Geophys.*, 49, RG3003, doi:10.1029/2011RG000355.

Harries, J. E., J. M. Russell III, A. F. Tuck, L. L. Gordley, P. Purcell, K. Stone, R. M. Bevilacqua, M. Gunson, G. Nedoluha, and W. A. Traub (1996), Validation of measurements of water vapor from the Halogen Occultation Experiment (HALOE), *J. Geophys. Res.*, 101(D6), 1020510216, doi:10.1029/95JD02933.

Hegglin, M. I., D. Brunner, T. Peter, J. Staehelin, V. Wirth, P. Hoor, and H. Fischer (2005), Determination of eddy diffusivity in the lowermost stratosphere, *Geophys. Res. Lett.*, 32, L13812, doi:10.1029/2005GL022495.

Highwood, E. J., and Hhoskins, B. J. (1998), The tropical tropopause, *Q. J. R. Meteorol. Soc.*, 124, 1579-1604, doi: 10.1002/qj.49712454911.

Hurst, D. F., A. Lambert, W. G. Read, S. M. Davis, K. H. Rosenlof, E. G. Hall, A. F. Jordan, and S. J. Oltmans (2014), Validation of Aura Microwave Limb Sounder stratospheric water vapor measurements by the NOAA frost point hygrometer, *J. Geophys. Res. Atmos.*, 119, doi:10.1002/2013JD020757.

Jensen, E., and L. Pfister (2004), Transport and freeze-drying in the tropical tropopause layer, *J. Geophys. Res.*, 109, D02207, doi:10.1029/2003JD004022.

Kodera, K., Funatsu, B. M., Claud, C., and Eguchi, N. (2014), The role of convective overshooting clouds in tropical stratospheretroposphere dynamical coupling, *Atmos. Chem. Phys. Discuss.*, 14, 23745-23761, doi:10.5194/acpd-14-23745-2014, in review.

Konopka, P., Günther, G., Müller, R., dos Santos, F. H. S., Schiller, C., Ravegnani, F., Ulanovsky, A., Schlager, H., Volk, C. M., Viciani, S., Pan, L. L., McKenna, D.-S., and Riese, M. (2007), Contribution of mixing to upward transport across the tropical tropopause layer (TTL), *Atmos. Chem. Phys.*, 7, 3285-3308, doi:10.5194/acp-7-3285-2007.

Konopka, P., J.-U. Grooß, F. Plöger, and R. Müller (2009), Annual cycle of horizontal in-mixing into the lower tropical stratosphere, *J. Geophys. Res.*, 114, D19111, doi:10.1029/2009JD011955.

Konopka, P., Ploeger, F., Tao, M., Birner, T. and Riese, M. (2015), Hemispheric asymmetries and seasonality of mean age of air in the lower stratosphere: Deep versus shallow branch of the Brewer-Dobson circulation. J. Geophys. Res. Atmos., 120: 20532066. doi: 10.1002/2014JD022429.

Kunz, A., Spelten, N., Konopka, P., Müller, R., Forbes, R. M., and Wernli, H. (2014), Comparison of Fast In situ Stratospheric Hygrometer (FISH) measurements of water vapor in the upper troposphere and lower stratosphere (UTLS) with ECMWF (re)analysis data, *Atmos. Chem. Phys.*, 14, 10803-10822, doi:10.5194/acp-14-10803-2014.

Liu, C., Zipser, E., Garrett, T., Jiang, J. H., and Su, H. (2007), How do the water vapor and carbon monoxide tape recorders" start near the tropical tropopause?, *Geophys. Res. Lett.*, 34, L09804, doi:10.1029/2006GL029234.

Livesey, N. J., et al. (2007), EOS MLS version 2.2 Level 2 data quality and description document, *Tech. Rep.*, JPL D-33509, Jet Propul. Lab., Pasadena, Calif.

Mote, P. W., K. H. Rosenlof, M. E. McIntyre, E. S. Carr, J. C. Gille, J. R. Holton, J. S. Kinnersley, H. C. Pumphrey, J. M. Russell III, and J. W. Waters (1996), An atmospheric tape recorder: The imprint of tropical tropopause temperatures on stratospheric water vapor, *J. Geophys. Res.*, 101(D2), 39894006, doi:10.1029/95JD03422.

Mote, P. W., T. J. Dunkerton, M. E. McIntyre, E. A. Ray, P. H. Haynes, and J. M. Russell III (1998), Vertical velocity, vertical diffusion, and dilution by midlatitude air in the tropical lower stratosphere, *J. Geophys. Res.*, 103, 86518666, doi:10.1029/98JD00203.

Neu, J. L., and R. A. Plumb (1999), Age of air in a leaky pipe model of stratospheric transport, *J. Geophys. Res.*, 104(D16), 1924319255, doi:10.1029/1999JD900251.

Newell, R. E. and Gould-Stewart, S. (1981), A Stratospheric Fountain?, *J. Atmos. Sci.*, 38, 27892796. doi:http://dx.doi.org/10.1175/1520-0469(1981)038¡2789:ASF¿2.0.CO;2

Niwano, M., Yamazaki, K., and Shiotani, M. (2003), Seasonal and QBO variations of ascent rate in the tropical lower stratosphere as inferred from UARS HALOE trace gas data, *J. Geophys. Res.*,108, 4794, doi:10.1029/2003JD003871.

Paulik, L. C. and Birner, T. (2012), Quantifying the deep convective temperature signal within the tropical tropopause layer (TTL), *Atmos. Chem. Phys.*, 12, 12183-12195, doi:10.5194/acp-12-12183-2012.

Plöger, F., Fueglistaler, S., Grooß, J.-U., Günther, G., Konopka, P., Liu, Y.S., Müller, R., Ravegnani, F., Schiller, C., Ulanovski, A., and Riese, M. (2011), Insight from ozone and water vapour on transport in the tropical tropopause layer (TTL), *Atmos. Chem. Phys.*, 11, 407-419, doi:10.5194/acp-11-407-2011.

Plumb, R. A. (1996), A tropical pipe model of stratospheric transport, *J. Geophys. Res.*, 101(D2), 39573972.

Plumb, R. A. (2002), Stratospheric transport, *J. Meteorol. Soc. Jpn.*, 80, 793801.

Plumb, R. A., and J. Eluszkiewicz (1999), The Brewer-Dobson circulation: Dynamics of the tropical upwelling, *J. Atmos. Sci.*, 56, 868890.

Plumb, R. A., and R. Ferrari (2005), Transformed Eulerian-mean theory. Part I: Nonquasigeostrophic theory for eddies on a zonal-mean flow, *J. Phys. Oceanogr.*, 35, 165174

Randel, W. and Jensen, E. (2013), Physical processes in the tropical tropopause layer and their role in a changing climate, *Nat. Geosci.*, 6, 169176, doi:10.1038/ngeo1733.

Richard, E. C., K. C. Aikin, E. A. Ray, K. H. Rosenlof, T. L. Thompson, A. Weinheimer, D. Montzka, D. Knapp, B. Ridley, and A. Gettelman (2003), Large-scale equatorward transport of ozone in the subtropical lower stratosphere, *J. Geophys. Res.*, 108, 4714, doi:10.1029/2003JD003884.

Rosenlof, K. H. (1995), Seasonal cycle of the residual mean meridional circulation in the stratosphere, *J. Geophys. Res.*, 100(D3), 51735191, doi:10.1029/94JD03122.

Sargent, M .R., J. B. Smith, D. S. Sayres, and J. G. Anderson (2014), The roles of deep convection and extratropical mixing in the tropical tropopause layer: An in situ measurement perspective, *J. Geophys. Res. Atmos.*, 119, doi:10.1002/2014JD022157.

Schoeberl, M., Douglass, A., Zhu, Z., and S. Pawson (2003), A comparison of the lower stratospheric age spectra derived from a general circulation model and two data assimilation systems, *J. Geophys. Res.*, 108, 4113.

Schoeberl, M. R., et al. (2006), Overview of the EOS Aura mission, *IEEE Trans. Geosci. Remote Sens.*, 44, 1066-1074.

Schoeberl, M. R., et al. (2008), QBO and annual cycle variations in tropical lower stratosphere trace gases from HALOE and Aura MLS observations, *J. Geophys. Res.*, 113, D05301, doi:10.1029/2007JD008678.

Schoeberl, M. R., A. R. Douglass, R. S. Stolarski, S. Pawson, S. E. Strahan, and W. Read (2008), Comparison of lower stratospheric tropical mean vertical velocities, *J. Geophys. Res.*, 113, D24109, doi:10.1029/2008JD010221.

Schoeberl, M. R., Dessler, A. E., and T. Wang (2012), Simulation of stratospheric water vapor and trends using three reanalyses, *Atmos. Chem. Phys.*, 12, 6475-6487.

Solomon, S., K. H. Rosenlof, R. W. Portmann, J. S. Daniel, S. M. Davis, T. J. Sanford, and G.-K. Plattner (2010), Contributions of stratospheric water vapor to decadal changes in the rate of global warming, *Science*, 327, 12191223, doi:10.1126/science.1182488.

Trenberth, .K.E., Stepaniak, D.P., Caron, J.M. (2000), The global monsoon as seen through the divergent atmospheric circulation, Journal of Climate, 13, 3969-3993.

Tung, K. K. (1982), On the Two-Dimensional Transport of Stratospheric Trace Gases in Isentropic Coordinates. *J. Atmos. Sci.*, 39, 23302355, doi: http://dx.doi.org/10.1175/1520-0469(1982)039¡2330:OTTDTO¿2.0.CO;2.

Vaughan, G., C. Cambridge, L. Dean, and A. W. Phillips (2006), Water vapour and ozone profiles in the midlatitude upper troposphere, *Atmos. Chem. Phys.*, 5, 963971.

Vömel, H., et al. (2007), Validation of Aura Microwave Limb Sounder water vapor by balloon-borne Cryogenic Frost point Hygrometer measurements, *J. Geophys. Res.*, 112, D24S37, doi:10.1029/2007JD008698.

Waters, J., et al. (2006), The Earth Observing System Microwave Limb Sounder (EOS MLS) on the Aura satellite, *IEEE Trans. Geosci. Remote Sens.*, 44, 1075-1092.

Wright, J. S., and S. Fueglistaler (2013), Large differences in reanalyses of diabatic heating in the tropical upper troposphere and lower stratosphere, *Atmos. Chem. Phys*, 13, 9565-9573.

Yang, Q., Fu, Q., and Hu, Y. (2010), Radiative impacts of clouds in the tropical tropopause layer, *J. Geophys. Res.*, 115, D00H12.

Zhang, Z. and Q Chen (2007), Comparison of the Eulerian and Lagrangian methods for predicting particle transport in enclosed spaces, *Atmospheric Environment*, 41, 5236-5248.